

Dissertation

“Development of a 14.5 GHz All-Permanent Magnet Multicharged ECR Ion Source for Remote Operation”

ausgeführt zum Zwecke der Erlangung des akademischen Grades eines
Doktors der technischen Wissenschaften
unter der Leitung von

o.Univ.Prof. Dipl.-Ing. Dr.tech. HP. Winter

E134

Institut für Allgemeine Physik

eingereicht an der Technischen Universität Wien
Fakultät für Physik

von

Dipl.-Ing. Ernst Galutschek

Matrikelnummer 9225367

Geusaugasse 10/14

1030 Wien

Wien, am 23.März 2005

Dipl.-Ing. Ernst Galutschek

Kurzfassung

Die Wechselwirkung langsamer, hoch geladener Ionen (Geschwindigkeit unter einer atomarer Einheit oder 25keV/amu) mit Atomen, Molekülen und Festkörperoberflächen ist für die verschiedensten Forschungsgebiete, wie z.B. Untersuchungen zur thermonuklearen Fusion, astrophysikalischer oder ionosphärischer Prozessen, Untersuchungen zur Oberflächenanalytik oder in der Nanotechnologie von Interesse. Die Nachfrage nach Quellen für langsame hochgeladene Ionen stieg daher in den letzten zwei Jahrzehnten dramatisch an. In diesem Zusammenhang wurde die von R. Geller entwickelte Elektronenzyklotronresonanzionenquelle (EZR Ionenquelle) zum Rückgrat für die Produktion langsamer hoch geladener Ionen.

Da eine Erhöhung der EZR Frequenz die Produktion hoch geladener Ionen begünstigt, werden entsprechen höhere Magnetfelder für einen ausreichenden Einschluß des Plasmas benötigt. Üblicherweise werden diese Magnetfelder von Spulen, oder Supraleitern erzeugt, deren Betrieb und Unterhalt einen erheblichen Energieverbrauch und auch hohe Kosten verursacht. Für den Laborbetrieb ist es daher vorteilhaft Permanentmagnete zur Erzeugung dieser Felder zu verwenden.

Im Rahmen dieser Arbeit wird die Entwicklung, der Aufbau und erste Betriebserfahrungen einer neuen, ausschließlich auf Permanentmagneten basierenden, 14.5 GHz EZR Ionenquelle beschrieben. Prinzipiell werden für den Betrieb keine elektrischen Verbraucher am Hochspannungsterminal der Ionenquelle benötigt.

Die neue EZR Ionenquelle wurde an einem Teststand und an einem kleinen Ionenbeschleuniger zur Untersuchungen von Stößen mit Atomen und Festkörperoberflächen getestet.

Über ein LabVIEW Programm können alle Parameter der Ionenquelle ferngesteuert werden. Falls gewünscht, kann die Ionenquelle auch über das Internet, von nahezu jedem beliebigen Rechner aus, gesteuert werden. Die dafür notwendigen Programme wurden im Rahmen dieser Arbeit installiert und getestet.

In diesem Zusammenhang werden auch Experimente zur Tauglichkeit der Strahlemissionsspektroskopie schneller Heliumstrahlen als Plasmarandschichtdiagnostik bei JET, dem weltweit führenden Fusionsexperiment in Culham, England, diskutiert.

Abstract

Impact of comparably slow (impact velocity below one atomic unit or 25 keV/amu) multiply charged ions (MCI) on atoms, molecules and solid surfaces is of considerable interest in various fields of modern research as, e.g., thermonuclear fusion plasmas, astrophysical and ionospheric processes, and surface analytics and nanotechnology. Consequently, demand for slow MCI beams has remarkably increased during the last two decades. In this respect, the so called ECR ion source invented by the French physicist Richard Geller (ECR stands for magnetically confined electron cyclotron resonance heated plasma) has become the working horse for producing slow MCI beams. Since an increase of the ECR frequency favours plasma conditions which are beneficiary for MCI production, accordingly higher magnetic fields which are needed for satisfactory ion source plasma confinement, have to be provided. Commonly these magnetic fields are produced by normal conducting or superconducting electromagnet coils, the use of which is energy-consuming and thus rather costly in operation. For common laboratory needs it is therefore desirable to use instead permanent magnets for magnetic field production. In this thesis, the construction of and initial operational results from a novel 14.5 GHz ECR ion source, based on permanent magnets only, is described. In principle, no power supply is needed on the high voltage terminal of the ion source. This ECRIS has been built and tested both on a test bench and with a small ion accelerator for atomic collision experiments both in gas phase and on solid surfaces in ultra-high vacuum. The new ECR ion source can be remotely operated via a LabVIEW program and the Internet, which capability has been implemented and also demonstrated. In this context we shortly recount some experimental activities on fast helium beam emission spectroscopy for boundary plasma diagnostics at JET, the world-leading "Joint European Torus" fusion experiment at Culham, England, where remote participation is the common feature and has served as a very good example for our respective aspirations with our new ECR ion source.

Contents

Introduction	1
1.1 ECR Ion Sources	5
1.2 Production of Multiply Charged Ions	7
1.3 Plasma Confinement	13
1.4 ECR Heating	20
1.5 Ion Extraction	27
2. The 14.5 GHz ECR Ion Source SOPHIE	33
2.1 The Permanent Magnet System	35
2.2 The Plasma Discharge Chamber	43
2.3 The Microwave System	46
2.4 The Ion Extraction System	50
2.5 Computer Control and Interlock System	54
2.6 Overall Performance of the ECRIS SOPHIE	59
2.6.1 Investigations at the Test Stand	59
2.6.2 Performance of SOPHIE at the Ion Accelerator	66
3. Remote Participation	73
3.1 VNC	75
3.2 VRVS	77
3.3 Yahoo! Messenger	79
3.4 LabVIEW Activities within the LEIF Network	80
3.5 Fast Helium Beam Diagnostics as a Learning Case for Remote Participation	82
3.5.1 Principles of Fast He BES	82
3.5.2 Measurements at JET in October 2002	85
3.5.2 Experimental Results	86
Conclusion and Outlook	89
Bibliography	91
List of Abbreviations	96

Introduction

Electron Cyclotron Resonance ion sources (henceforth named ECR ion sources or ECRIS) of different kind have already been developed and operated at the Institut für Allgemeine Physik of the University of Technology in Vienna.

For the purpose of tokamak edge plasma spectroscopy with fast neutral lithium beams, the compact, high current 2.45 GHz ECRIS "ERNST" [1-3] has been developed and constructed. The source has been designed based on the heat pipe technology for continuous operation with gas and/or lithium vapour to provide mainly singly charged ions.

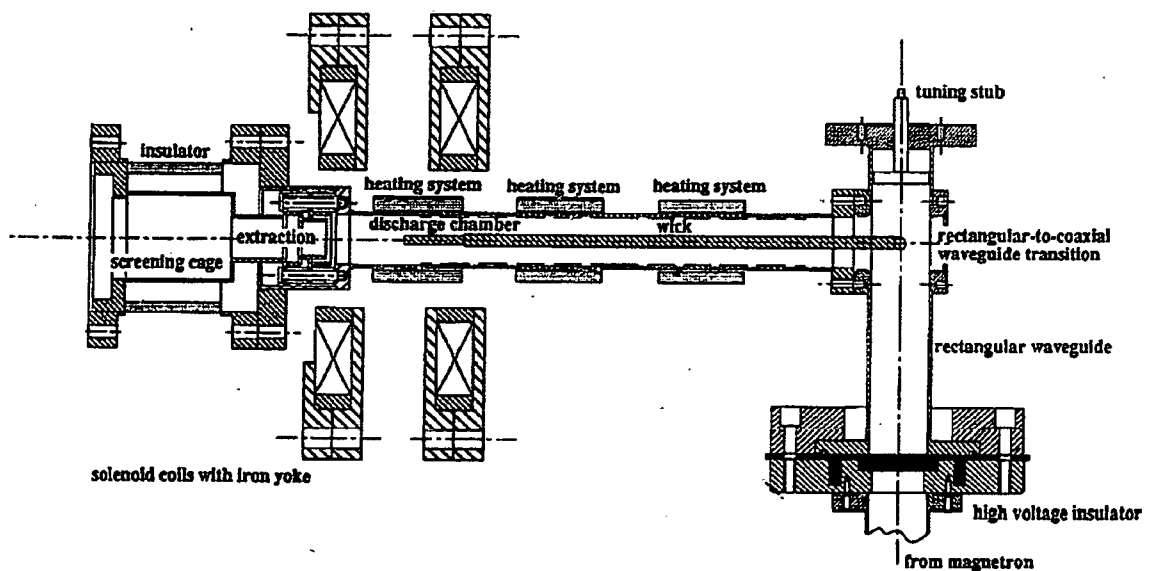


Fig. 1.1: Schematic drawing of the 2.45 GHz ECRIS "ERNST" [3].

The 5 GHz ECRIS “BERTA” [4] ion source has been used for production of slow multiply charged ions for atomic collision experiments in the “AUGUSTIN” laboratory at the University of Technology in Vienna.

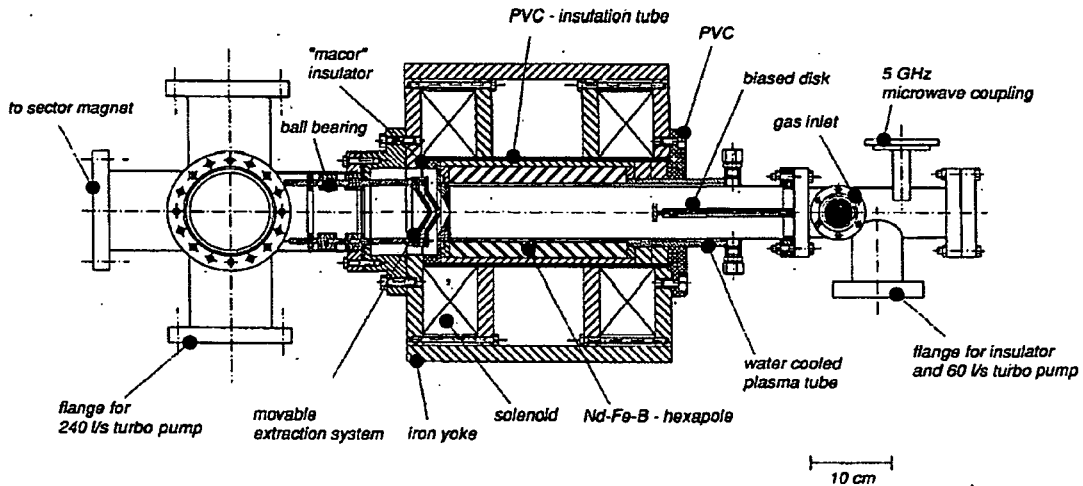


Fig. 2: Schematic drawing of the 5 GHz ECRIS “BERTA” [4].

Research focusing on the interaction of slow highly charged ions with matter (surfaces, atoms, molecules and, clusters) requires beams of multiply charged ions. Empirical Scaling laws for ECR ion sources predict a dramatic increase of the extractable currents of multiply charged ions with higher microwave frequencies.

Recently available NdFeB alloys for strong permanent magnets and comparably low priced microwave equipment for the Ku-band therefore led to the decision to replace the 5 GHz ECRIS “BERTA” by a compact 14.5 GHz ECR ion source based on permanent magnets only. This way not only higher charge states became accessible for experiments, but also the overall power consumption of the laboratory could be reduced dramatically.

The Institut für Allgemeine Physik and the Strahlencentrum at the Justus Liebig University in Gießen therefore decided to develop a new 14.5 GHz ECR ion source, based on the well established all permanent magnet ECRIS family developed in Gießen [5-10].

A schematic drawing of the new 14.5 GHz ECRIS “SOPHIE” (SOurce for Production of Highly charged Ions using ECR) is shown in fig.3.

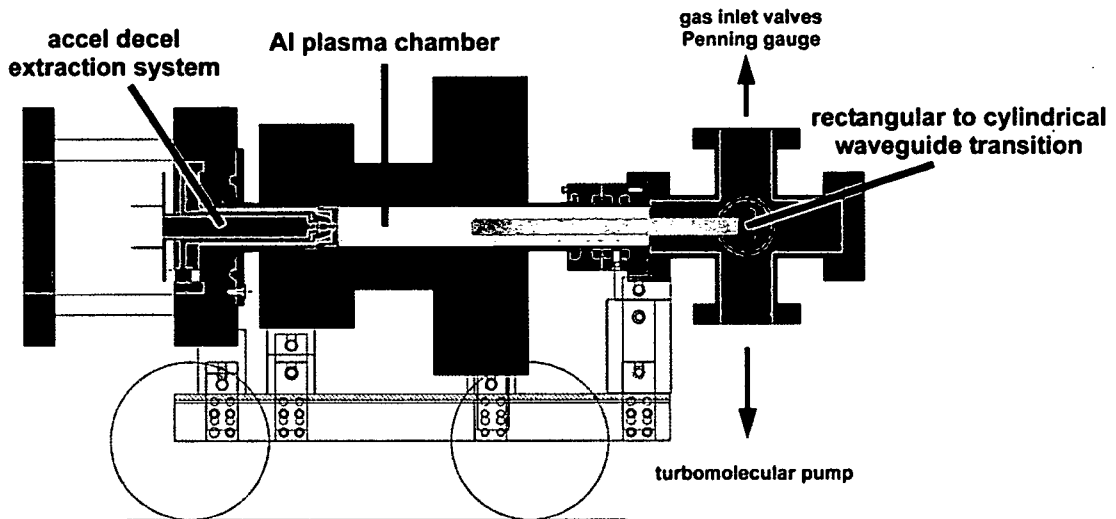


Fig. 3 Schematic drawing of the compact 14.5 GHz ECRIS “SOPHIE”.

This co-operation was part of the “Low Energy Ion beam Facilities” (LEIF) EU network, an I3 research activity carried out within the 5th framework programme of the European Union [13]. The LEIF network was established to improve co-operation between various low-energy ion beam facilities in Europe, combining these facilities to a European virtual facility.

Within the LEIF network, a so-called “Remote Participation and Online Access” project aimed to organise and provide online access to all network participants at the experimental facilities of institutions involved in LEIF.

The 14.5 GHz ECRIS “SOPHIE” was a model project within this activity. It allowed all parameters of the ion source to be remotely controlled by using the LabVIEW-based programme “CODIAN” developed by J. Bundesmann at the Hahn-Meitner Institute in Berlin [14,15,16], and a VNC client/server software [17]. The VNC client/server software had previously been used at the Institut für Allgemeine Physik for remote-participation in meetings and talks given at the JET (Joint European Torus) fusion research facility in Culham, England.

In this thesis the development, design and first results on the performance of the 14.5 GHz ECRIS "SOPHIE" will be discussed.

A brief, very simplified summary of the principles of ECR ion sources, based on available literature [18-21], is given in chapter one. For a more detailed description the book by R. Geller [18] is recommended. Ion sources in general are covered in the book by I.C. Brown [19], which features a chapter on ECR ion sources. Articles by A.G. Drentje [20] and Girard *et al.* [21] give general short reviews on ECR ion-sources.

The 14.5 GHz ECRIS "SOPHIE" is described in chapter two, giving an overview of its different subsystems. In subsection 2.6 first results on the performance of "SOPHIE" are presented. Some of the construction drawings of "SOPHIE" are included in an appendix.

Chapter three describes remote participation activities within the LEIF "Remote Participation and Online Access" project, exemplified by some fusion related research at the Institut für Allgemeine Physik. Also another closely related project is described, which has been conducted in parallel to the design and construction of the ECRIS "SOPHIE", i.e. the development of an edge plasma diagnostics with fast Helium beams. During the course of this thesis, experimental sessions at the fusion experiment JET, in Culham, England, have been attended, using the here described remote participation tools. The experience and know-how obtained in this project has been transferred to the LEIF "Remote Participation and Online Access" project.

1.1 ECR Ion Sources

ECR ion sources are delivering ion beams for a wide range of applications in many laboratories. Following the research on nuclear fusion devices based on magnetic mirror confinement, the development of ECR ion sources has been to a large extent an intuitive and experimental enterprise, still without a consistent theoretical description.

Fig. 1.1.1 gives a schematic view of a typical ECR ion source. ECR ion sources provide ions from a plasma heated via electron cyclotron resonance.

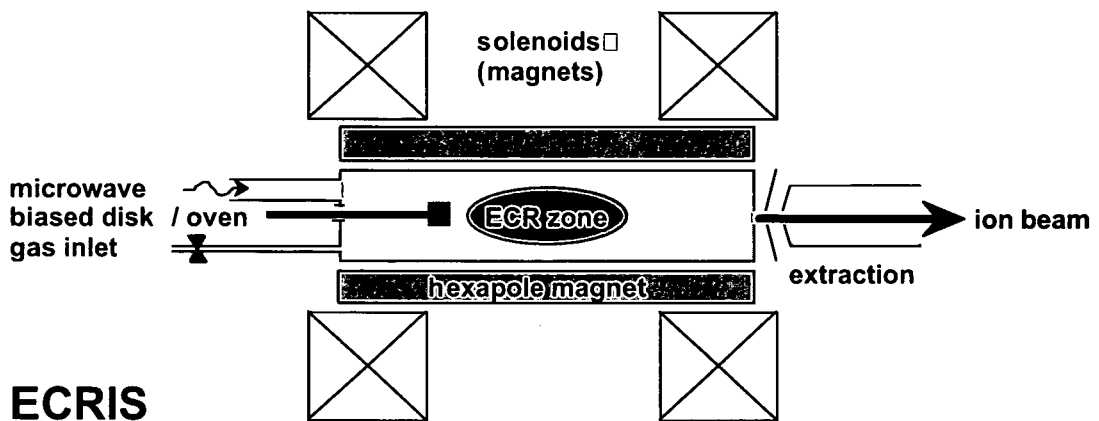


Fig. 1.1.1: Operation principle of an ECR ion source [23].

To confine the plasma, usually a magnetohydrodynamically stable “minimum-B” field structure is formed by the superposition of an axial magnetic mirror field with the radial field of a magnetic multipole. The axial field may be generated by solenoids, superconducting coils or, as in the case for the ECRIS “SOPHIE” described within this thesis, by permanent magnets, whereas the multipole field is in most cases generated by a permanent magnet hexapole.

The injected microwaves are resonantly absorbed in a region where their frequency coincides with the frequency of the electron gyromotion (see chapter 1.3). For “minimum-B” field structures, the “ECR-zone” is a closed surface around the centre of

the plasma. Some ECR ion sources operate not only with one but with two or even more microwave frequencies.

The plasma electrons, being heated by the microwaves, involve two components, a cold population (about 20 eV) and a hot population with a high energy tail reaching up to 100 keV or more. Typical ion energies are a few eV. Multiply charged ions are primarily produced via sequential electron impact ionization. The ions and electrons must be confined for sufficient time for sequential ionization to take place. Charge exchange, being the dominant loss mechanism for the multiply charged ion population, must be minimized by operating at low background gas pressure.

The plasma chamber is biased positively such that the ions can be extracted from the ion source via a suitable electrode geometry. In many cases a so-called "Accel-Decel" extraction system consisting of three electrodes is used, to obtain a parallel and intense ion beam.

Production of multiply charged ions can be enhanced by using plasma-chamber wall materials with high secondary electron emission. A so-called "biased-electrode" or "biased-disk" operated at negative potential with respect to the ion source is often used to influence the diffusion mode of the plasma, yielding higher extractable currents for multiply charged ions. Adding a suitable, usually lighter, gas to the working gas of the discharge improves the performance of the ion source as well.

1.2 Production of Multiply Charged Ions

There are various possibilities to produce multiply charged ions like field ionisation, photoionisation, electron impact ionisation, collisions with atoms, molecules (or their ions) or heavy particles, surface ionisation etc.. In fig. 1.2.1 cross sections for ionisation of argon by collision with photons, electrons and protons are given.

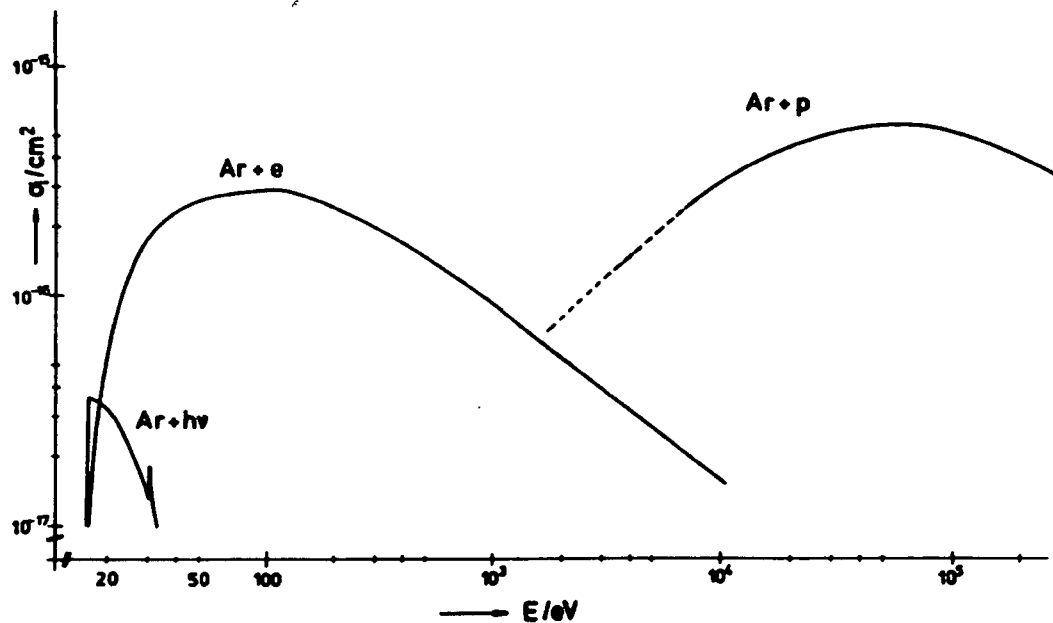


Fig. 1.2.1: Cross sections for ionisation of argon by photons, electron- and proton impact [18].

For the efficient production of multiply charged ions photo ionisation can be ruled out due to the comparably small cross section and the lack of a intense source of photons in the required energy range. Compared to the case of proton collision, the cross section of electron impact ionisation has a maximum at much lower energies. It is also much easier to produce high electronfluxes. Therefore many ion source designs, like ECR ion sources, are based on electron impact ionisation.

A certain ion charge state q can be reached in the following ways:

- Single impact ionisation: $X^0 + e \rightarrow X^{q+} + (q+1)e$
- Step-by-step ionisation: $X^0 + e \rightarrow X^+ + 2e$
- ...
- $X^{q-2} + e \rightarrow X^{(q-1)+} + 2e$
- $X^{q-1} + e \rightarrow X^{q+} + 2e$

Cross sections for direct ionisation are much smaller than the cross sections for step-by-step ionization. It is therefore advantageous to produce multiply charged ions via step-by-step ionisation [18]. Fig. 1.2.2 gives the step-by-step electron impact ionisation cross sections for argon.

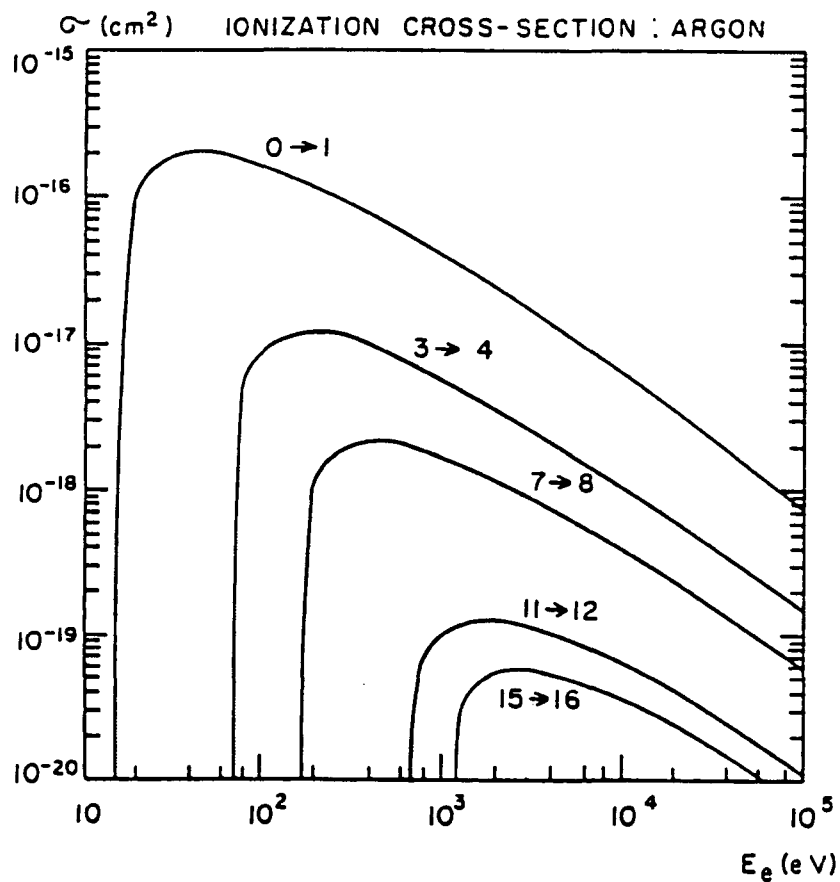


Fig 1.2.2: Electron impact ionization cross sections for argon [19].

For the projectile electrons, a minimum energy for removing the respective bound electrons is required. The probability for ionisation increases with the projectile electron energy to a maximum of about three or four times the binding energy of the electron to be removed from the atom or ion. The cross-sections are decreasing with growing charge state and their maxima are shifted towards higher impact energies. Step-by-step electron impact ionization therefore requires a wide spectrum of energies up to sufficiently high values for ionizing atoms to the desired charge state.

For a given ion-confinement time τ_i and electron density n_e a “quality-factor” $n_e\tau_i$, being a criterion for a specific ionization process to take place, can be defined as [19]:

$$n_e\tau_i \geq \frac{1}{R_{q_1 \rightarrow q_2}} \quad (1.1)$$

where $R_{q_1 \rightarrow q_2}$ is the reaction rate coefficient for a specific ionization channel from charge state q_1 to charge state q_2 , with a characteristic transition-time $\tau_{q_1 \rightarrow q_2}$ [19]:

$$\tau_{q_1 \rightarrow q_2} = \frac{1}{n_e \cdot R_{q_1 \rightarrow q_2}} \quad (1.2)$$

To allow such an ionisation to take place, a confinement time τ_i longer than the corresponding characteristic transition time is needed. So for a hot, not well confined plasma, multiple ionisation in single collisions will be responsible for relatively low charged ion production, whereas for ECR plasmas with comparably long particle confinement the step-by-step ionization gives primarily rise to multiply charged ions production. Fig. 1.2.3 shows values for the “quality factor” $n_e\tau_i$ in dependence of the electron temperature T_e for hydrogen like ions to become bare nuclei. These values are upper limits for $n_e\tau_i$, as the step-by-step ionization channel is considered only, while for partially ionized ions the “quality factor” could be lower, as other processes may contribute. It is clearly shown that an increase of the average charge state can only be obtained through a large increase in the “quality-factor”; e.g. an order of magnitude higher $n_e\tau_i$ value is required to obtain bare argon ions than for bare oxygen ions.

So a sufficient ion confinement is necessary for efficient step-by-step ionization as ions being longer exposed to the electron flux will reach higher charge states.

Obviously, all ion recombination processes have to be minimized. In ECRIS plasmas charge exchange with neutrals becomes the dominant recombination process, with a several orders of magnitude larger reaction rate coefficient than recombination with electrons or dielectronic recombination.

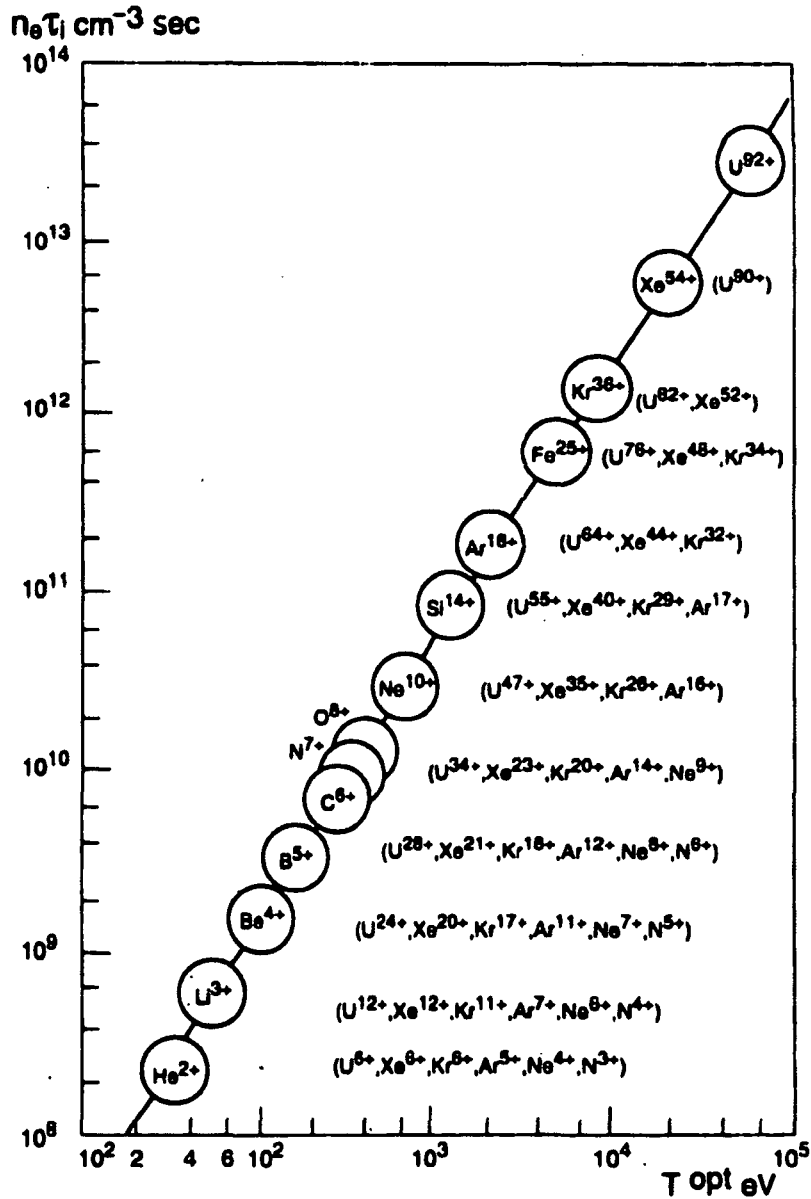


Fig.1.2.2: Golovanivsky's diagram of the $n_e \tau_i$ vs. T_e criteria.
Circles: completely stripped ions, bracket: other ions [19].

The most relevant processes for multiply charged ion production may therefore be summarized in the following balance equation [21,22], see also [19]:

$$\frac{dn_i^q}{dt} = +n_e \cdot n_i^{q-1} \cdot R_{(q-1) \rightarrow q}^{ION} - n_e \cdot n_i^q \cdot R_{q \rightarrow (q+1)}^{ION} + n_0 \cdot n_i^{q+1} \cdot R_{(q+1) \rightarrow q}^{CX} - n_0 \cdot n_i^q \cdot R_{q \rightarrow (q-1)}^{CX} - \left(\frac{n_i^q}{\tau_i^q}\right)$$

n_i^q ion density the of species i in charge state $q-1, q, q+1$ respectively

n_e electron density

n_0 neutral density

$R_{q_1 \rightarrow q_2}^{ION}$ reaction rate coefficients for electron impact ionization
to charge state $q, q+1$ respectively

$R_{q_1 \rightarrow q_2}^{CX}$ reaction rate coefficients for charge-exchange recombination
to charge state $q, q-1$ respectively

τ_i^q confinement time for ion species i in charge state q

(1.3)

In equilibrium the electron impact ionization has to balance the losses by charge-exchange and imperfect confinement. Typical charge exchange cross sections are three or four orders of magnitude larger than the corresponding electron impact ionization cross section. In the here relevant energy range, the reaction-rate coefficients are fortunately proportional to the projectile velocity, and neutral atoms are much slower than the hot electrons.

However, to keep the rate of production by electron impact ionization equal to the rate of loss by charge exchange, it is necessary for the neutral atom density to be about two orders of magnitude smaller than the electron density.

The relevant parameters for the production of multiply charged ions are therefore the electron density and -energy distribution, the ion density and confinement time and the density of neutral particles. Their influence on the production of multiply charged ions may be summarized as follows:

- A high ion density would be favoured by a high density “feeding gas”. On the other hand the neutral pressure has to be kept as low as possible to minimize loss via charge-exchange. However, the low density of “feeding gas” can be compensated by a longer ion confinement time or an increased electron flux.
- Ion confinement is a therefore a very critical parameter. If the confinement is too short, ions do not have sufficient time to reach the desired charge states, whereas too well confined ions might not be accessible for extraction.
- To allow step-by step ionization, electrons in a broad range of energies, sufficient to reach high charge states, are necessary.
- Since electron impact ionization cross section for high charge states are very small, a high flux of high energy electrons is needed to produce a significant density of multiply charged ions. Therefore the electron density has to be orders of magnitude higher than the neutral density. This may be achieved by improving the electron confinement but also by providing electrons by other means to the plasma.

1.3 Plasma Confinement

Good confinement of the plasma is necessary to allow the electrons to reach the required energies, and to expose the ions for a sufficient time to the electron flux allowing them to reach higher charge states.

In most ECR ion sources the plasma is confined in a so-called “minimum-B” multi mirror magnetic field structures. The two basic functions of the magnetic field are to confine the plasma and to allow an efficient energy transfer from the electromagnetic waves to the plasma.

In a magnetic mirror, charged particles are confined due to the conservation of their kinetic energy and their magnetic momentum, which is basically equivalent to conservation of the angular momentum about the guiding centre. (as described in plasma physics textbooks like [23,24] or in [19]) The magnetic momentum μ of a charged particle gyrating in a magnetic field B is defined as:

$$\mu = A.I = \pi.r_L^2 \frac{|q|v_{\perp}}{2.\pi.r_L} = \frac{m.v_{\perp}^2}{2.B} \quad (1.3.1)$$

where A is the surface of the current “loop” created by the gyromotion, I the electric current due to the particle motion, r_L the lamor-radius, q the charge, v_{\perp} the velocity component of the particle perependicular to the magnetic field B , and m the mass of the particle. To avoid any disturbance of the electron gyromotion by plasma fluctuations the plasma frequency ω_p should be kept smaller than the gyrofrequency ω_{CE} (as shown in [19]).

$$\omega_p = \sqrt{\frac{n e^2}{\epsilon_0 . m_e}} < \omega_{CE} = \frac{e.B}{m_e} \quad (1.3.2)$$

where m_e is the mass of the electron, n the plasma density, ϵ_0 the dielectric constant.

Entering an increasing magnetic field region the particle is experiencing a retarding force, as the kinetic energy contained in the gyro motion perependicular to the magnetic

field increases on the expense of the kinetic energy of the particle motion parallel to the magnetic field.

$$\vec{F} = (\mu \cdot \nabla) \vec{B} \quad (1.3.3)$$

This force may reflect the particle from the high field region, if the velocity component $v_{||}$ parallel to the magnetic field exceeds a certain value:

$$v_{||}^2 \geq v_{\perp}^2 \cdot (R - 1) \quad (1.3.4)$$

where v_{\perp} is again the velocity perpendicular to the magnetic field and R the so-called “mirror ratio”, which is defined as the ratio of the maximum to the minimum magnetic field of the mirror field structure. (v being velocity of the particle)

$$\frac{1}{\sin^2 \alpha} = R = \frac{B_{MAX}}{B_{MIN}}, \text{ with } \sin \alpha = \frac{v_{\perp}}{v} \quad (1.3.5)$$

In the velocity space, we find the so-called loss-cone (angle α), containing the not confined particles (fig 1.3.1). The higher the mirror ratio, the smaller the cone-angle α , the better the confinement.

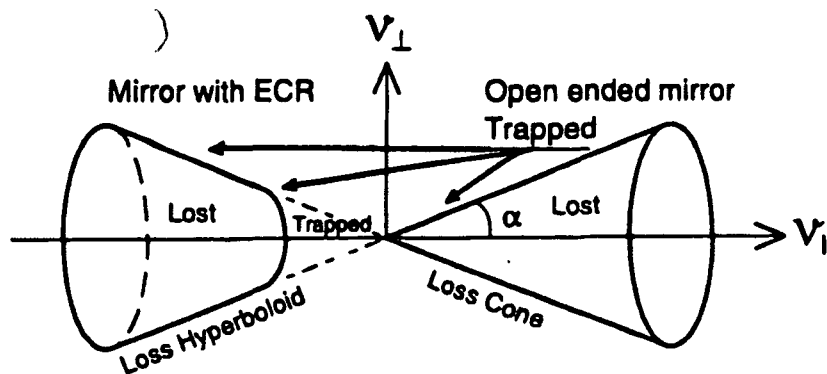


Fig. 1.3.1: Loss cone in velocity space: Loss cone in a simple mirror and loss hyperboloid in an ECR heated mirror [19].

As already mentioned, most ECR ion sources use multi-mirror confinement structures. By superimposing an axial mirror with a radial multipole field a so-called “minimum-B” field configuration is created (see fig 1.3.2). In such a configuration, the magnetic field increases from the centre of the field structure in every direction.

This way MHD instabilities are suppressed. The “minimum-B” structure also makes the ECR heating more efficient. The ECR condition is met on a closed surface around the

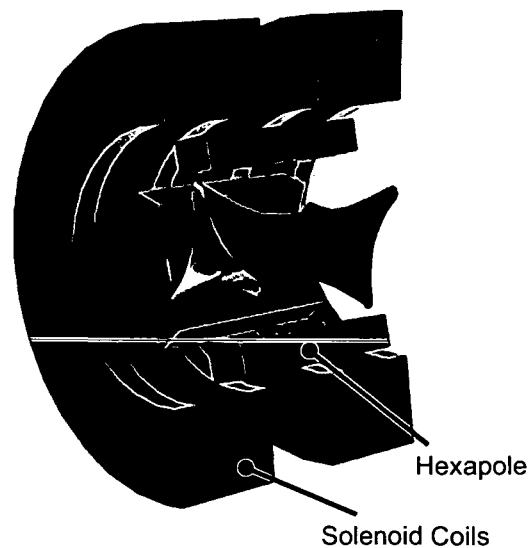
centre of the plasma, and the better confinement allows the electrons to make several passes through the “ECR-zone”, thus reaching higher energies.

Confinement in “minimum-B” configurations may be studied by making use of the second adiabatic invariant. When the particle has a larger scale periodic motion than the gyromotion around the field lines, like the bouncing motion of a trapped particle in an axial mirror, other invariants may be defined. The so-called second adiabatic invariant J is defined as the integral over the period of such a periodic motion (infinitesimal path length dl):

$$J = \oint v_{\parallel} dl \quad (1.3.6)$$

A particle with a given ratio of the kinetic energy to its magnetic momentum will move on a drift surface defined by the second adiabatic invariant J . As long as these surfaces do not intersect a wall, the particle is confined.

For the radial multipole usually a hexapole is used, as multipoles of higher order shift the “ECR-zone” closer to the plasma-chamber wall. In this case, the drift surfaces being of circular shape in the centre tend to form the characteristic triangular shape towards the outer region of the plasma (see fig. 1.3.2).



© D. Leitner

Fig. 1.3.2: Schematic view of a “minimum-B” configuration created by the superposition of an axial mirror field, here provided by solenoid coils, with the (radial) field of a hexapole magnet. Courtesy of D. Leitner, 2004 [26].

In ECR plasmas, only the hot electrons, encountering less collisions, are confined by the mirror-field structure. Low energy electrons, being more easily scattered into the loss cone, are subject to only poor mirror confinement. The often colliding heavier and cold ions are nearly not affected by the magnetic field [19]. ECR heating is particularly well suited for mirror confinement of a high-energy electron population, as the kinetic energy of the gyromotion perpendicular to the magnetic field is increased, the heated electrons will be kept in the plasma (see fig.1.3.1). The loss rate of these low energy electrons is higher than for the much slower, heavier ions, resulting in a positive plasma potential. The loss cone is modified according to this potential. [27]:

$$\frac{1}{\sin^2 \alpha_{eff}} = R - 2.e.(U_0 - U_{B_{MAX}}) / m_e v_{\perp} \quad (1.3.5)$$

Here U_0 ist the potential in the mid-plane of the mirror, $U_{B_{MAX}}$ the potential in the maximum of the mirror, e the charge of the electron and α_{eff} the modified loos-cone angel (see also formula 1.3.5 and fig. 1.3.1).

At the plasma core the hot electron density is high. The hot electrons have a low collision rate and their confinement time is much longer than the lower energy electrons in the plasma edge. The high density of hot electrons can produce a local negative potential in the centre of the trap, retaining the multiply charge ions and increasing their confinement time [19].

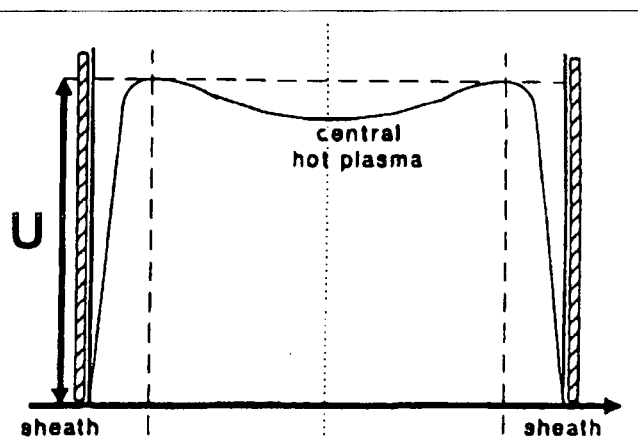


Figure 1.3.3 Plasma potential U along a cross-section perpendicular to the axis of a "minimum-B" field structure: The hot electrons create a small negative potential dip in the plasma-core, confining the cold ions. Due to collisions the cold electrons leak trough the loss cone. In order to maintain ambipolar loss flow, an ambipolar potential is created in the sheat [19].

The different ion charge states have therefore potential barriers of different value proportional to their charge. Thus differently charged ions have equal temperature but different potential barriers, thus different loss rates. The ions are predominantly heated via interaction with the hot electrons [19]:

$$\frac{dT_q}{dt} \propto \frac{n_e \cdot q^2}{m_{ion} \cdot \sqrt{T_e}} \cdot \ln \Lambda \quad (1.3.6)$$

T_q ... ion temperature; T_e ... electron temperature; m_{ion} ... mass of the ion; q ... charge of the ion; $\ln \Lambda$... Coulomb logarithm

Even if the heating is only weak, ions with higher charge are heated up more quickly, reaching higher kinetic energies, allowing them to leave the confinement by the electrostatic potential well more easily. Conversely, all possible mechanisms cooling the highly charged ions would raise their lifetimes and therefore the mean ion charge state in the plasma. Ion thermalization is due to elastic collision of the ions amongst each other. The collision frequency for the species i,k is [19]:

$$\nu_{ik} \propto \sum_{k=1}^q \frac{k^2 \cdot \ln \Lambda \cdot n_k \sqrt{A_i \cdot A_k}}{(A_k \cdot T_i + A_i \cdot T_k)} \quad (1.3.7)$$

where $A_{i,k}$ is the atomic mass and $T_{i,k}$ the temperature of the ion species i,k . In these collisions energy is transferred from the hotter, higher charged ion, to the cooler, less charged ion. The ions in lower charge state can due to their lower charge more easily leave the electrostatic potential well. This way energy of the multiply charged ions is transported out of the plasma via the ions in lower charge states.

Adding a lighter gas to the working gas of the ion source increases the ion confinement time, as the lighter gas reaches in the average a lower charge state and therefore cools the heavier, multiply charged ions, thus increasing their confinement time, and allowing them to reach even higher charge states. Additionally, the average charge of the plasma is reduced, also improving the ion confinement. Beside that, the ionization energy of the added gas plays an important role, which might explain why oxygen is such a most "mixing-gas" [33].

An empirical scaling law found by R.Geller [34,35] reflects the fact, that increasing the magnetic field strength and the mirror ratio gives a better confinement and thus a higher average ion charge state \bar{q} :

$$\bar{q} \propto \log\left(\frac{B_{\min} + B_{\max}}{2}\right)^{1.5} \quad (1.3.6)$$

Where B_{\min} is the minimum and B_{\max} the maximum magnet field of the mirror configuration. For the magnetic field-structure the following “optimum” values are found in literature [22]:

$$\frac{B_{INJ}}{B_{ECR}} \geq 2.5 \quad \frac{B_{EXTR}}{B_{ECR}} \approx 1.8 \quad \frac{B_{RMAX}}{B_{ECR}} \approx 2 \quad \frac{B_{MIN}}{B_{ECR}} \approx 0.8 \quad (1.3.7)$$

B_{INJ} ... magnetic field at the maximum closer to the microwave/gas injection side

B_{ECR} ... magnetic field at the ECR resonance zone

B_{EXTR} ... maximum magnetic field at the maximum closer to the extraction side

B_{RMAX} ... maximum radial magnetic field (or field at the last closed flux surface)

Here, the “ECR-zone” and not so much the minimum of the magnetic field is considered, which is justified insofar, as the plasma density is higher near the “ECR-zone” (see also fig. 1.4.3).

With nowadays available permanent magnet alloys, which have a remanence in the range of one Tesla, operation at 14 GHz ($B_{ECR} \approx 0.5$ Tesla) is somehow an upper limit for building an all permanent magnet system according to these requirements.

The overall positive plasma potential, which has been measured to be in the order of magnitude of 10 V to 40 V, reduces the ion confinement time [28]. Therefore many methods to improve the performance of the ion source aim at lowering the plasma potential. This may be achieved by providing electrons to the plasma, not only reducing the plasma potential, but also compensating the (cold) electron losses. A higher electron density allows operation at lower neutral-gas pressure and lower microwave power.

Using plasma chamber wall materials with high secondary electron emission is a very efficient method to provide cold electrons [29,30]. Also, the sputtering of the plasma chamber wall is reduced this way. Materials like SiO_2 , ThO_2 , Al_2O_3 or Al, which may be covered by an oxide layer, have been successfully used to improve the multiply charged ion production.

Early ECR ion sources were operating with two plasma stages, where it has been found that the predominant function of the first stage was to provide additional electrons to the second stage [31,32].

In nowadays used ECR ion sources the first stage has been replaced by a negatively biased electrode at the microwave injection side [31,32]. Here, not so much the secondary electrons, but reflection of electrons back into the plasma is the dominant mechanism to influence the plasma potential. In ECR plasmas electrons predominantly diffuse along the magnetic field lines, whereas ions dominate the radial losses. Compensating currents in the plasma-chamber wall, so-called "Simon-currents" can be influenced by such an electrode thus forcing the plasma to a modified diffusion regime which increases radial confinement [36,37].

Ions with higher charge states can not be so easily extracted from the core plasma. When the microwave power is switched off, the then cooling down electrons are not so well confined anymore, reducing the electron density (in the plasma core). Operating the microwave heating in pulsed operation ions may be released from the core plasma. The steady state of the plasma is replaced by this so-called pulsed "after-glow" regime [19], where because of the loss of electrostatic confinement by the electrons the ions are released from the core plasma.

1.4 ECR Heating

A large flux of fast electrons is needed to produce a significant density of multiply charged ions. Electron cyclotron resonance heating (ECRH) is a very efficient way to generate such hot electrons for which energies of up to 1 MeV have been observed [21]. Although inelastic collisions are essential to the avalanche process sustaining the plasma, at low gas pressure they contribute only weakly to the electromagnetic absorption. Collisionless absorption of electromagnetic waves from a resonant wave-particle interaction will damp the wave [19].

The electrons of the plasma gyrate around the magnetic field with the electron cyclotron frequency:

$$\omega_{CE} = \frac{e \cdot B}{m_e} \quad (1.4.1)$$

The right-handed circularly polarized component of an electromagnetic wave is absorbed in regions, where the frequency of the gyromotion of the electrons, which is a function of the magnetic field, coincides with the frequency of the electromagnetic wave.

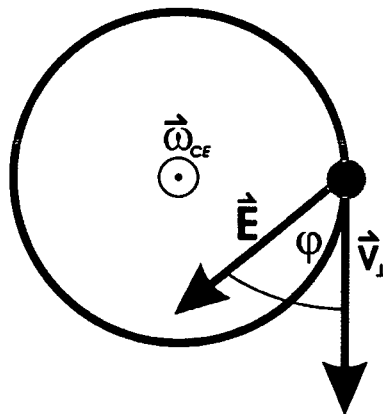


Fig. 1.4.1 \vec{E} is the electric field of an right-handed circularly polarized electromagnetic wave rotating with the same frequency $\bar{\omega}_{CE}$ (pointing to the reader) as the electron gyrating with the velocity \bar{v}_\perp perpendicular to the magnetic field.

If the gyrovelocity of the electron is synchronized with the electromagnetic field and the phase between them is fixed and favourable for acceleration, the electron is speeding up, thus absorbing energy from the electromagnetic wave. The region, where the criterion for such an absorption is met, is called “ECR-zone”.

Generally, four modes of propagation have to be distinguished for electromagnetic waves propagating in a magnetized plasma: The right- and left-handed circularly polarized modes for electromagnetic waves propagating parallel to the static magnetic field, and the ordinary- and the elliptically polarized extraordinary mode for electromagnetic waves propagating perpendicular to the magnetic field (see fig. 1.4.1). The dispersion diagrams for the different modes, base on the so-called “cold-plasma” model, are given in fig. 1.4.2. Although based on the approximation of the “cold-plasma” model (as described in plasma physics books like: [23,24]), the here given dispersion relations allow to investigate the cutoffs and resonances of the different propagation modes.

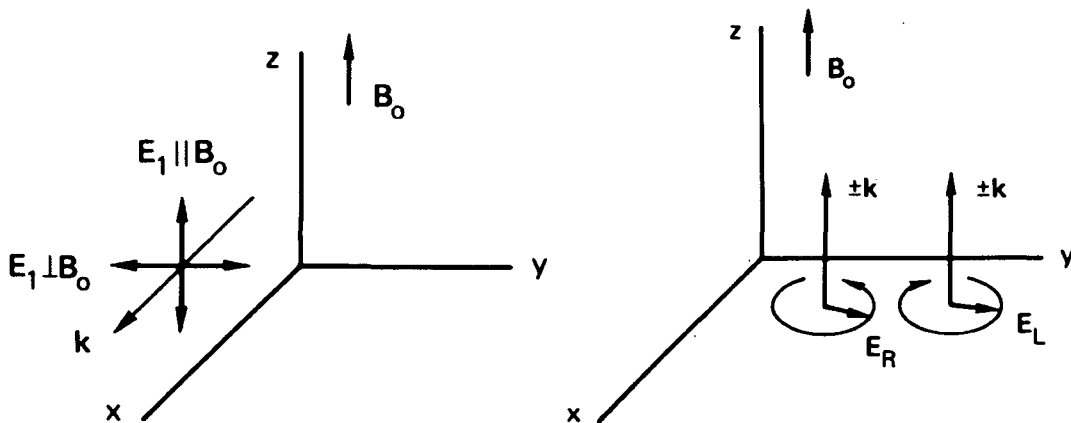


Fig. 1.4.1: Geometry for electromagnetic waves propagating in a magnetized plasma. (static magnetic field B_0).

Left diagram: wave-vector k perpendicular to B_0 :

extraordinary wave: electric field E_1 perp. to B_0 ; ordinary wave: E_1 parallel to B_0 .

Right diagram: wave-vector k parallel to B_0 :

right- (E_R) and left-handed (E_L) circularly polarized waves [24].

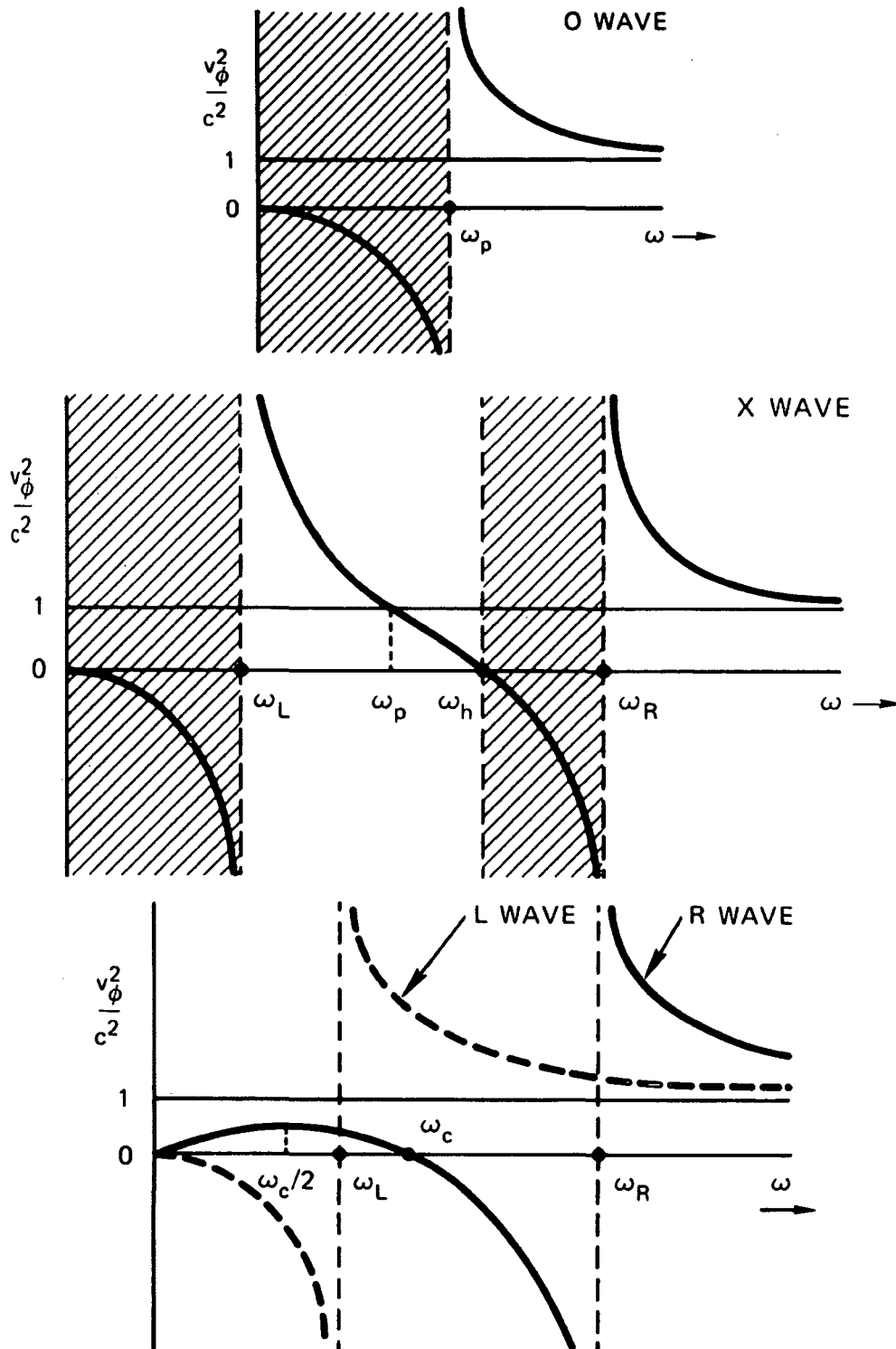


Figure 1.4.2: Dispersion diagrams (from top to bottom) for the ordinary (O-WAVE), extraordinary (X-WAVE) and the right- and left-handed circularly polarized (R & L WAVE) electromagnetic waves [24].

The ordinary wave is not affected by the magnetic field. The dispersion relation is the same as for an electromagnetic waves propagating in a plasma without magnetic field:

$$n = \frac{c^2 k^2}{\omega^2} = \frac{c^2}{v_\phi^2} = 1 - \frac{\omega_p^2}{\omega^2} \quad (1.4.2)$$

where n is the refractive index, c the speed of light, k the wave-number, ω the frequency, v_ϕ the phase velocity and the plasma frequency $\omega_p = e \sqrt{\frac{n_e}{\epsilon_0 m}}$.

For the extraordinary waves a resonance is found at the upper hybrid frequency ω_{UH} which is defined as:

$$\omega_{UH}^2 = \omega_p^2 + \omega_{CE}^2 \quad (1.4.3)$$

The extraordinary waves has two cutoffs at ω_R and ω_L : (+ for ω_R ; - for ω_L):

$$\omega_{R,L} = \frac{1}{2} \left(\pm \omega_{CE} + \sqrt{(\omega_{CE}^2 + 4\omega_p^2)} \right) \quad (1.4.4)$$

The cutoffs and the resonance divide the dispersion diagram in the following regions:

The phase velocity increases until ω_R is reached, where v_ϕ becomes infinite. Between ω_R and ω_L the phase velocity is negative, no propagation is possible. At the resonance $\omega = \omega_{UH}$ the phase velocity is zero. The phase velocity is slower than the speed of light for regions where ω is larger than ω_p .

The dispersion relation for right- and left handed circularly polarized waves is (+ for L-wave; - for R-wave):

$$n = \frac{c^2 k^2}{\omega^2} = \frac{c^2}{v_\phi^2} = 1 - \frac{\omega_p^2 / \omega^2}{1 \pm (\omega_{CE} / \omega)} \quad (1.4.5)$$

For the right handed polarized wave, there is a resonance at the electron cyclotron resonance ω_{CE} . The cutoffs for electromagnetic waves propagating parallel to the static magnetic field are the same as for the extraordinary wave, where the right handed polarized wave has the higher cutoff at ω_R . The left handed polarized wave behaves like the ordinary wave, except that the cutoff occurs at ω_L . The right hand polarized wave has a stop-band between ω_c and ω_R but there is a second band of propagation with a phase velocity below the speed of light below ω_{CE} . The wave in this lower region is called the "whistler-mode".

In this model, only right handed circularly polarized waves and extraordinary waves can transfer energy to the electrons via the electron cyclotron or the upper hybrid resonance. In most ECR ion sources the microwaves are coupled axially to the plasma, which means more or less parallel to the magnetic field to the plasma. Travelling in a region of decreasing magnetic field towards the “ECR zone”, the right-handed circularly polarized “whistler-mode” is the important mode for heating the plasma via electron cyclotron resonance. However the other components of the emitted microwave may well be converted into partly extraordinary or right-handed circularly polarized waves after some reflections in the plasma vessel. Also, the incident electromagnetic wave may be converted to other plasma oscillation modes via nonlinear processes. This way, most of the wave energy will be finally absorbed. Therefore it is not necessary to preselect the wave mode to generate an ECR plasma.

Even if the idea of ECRH is rather simple, it is very difficult to obtain a quantitative description of the wave absorption. The principal reason is that the electrons behave non-uniquely during resonance zone crossing. Their acceleration is strongly dependent on the phase difference between the electron cyclotron motion and the circularly polarized electromagnetic field. Moreover the favourable phase difference is not fixed. Those electrons with correct phase relative to the electric field will continuously gain energy. Since the energy change is the force multiplied by distance, the accelerated electrons gain more energy per unit time than the decelerated electrons lose. There is therefore a net gain of energy, at the expense of the wave energy, and the wave is damped.

In a “minimum-B” configuration the condition for ECR absorption is fulfilled on a closed surface, the “ECR-surface”. Good confinement of the hot electrons allows several passes of the resonance zone, thus enabling the electrons to reach relativistic energies.

Different circumstances limit the electron energy. An electron does not remain permanently in the “ECR zone”. The time the electron spends there is limited, because the magnetic field is generally not homogenous, and the ECR is in a region of a magnetic field gradient which limits the transit time of the electron. This is why the final energy of the electron depends on the gradient of the magnetic field [19]. As ions are predominantly produced near the (hot) “ECR-zone”, an “ECR-zone” near the axis,

in a region of a not too steep magnetic field seems to be favourable [7]. This is achieved with a so-called “flat field” magnetic field structure. Fig. 1.4.3 shows the result of a simulations comparing such a structure with that of a “conventional” ECRIS. As can be seen much higher electron energy densities can be reached with such a “flat-field” structure, having an “ECR-zone” close to the axis, although the “ECR-zone” of the “flat-field” structure is smaller than for the “conventional” ECRIS.

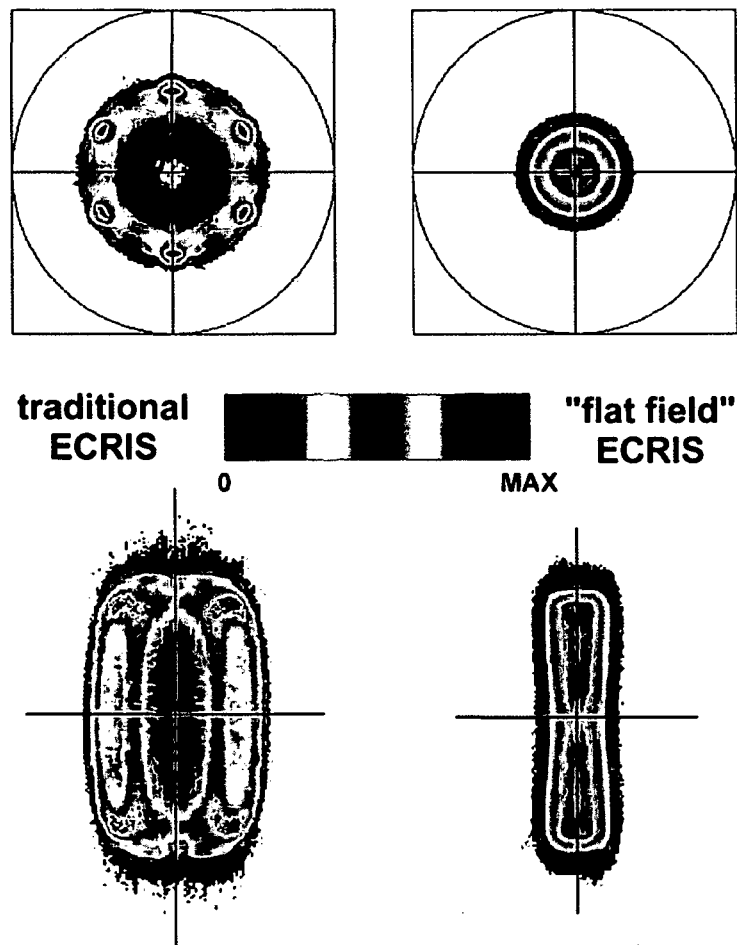


Figure 1.4.3: Simulation of the spatial electron energy distribution of a “traditional” and a “flat-field” ECRIS. (energy increased from (black) red to blue) Note the high-energy region at the centre of the flat-field configuration [39].

An upper bound for the useful plasma density that can be achieved in ECR ion sources is the critical density. Measurements of plasma densities in ECR ion sources have shown that the hot electron population makes up roughly 10% of the total electron density,

which can be close to the critical density [39]. Therefore the use of higher frequencies seems the only practical way to reach higher plasma densities in ECR ion sources

For hot electrons when the classical diffusion becomes absolutely negligible and when no turbulence appears RF diffusion might dominate the loss mechanism [19]. As a result there is a maximum power density for each ECR source, that can be coupled in and a maximum plasma density, typically lower than the cut-off density, that can be achieved before instabilities begin to inhibit the high charge state performance. This limit increases with the frequency of the microwave and the strength of the magnetic field.

As for the magnetic field, empirical scaling laws for the dependence on the microwave frequency can be given [34,35]: Operating with higher magnetic fields is not only improving the confinement, but allows to use microwaves of higher frequency. For a similar magnetic field configuration (same mirror ratio) the average charge state and the extractable ion currents are changing according to the followings empirical scaling-laws [19]:

$$\bar{q} \propto \log \omega^{3.5} \quad (1.4.6)$$

$$I_q \propto \omega^2 \cdot M^a \quad (1.4.7)$$

So, for a change from 5 GHz (“BERTA”) to 14 GHz microwave frequency (“SOPHIE”) a substantial increase of the extracted currents, and the average charge state could be expected. Also, it becomes clear, why the microwave-frequency is a very sensitive parameter: Changing the frequency does not only change the efficiency for coupling the microwaves to the plasma chamber cavity and the position of the “ECR-zone”, but also the efficiency of the heating mechanism. To prevent nonlinear phenomena, the injected microwave power should stay below 1 W/cm³. In this range the mean charge state scales with the microwave power P according to [19]:

$$\bar{q} \propto P^{1/3} \quad (1.4.8)$$

For a compact ECRIS like “SOPHIE”, the applied 200 W microwave amplifier should therefore be more than sufficient, even with a very inefficient microwave transmission system.

1.5 Ion Extraction

Ion extraction from a plasma and ion beam formation is done by the extraction system. The simplest type is a diode system consisting of a plasma electrode at positive ion source potential and an extraction or ground electrode at ground potential (fig. 1.5.1.). The emission surface of the ions at the plasma boundary is called plasma meniscus. Its shape depends on the parameters of the plasma, the extraction voltage, the magnetic field in the extraction region and the shape of the electrodes.

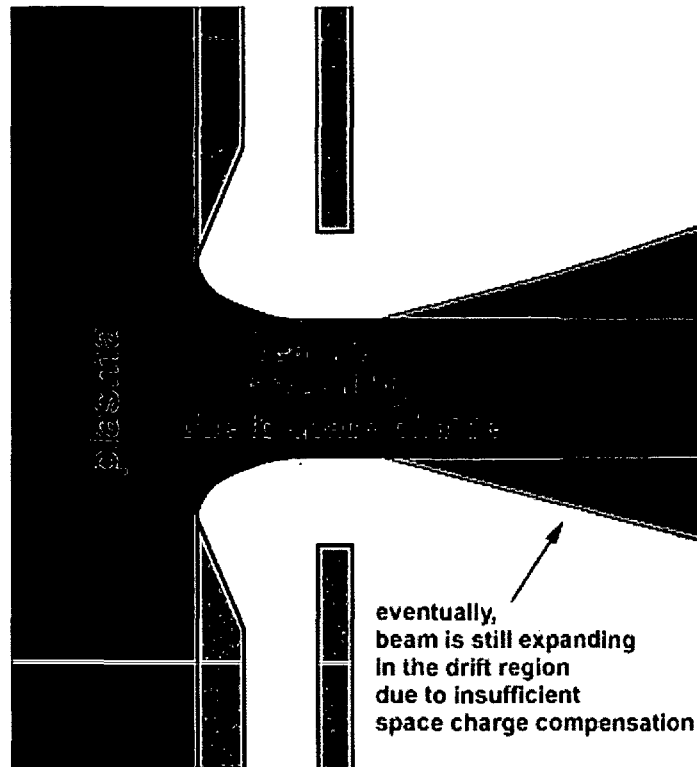


Fig. 1.5.1: Scheme of a diode extraction system. The concave shape of the plasma-meniscus and the stray-field of the extraction electrode counteract the blow-up of the beam due to space-charge.

An ideal plasma is an equipotential region. When the plasma stays in contact with an electrode held at different potential, a sheath is formed, and the whole potential difference between the plasma and the electrode is localized within this sheath. Electrons

emitted from the plasma are reflected at this boundary if their energy is less than the potential drop between these two electrodes. The extracted current is either limited by space charge or by the current density the plasma can provide. The Child-Langmuir law gives the extractable current density j_{SC} , assuming a plane emission area, and zero initial energy of the ions [20]:

$$j_{SC} = \frac{4}{9} \epsilon_0 \sqrt{\frac{2.e.q}{m}} \cdot \frac{1}{d^2} \cdot U^{\frac{3}{2}} \quad (1.5.1)$$

where d is the “extraction-gap”, the distance between the two electrodes, and U the potential difference. The current density j_{PE} which the plasma can provide is given by the Bohm criterion [19]:

$$j_{PE} = q.n_i \sqrt{\left(\frac{k.T_e}{m_i}\right)} \quad (1.5.2)$$

Multiplying 1.5.1 with the area of the emitting surface, we can define the perveance P of an ion beam with the total extracted current I as:

$$P = \frac{I}{U^{\frac{3}{2}}} \quad (1.5.3)$$

The shape of the plasma meniscus reflects the condition, that the emitted current density has to be equal to the space charge limited current density. The distance between meniscus and extraction electrode adjusts in such a way, that the electric field at the meniscus is zero. If the plasma density is too low, a concave meniscus is formed. If the density is too high, the meniscus is plane or even convex (see fig. 1.5.2).

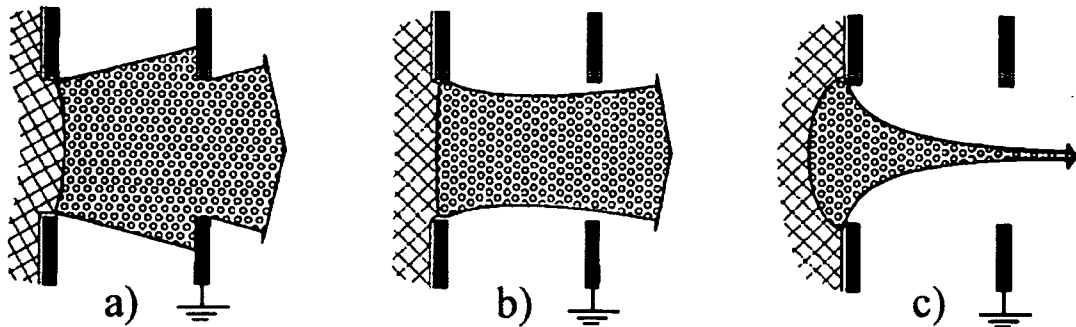


Fig. 1.5.2: Plasma meniscus for $j_{PE} > j_{SC}$ (a), $j_{PE} = j_{SC}$ (a) and $j_{PE} < j_{SC}$ (c) [40].

To obtain a least divergent ion beam for a given plasma density, the voltage or the extraction gap have to be adjusted according to 1.5.1. with $j_{PE} = j_{SC}$. This condition is called “perveance-match”. To obtain a parallel ion beam, compensation of the ion-beam space charge is crucial.

Two processes are responsible for the passive production of space charge neutralizing particles: Collisions of ions of the primary beam with residual gas atoms and ion hitting a surface inducing electron emission [20].

Particles of a charged beam drifting in a vacuum chamber will collide with residual gas atoms or molecules. Depending on the specific condition of the collision, the residual gas atoms can be ionized. In the case of a positive primary beam secondary ion in the beam will be repelled by the space charge whereas the electron will be trapped. If the ions of the primary beam hit a metallic surface, secondary particles are created. Again, for a positive ion beam, electrons will be trapped in the space charge potential well, whereas positive particles will be repelled. The cross section for ion induced electron emission from surfaces is huge compared to the cross section for residual ionization.

The electrons generated in the extraction region of the diode are accelerated towards the plasma. Therefore these electrons can not contribute to the space charge compensation of the beam behind the extraction electrode. Without space charge compensation of the ion beam the divergence angle increases rapidly after extraction. Therefore a third electrode, the so-called suppressor electrode, is placed between the plasma electrode and the extraction electrode. Fig. 1.5.2 shows a scheme of such an triode “Accel-Decel” extraction system [20].

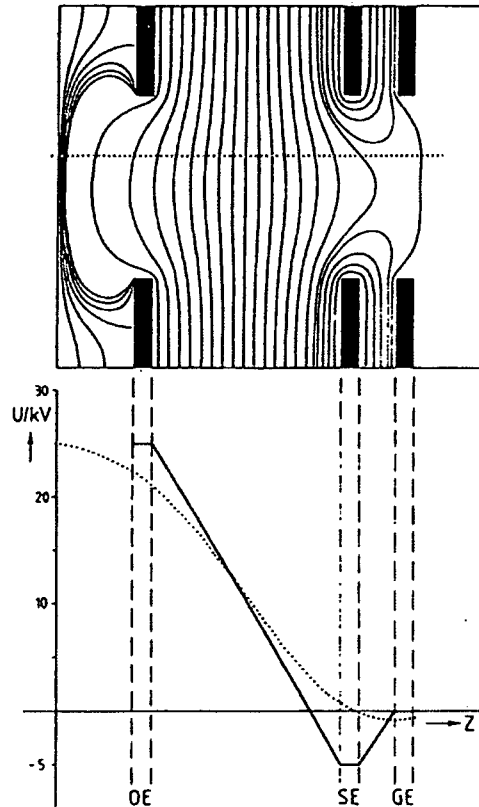


Fig. 1.5.3 Scheme of an "Accel-Decel" Extraction system. The potential with (dashed line) and without ion beam (full line) is given along the symmetry-axis of the system [39].

Biased at negative potential, the suppressor electrode gives rise to a potential barrier for the electrons. Electrons generated in the ion beam have energies of a few eV up to a few tens of eV, so a barrier of -100 V on the axis is high enough in most cases to stop the electrons.

An important quantity to characterize an ensemble of beam trajectories is the beam emittance [20]. The multidimensional distribution function ρ of a particle in the ion beam can be written as:

$$\rho = \rho(x, y, z, p_x, p_y, p_z, t) \quad (1.5.3)$$

where, x, y, z are the coordinates in space, p_x, p_y, p_z the momenta in the x, y, z direction and t the time.

In the stationary case the time can be replaced by the position z . In the case of a momentum in z -direction being much greater than in the transverse directions, the radial momenta can be replaced by the angles x', y' :

$$x' = \frac{p_x}{p_z}; y' = \frac{p_y}{p_z} \quad (1.5.4)$$

The emittances ϵ_x and ϵ_y are defined as the smallest area in the $x-x', y-y'$ plane which contains all trajectories divided by π . In the presence of conservative forces only, the emittance is constant along the beam. It is common to match the emittance to an ellipse (see fig.1.5.4):

$$\epsilon = \gamma \cdot x^2 + 2 \cdot \alpha \cdot x \cdot x' + \beta \cdot x'^2; \quad \beta \cdot \gamma - \alpha^2 = 1 \quad (1.5.5)$$

A long vertical, narrow emittance ellipse corresponds to a small spot with large divergence, a horizontal ellipse enclosing only points with small x' represents a large diameter, parallel beam. Due to aberrations, the extremities of the emittance diagram might be twisted around, making it impossible to refocus the beam.

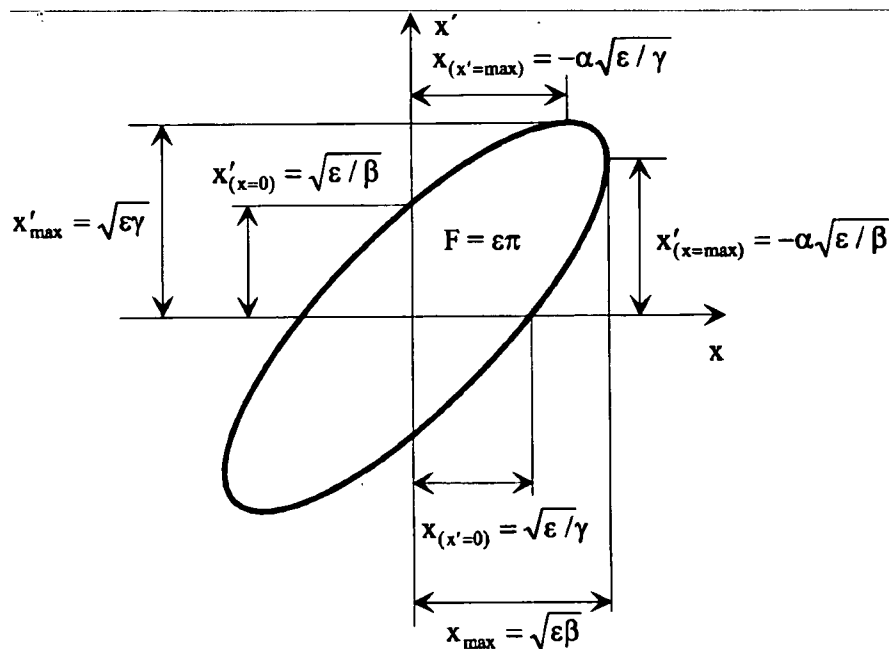


Fig. 1.5.4: The emittance ellipse [19].

For comparison of different ion sources, considering the intensity of the ion beam, the commonly used brightness should also be mentioned, indicating the ion current I normalized by the emittances of the two-dimensional sub-spaces.

$$B = \frac{I}{\varepsilon_x \cdot \varepsilon_y} \quad (1.5.6)$$

Extraction from ECR-plasmas is characterized by a not uniform plasma density across the meniscus, reflecting the (for hexapoles triangular) shape of the drift surfaces, the magnetic field in the extraction- and drift region and the different ion charge state components of the total extracted current. Generally, the emittance of an ECR ion source is dominated by the magnetic field. The by the hexapole field caused inhomogenous plasma density at the plasma meniscus causes electrostatic fields pointing to the maxima of the density distribution, which, together with the magnetic field cause emittance growth. It has been found experimentally, that the emittance decreases for higher charge states, reflecting the ion distribution in the plasma.

2. The 14.5 GHz ECR Ion Source SOPHIE

The compact, low cost 14.5 GHz ECR ion source “SOPHIE” (**S**ource for **P**roduction of **H**ighly charged **I**ons using **E**CR) was developed in co-operation between the Vienna University of Technology and the Justus-Liebig University in Gießen. The design has been based on the 10 GHz all permanent magnet ECRIS type developed in Gießen. [5-12] A schematic view of the ion source “SOPHIE” is shown in fig. 2.1.

The magnetic field configuration for confining the plasma is provided by four permanent magnet rings and a Halbach-type hexapole. Microwaves with a total power of up to 200 W in the frequency range of 12.75 to 14.5 GHz are transmitted from the microwave system at ground potential through a PTFE window into the water cooled 25 mm diameter plasma chamber. The waveguide coupling system is also used as biased electrode. An aluminium liner enhances the production of highly charged ions. The plasma chamber may be evacuated by a small turbomolecular pump at ground potential through an insulating break, and it can be shifted along the magnetic axis. The triode “Accel-Decel” extraction system permits ion acceleration voltages between 1 and 10 kV. Two gas inlet valves, connected via an insulating break, permit operation in the gas-mixing mode.

“SOPHIE” was a pioneering subpart within the LEIF project, allowing all parameters of the ion source to be controlled remotely by using the LabVIEW based programme “CODIAN” developed by J. Bundesmann at the Hahn-Meitner Institute in Berlin, with a VNC client/server software [14-17].

Large parts of standardized components in the design of “SOPHIE” resulted in low equipments costs, easy maintainance and high reliability.

In September 2003 “SOPHIE” started routine operation. After extensive tests with various discharge gases “SOPHIE” is now routinely used for investigations with various slow multiply charged ion species. First results concerning the performance of this new ECR ion source are presented and discussed in chapter 2.6.

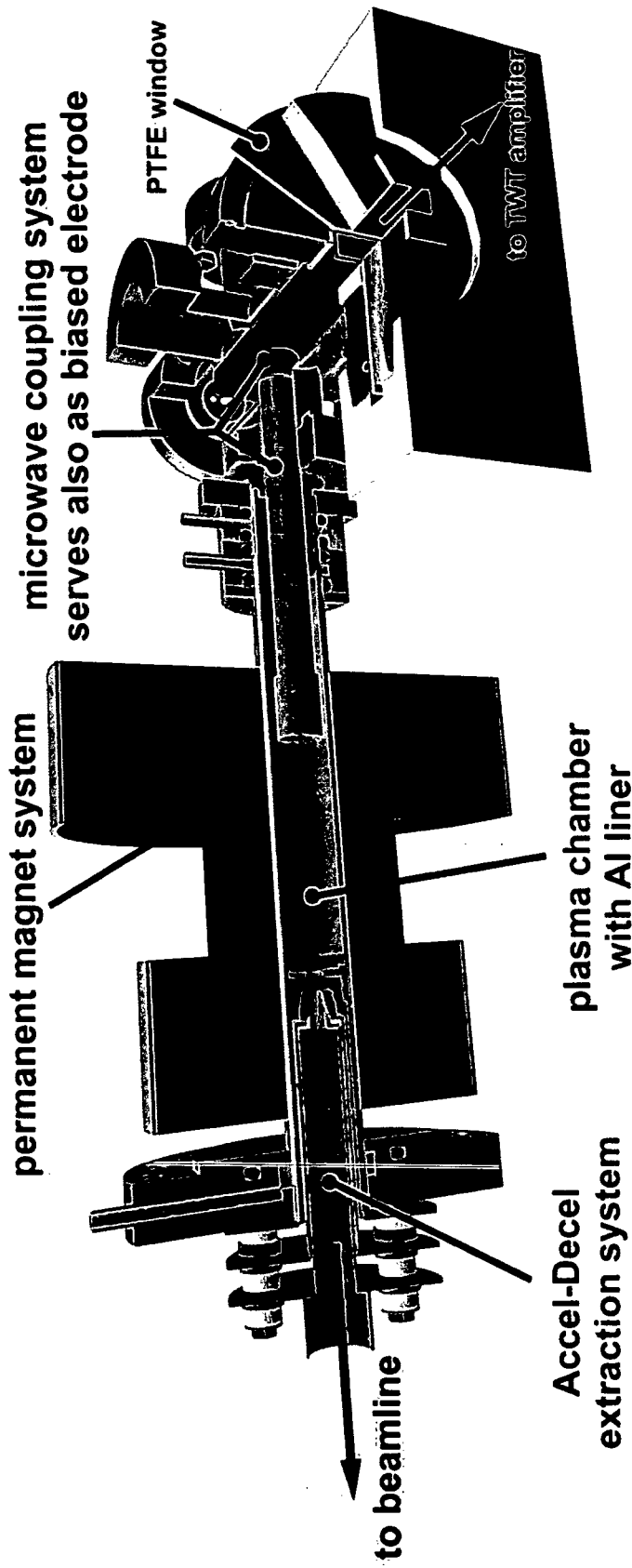


Figure 2.1: Cutaway view of the 14.5 GHz all permanent magnet ECRIS "SOPHIE" (total length app. 50 cm).

2.1 The Permanent Magnet System

The magnet system of “SOPHIE” is based on the design of the so called “high-B” 10 GHz Gießen-typ all permanent magnet ECRIS [5-12].

Two radially and two axially magnetized rings together with a Halbach type hexapole magnet [41] provide a “minimum-B” field structure within the plasma chamber.

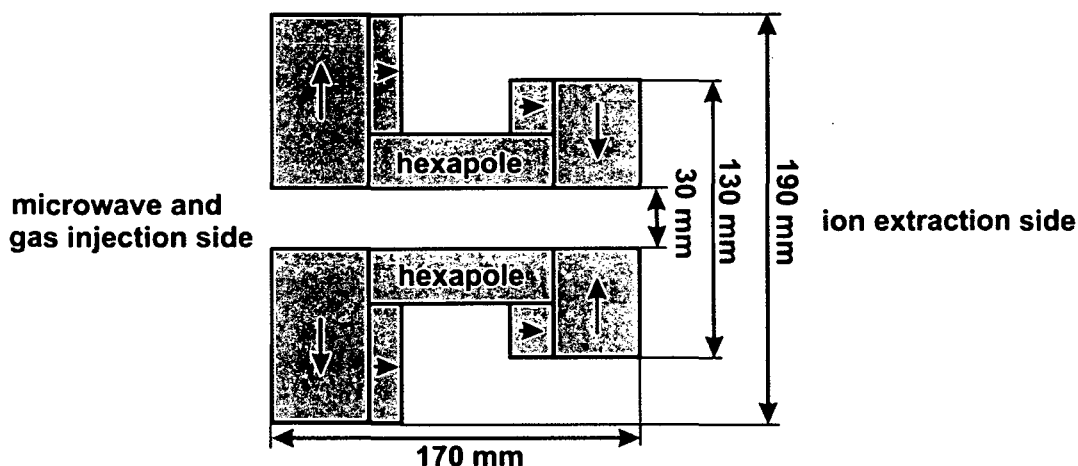


Figure 2.1.1: Schematic view of the permanent magnet system of “SOPHIE”.

The magnet system has been manufactured by VacuumSchmelze Hanau, Germany. The NdFeB alloy “VACODYM® 655 HR” chosen for this system belongs to a family of alloys known for their high energy density ($B \cdot H_{\max} = 315 \text{ kJ/m}^3$ for “VACODYM® 655HR”). It has been developed for applications where a high remanence (1.28 T for “VACODYM® 655 HR”) and a good thermal stability are required. Figure 2.1.2 shows typical demagnetization curves for the used alloy. With fields in the order of magnitude of one Tesla, the working point of the magnet can be in a region where it is already necessary to take precautions against demagnetization by heating up the magnet system.

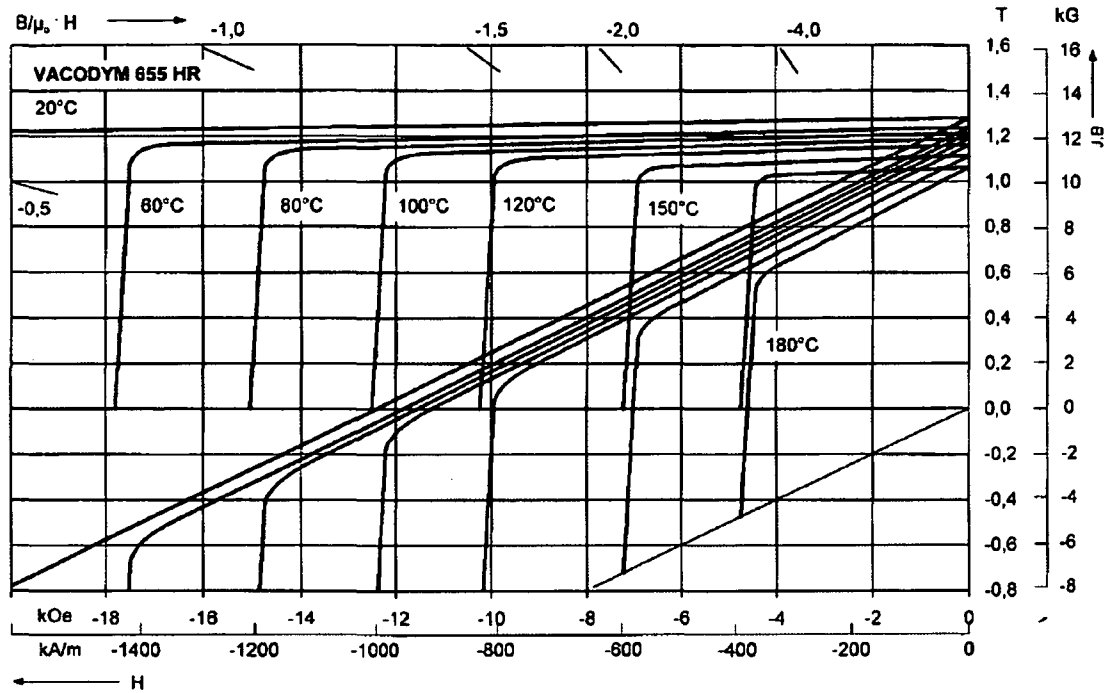


Figure 2.1.2: Typical demagnetization curves (magnetic field B [T] and magnetization J [T] vs. magnetizing field $B/\mu_0 H$ [T] or demagnetizing field H [kA/m]) at different temperatures for the alloy "VACODYM®655 HR" [42].

Calculations for the design of the magnet system have been done with the program "PANDIRA" [43], part of the "SUPERFISH" group of codes maintained and distributed by the Los Alamos Accelerator Code Group. "PANDIRA" provides static magnetic fields in two Cartesian dimensions or cylindrically-symmetric configurations in three dimensions. The code solves ferroelectric problems and handles permanent magnet materials as well as permeable iron components and current-carrying coils. Figure 2.1.3 shows results of such calculations. Calculations for the longitudinal field provided by the four ring magnets and the radial field from the Halbach type hexapole have been done separately. The results have been verified for different boundary conditions and different mesh size, showing only small differences in the outer part of the calculated region.

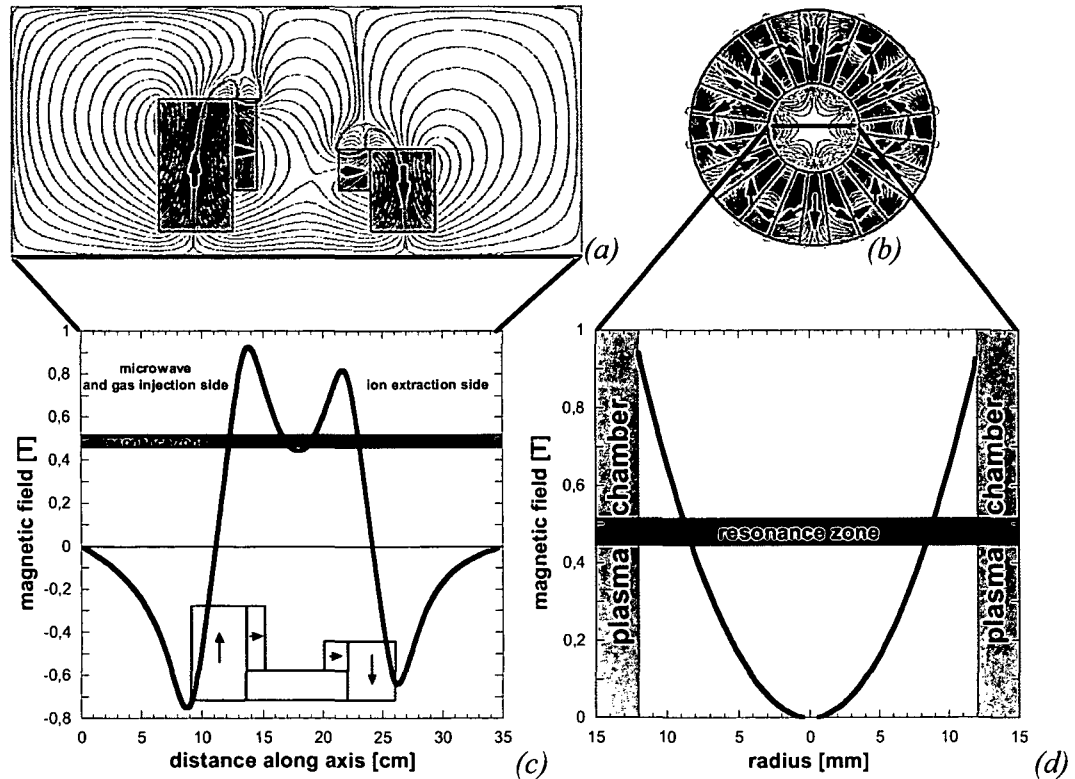


Figure 2.1.3 Longitudinal (a,c) and radial (b,d) magnetic field of “SOPHIE” permanent magnet system, calculated by “PANDIRA”. Figures (c,d) give the magnetic field (red line) along the axis and across the hexapole as indicated by the orange line in(a,b).

Figures 2.1.4 (a) to (e) show the dependence of the longitudinal and the radial magnetic field vs. the dimensions of the magnet system.

In order keep the magnet system as small as possible, the outer diameter of the plasma chamber has been chosen with 30 mm based on the Gießen ECRIS design.

Based on the experience with the “high-B” 10 GHz Gießen-type all-permanent magnet ECRIS, the geometry has been chosen for an axial mirror ratio of 2.1 at the microwave- and gas-injection side and 1.9 at the extraction side respectively. A concomitant requirement was the resonance zone to cover the frequency range of 12.75 GHz to 14.5 GHz. Based on [6,7,39] an “ECR-zone” close to the minimum of the magnetic mirror is favourable for efficient plasma heating and the extraction of multiply charge ions.

The radial field is provided by a so-called Halbach hexapole [41]. Such a configuration consists of 24 trapezoid-shaped magnets, where the magnetization is rotated for 45° with respect to its neighbouring elements. This way the field inside the hexapole is increasing, while there is nearly no radial stray field on the outside. To keep the resonance zone as far away as possible from the plasma chamber wall (at 12 mm radius) a comparably strong hexapole with an outer diameter of 80 mm has been chosen. As can be seen in figure 2.1.4, further increase of the outer radius of the hexapole would not have resulted in a higher field within the plasma chamber.

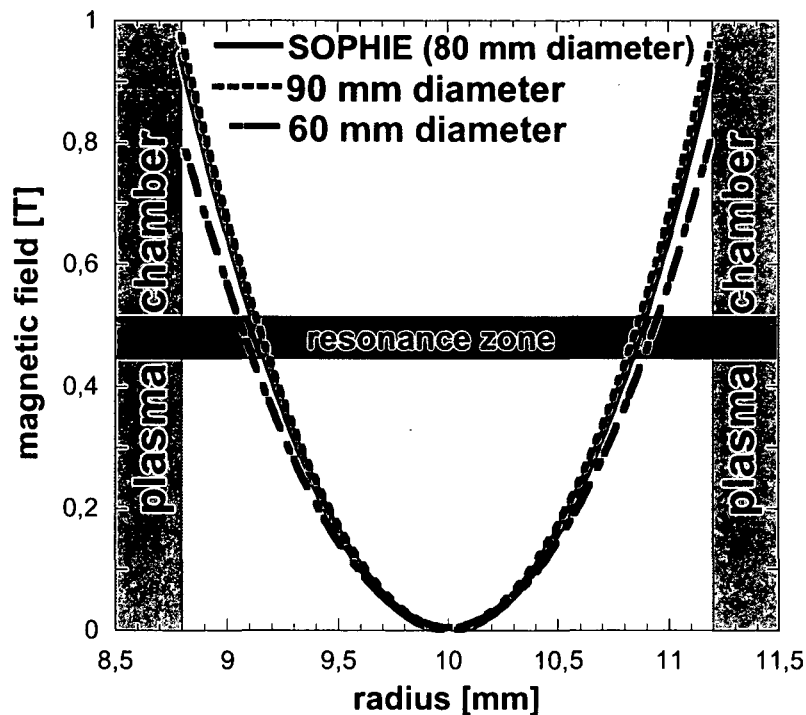


Fig. 2.1.4: Results of radial magnetic field calculations for different outer diameter of the Halbach hexapole. Red line for finally selected configuration.

Having define the outer diameter of the hexapole, the inner diameter of the axially magnetized rings has been fixed. These rings are very efficiently increasing the maxima of the axial field (see fig. 2.4.8).

The extraction region had to be kept as short as possible to minimize the distance for ions travelling across the narrow extraction system (distance from the maximum of the mirror field to the edge of the magnet system). Therefore the length of the radially

magnetized rings had to be kept as short as possible. Fig. 2.4.5 and 2.4.6 show the influence of the length and diameter of the radially magnetized rings on the axial field.

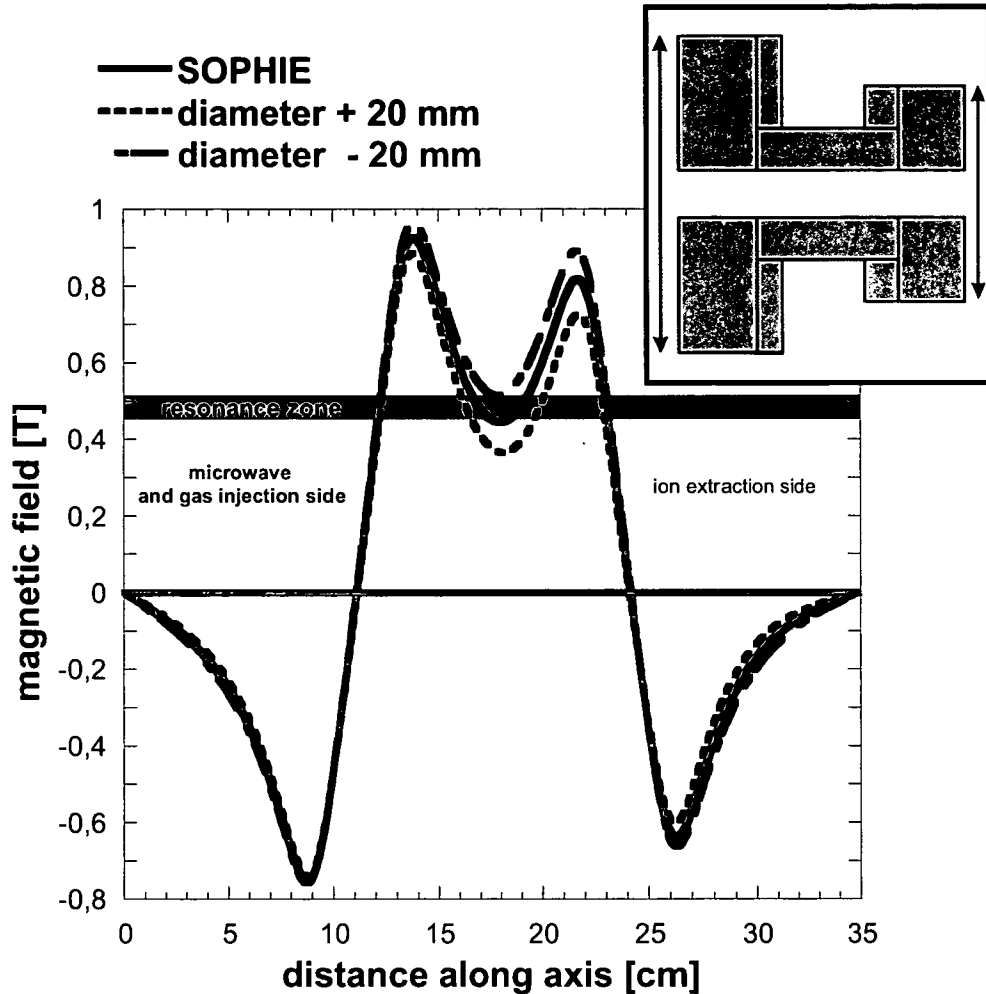


Fig 2.1.5: Variation of the diameter of the four rings providing the axial field. Red line for finally selected configuration.

As can be seen a strong increase of the diameter (of 20 mm), and thus of the volume of the system does not really increase the maximum at the injection side anymore. Comparing the variation of the rings at the injection side with the variation of the smaller ring at the extraction side, 190 mm seems to be a reasonable compromise for the required “mirror-ratio” and efficient material use.

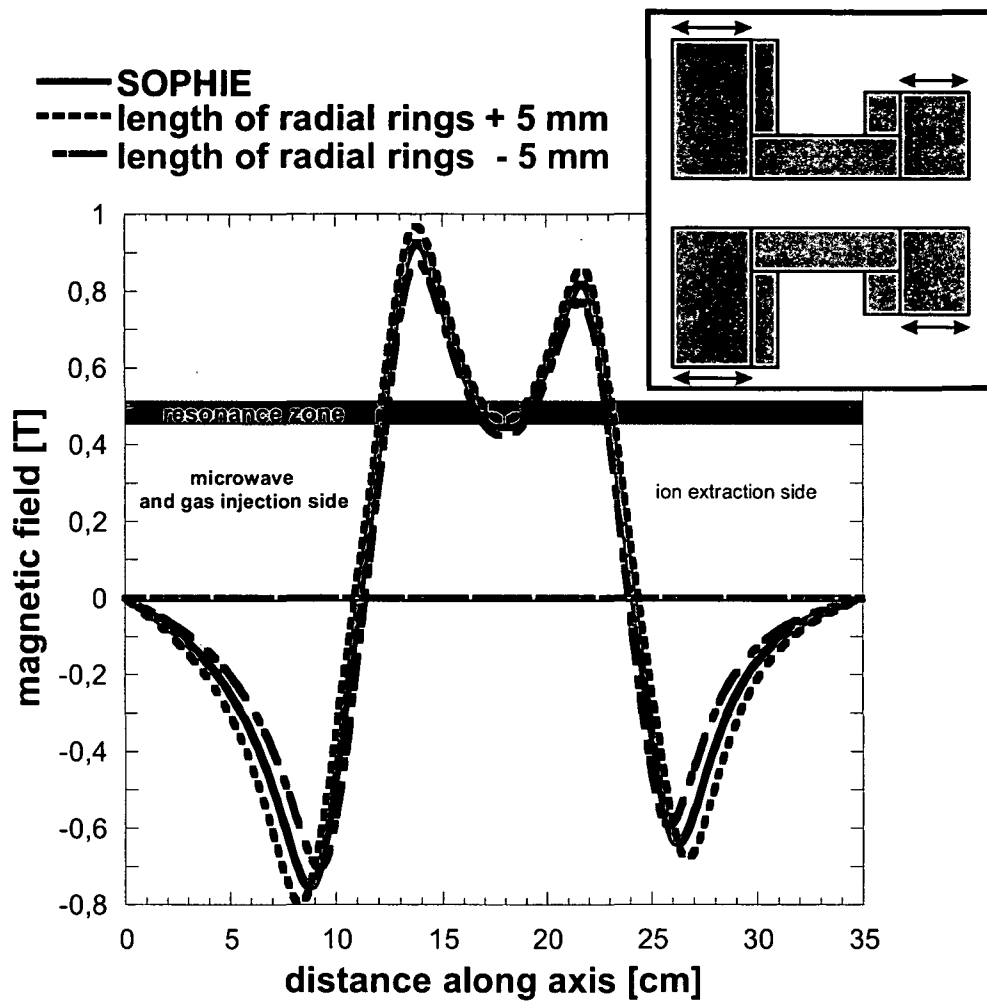


Fig 2.1.6: Variation of the length of the radially magnetized rings. Red line for finally selected configuration.

The length of the radially magnetized rings is the more efficient parameter to influence the maxima of the field. Nevertheless, the system had to be kept as short as possible, for an efficient extraction, high pumping speed and low system costs.

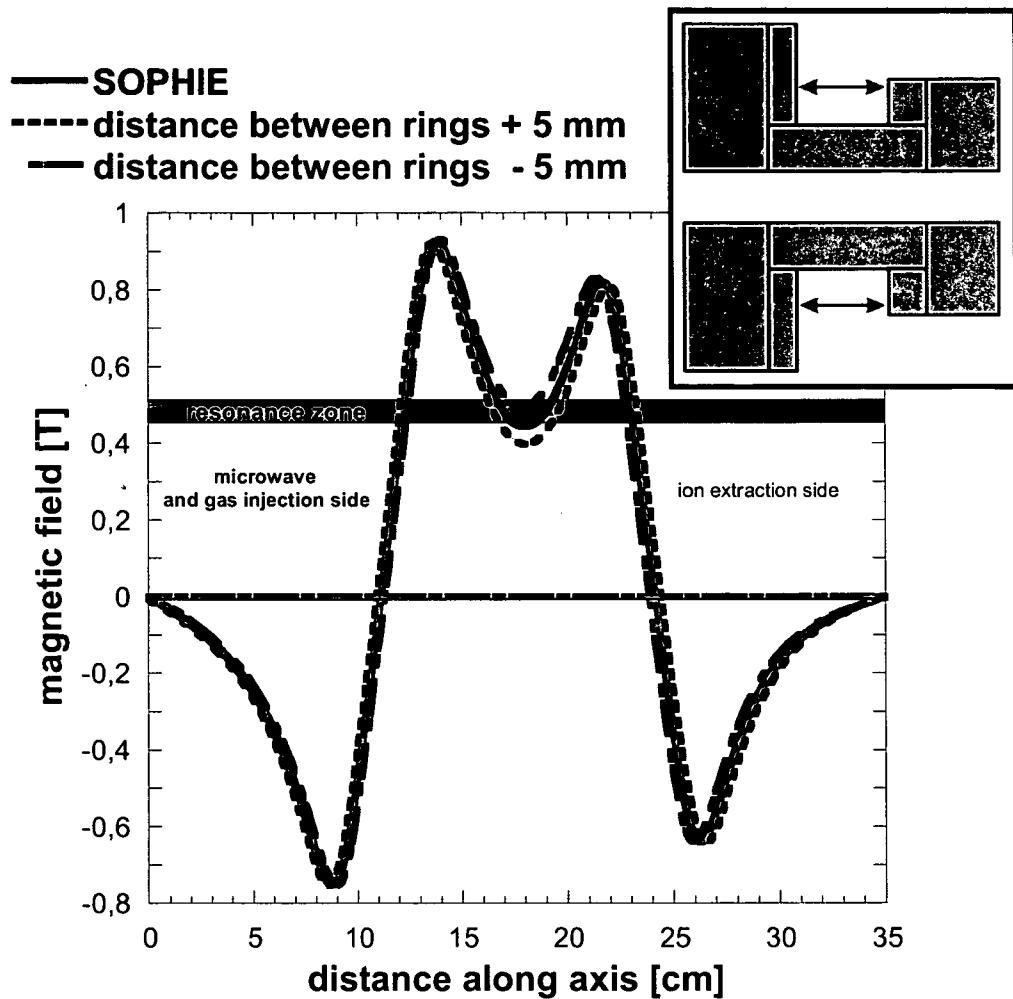


Fig 2.1.7: Variation of the distance between the rings providing the axial field. Red line for finally selected configuration.

The distance between the four ring magnets defines the depth of the minimum of the axial mirror field (and therefore the mirror-ratio). Here the position of the “ECR-zone” had to be considered: An “ECR-zone” close to the minimum is preferable, where at the same time a shorter distance, with a higher minimum, results in a shorter, (and therefore cheaper) hexapole. A small safety margin had to be included when moving the “ECR-zone” towards the minimum, in order to make sure a resonance-zone exists at all.

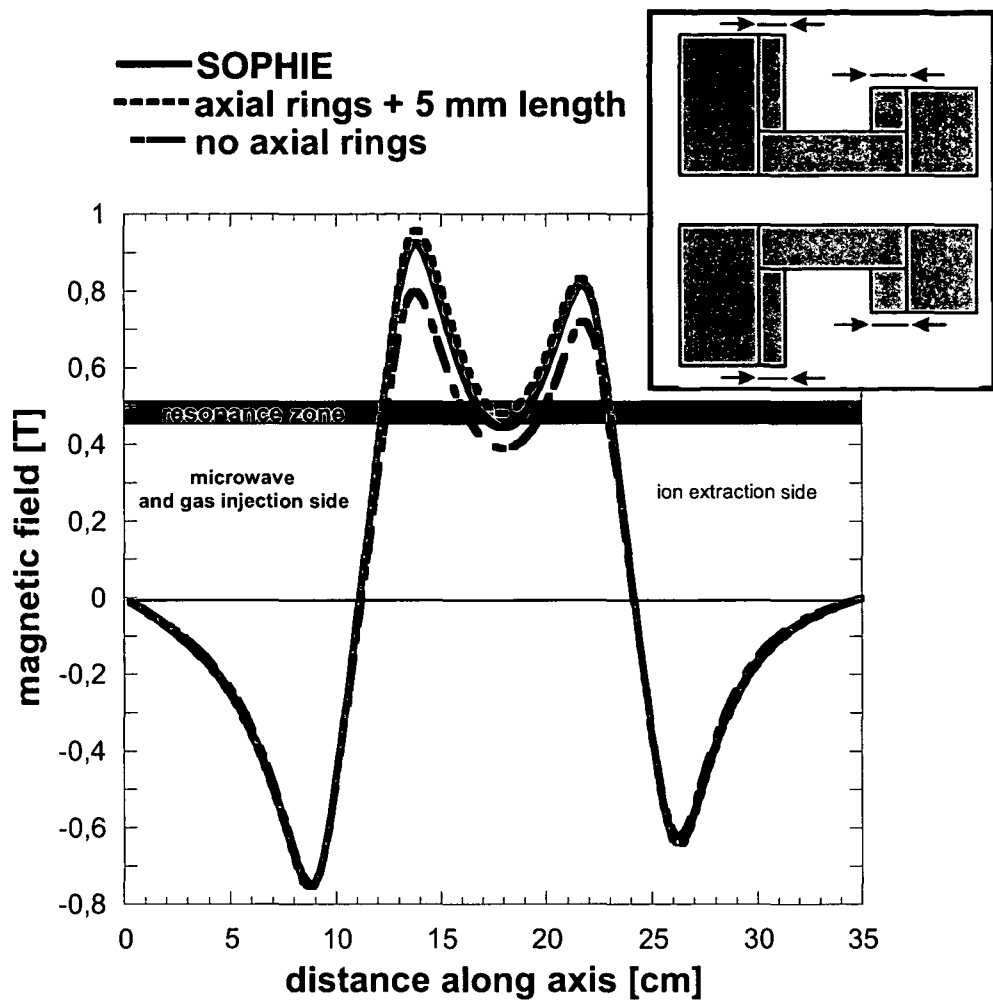


Fig 2.1.8: Influence of the axially magnetized rings on the the axial field. Red line for finally selected configuration, green line: no axially magnetized rings and blue, dashed line: longer rings.

The axially magnetized rings shift the whole field upwards, showing only a weak dependence on the length. A length close to the saturation value, where a further increase would not be reasonable, has been chosen.

2.2 The Plasma Discharge Chamber

“SOPHIE” is equipped with a water cooled stainless steel plasma chamber. An aluminium liner with an inner diameter of 24 mm, serves for enhancement of the production of highly charged ions. Fig. 2.2.1 shows a cutaway view of the plasma chamber of “SOPHIE” (see also fig. 2.1).

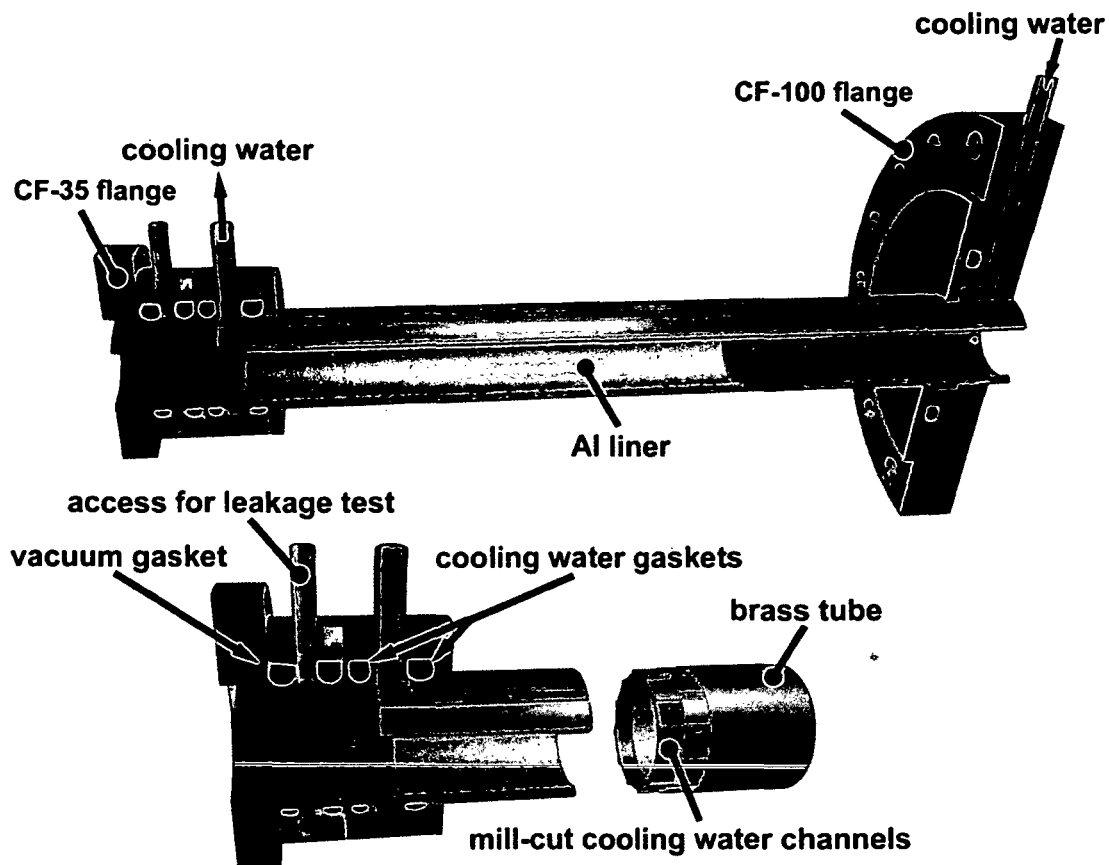


Figure 2.2.1 Cutaway view of the plasma chamber

A 280 mm long stainless steel tube with 25 mm inner diameter was welded into a modified CF-100 blank flange. In this manner not only the number of gaskets could be reduced, but also the extraction system is thereby kept as short as possible. A brass tube with 30 mm outer diameter covers the mill-cut channels for the cooling water. To use the full diameter of the permanent magnet system bore, while still allowing the removal

of the permanent magnet system, a system of Viton gaskets seals the plasma chamber at the injection side. This system of seals allows the introduction of helium to the site of the vacuum gasket for leakage testing or, if necessary, to facilitate differential pumping of the system. The transition to a standard CF-35 flange size permits connection of the plasma chamber to other standard CF components.

The dimension of the plasma-chamber has been defined by the 30 mm diameter bore of the previously described permanent-magnet system. Based on the Gießen design [5-12], where the dimension of the plasma-chamber has been chosen to just allow 10 GHz microwaves to propagate, it could safely be assumed that a plasma-chamber for 14 GHz operation could be built to fit nicely into a 30 mm bore. Fig. 2.2.2 shows the setup of the vacuum system of "SOPHIE".

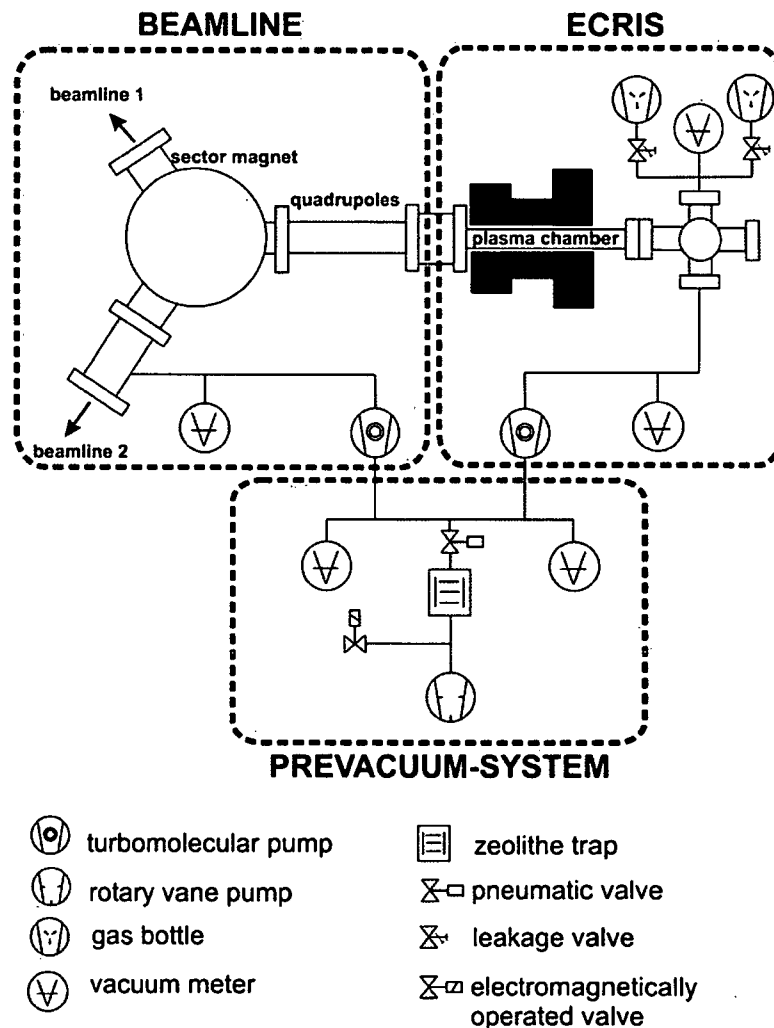


Figure 2.2.2 Scheme of the vacuum system of "SOPHIE".

At the injection side, a CF-35 six-way cross-piece is connected to the plasma chamber. It houses the microwave coupling system with the PTFE window and the feed-through for the biased voltage electrical connection. Atop of it there are two gas leakage valves and a Penning gauge, connected via a CF-35 ceramic insulator to allow their operation at ground potential. "Minican" bottles can be connected to the gas line of each leakage valve and a small rotary vane pump serves for evacuation of the gas lines when changing a gas bottle.

Two turbomolecular pumps are fitted below the six-way cross-piece (60 l/s) and one of the beamlines (240 l/s) to maintain vacuum. The latter is located at the beam-line to minimise the distance traversed by the extracted ions before separation. Both turbomolecular pumps are connected to one rotary-vane pump equipped with a zeolite trap. A pneumatic valve to isolate the prevacuum system from the plasma chamber and an electromagnetic valve for venting the chamber are controlled via the SPS interlock system.

2.3 The Microwave System

The main part of the microwave system is a 200 W Ku-Band compact travelling wave tube (TWT) amplifier VZU-6992EC by “Communication and Power Industries” (CPI, formerly known as “Varian”). The VZU-6992EC amplifier is a member of a comprehensive line of communication amplifiers, specifically designed for uplink service in satellite communication. It permits continuous operation in the range of 12.75 GHz to 14.5 GHz. The system incorporates a microprocessor control system, a solid state intermediate amplifier, input/output isolation circuits, input attenuator, RF detectors and an output harmonic filter. The maximum reflected power accepted by the built-in circulator is limited to 20 W only. Therefore an additional circulator together with an air cooled dummy load, capable of handling a reflected power of up to 200 W had to be installed, since during operation with “SOPHIE” constant reflected power well above 20 W might not be avoidable. A schematic view of the microwave system is given in fig. 2.3.1.

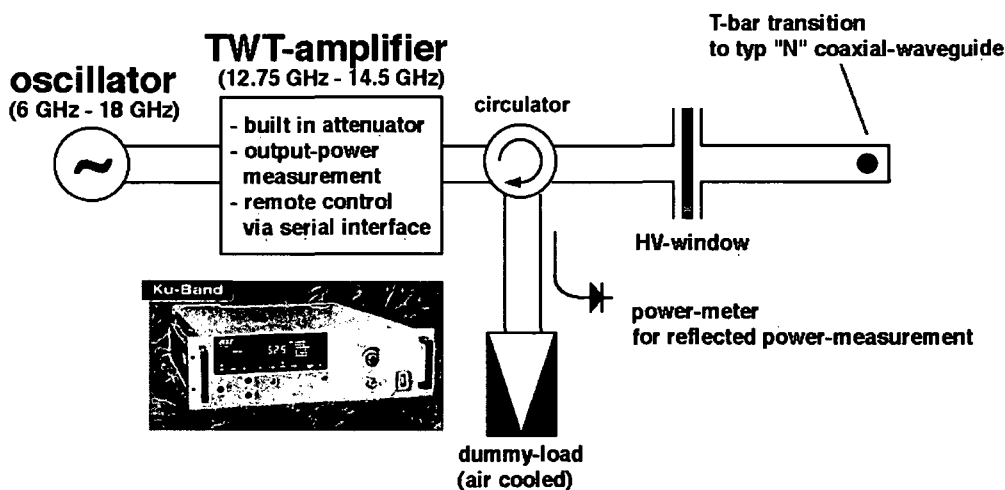


Figure 2.3.1: Scheme of the microwave system.

The microwave signal produced by an OMNIYIG 1518 YIG thin film oscillator propagates via a “Typ-N” coaxial waveguide to the TWT amplifier and then via a “WR-75” rectangular waveguide to the circulator and the ion source.

A custom-built power supply and control unit allows to tune the oscillator manually or by the LabVIEW-based computer control system. For operation with “SOPHIE” the output signal of the oscillator is limited to the range of 12.75 GHz to 14.5 GHz in order to prevent the TWT amplifier from damage by a not suitable input signal. In addition, the oscillator is switched off automatically in the case of insufficient cooling water supply to protect the permanent magnet system from overheating.

The transition into the vacuum chamber and the insulation from the ion source potential are provided by a PTFE window of 2 mm thickness. This thickness is a compromise between optimum transmission and the required low gas leakage and potential difference of 10 kV. Figure 2.3.2 shows a cross-sectional view of the microwave window and the coupling system (see also fig. 2.1). A PTFE sheet is held between two relatively large stainless steel flanges in order to prevent the viton gasket from damage by microwave leaking. In this way also the option to replace the PTFE by another suitable material is maintained.

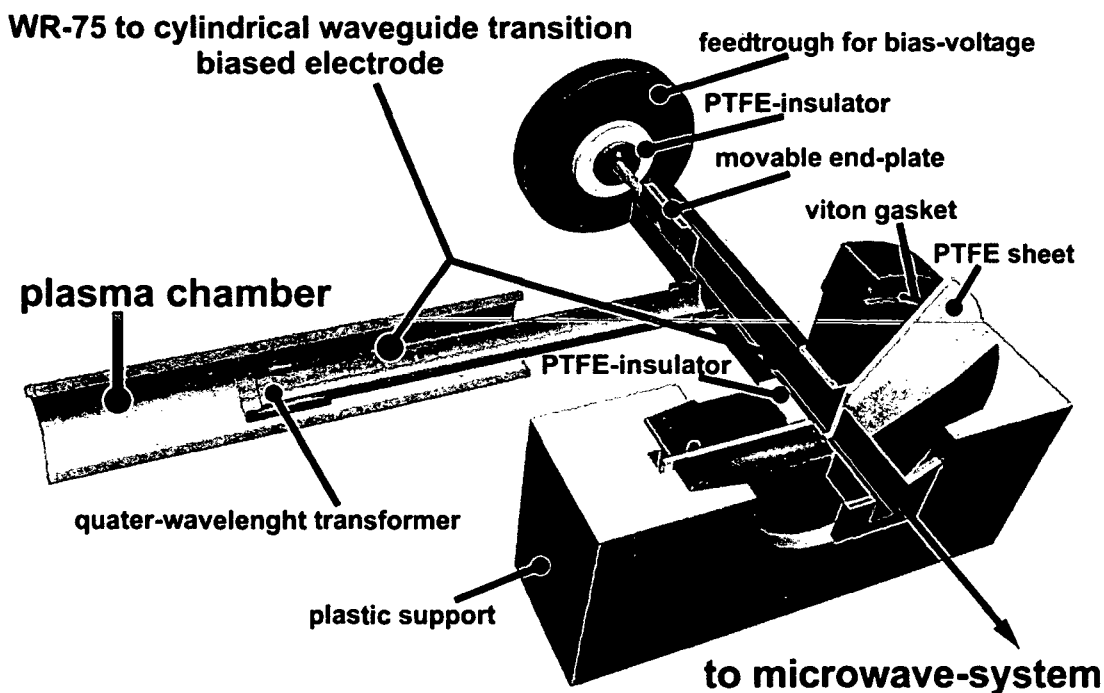


Figure 2.3.2: Cross-sectional view of the microwave window and the coupling system.

The coupling system is a simple transition from “WR-75” rectangular- to a 13 mm inner diameter cylindrical waveguide. The whole system is insulated from the ion source potential to be used as biased electrode with a maximum potential difference of 2 kV. Avoiding any coaxial waveguide, the microwaves are efficiently transmitted into the comparably small plasma chamber, maintaining the necessary pumping speed but still allowing operation with a biased electrode, which is crucial for the production of multiply charged ions. Transmission into the plasma chamber is significantly improved by a “quarter-wavelength” transformer at the end of the cylindrical waveguide. A moveable end-plate in the rectangular waveguide allows to tune the system. The rectangular geometry “hides” the window from the plasma, avoiding the window from being covered by sputtered metal vapour.

For operation at the ion source test stand in Gießen “SOPHIE” has been equipped with a less sophisticated coaxial microwave coupling system (see fig. 2.3.3). Although guaranteed by the manufacturer, the used feed-through proved to be not suitable for operation at 14 GHz. Also, the losses in the coaxial line were not acceptable for a routinely used system.

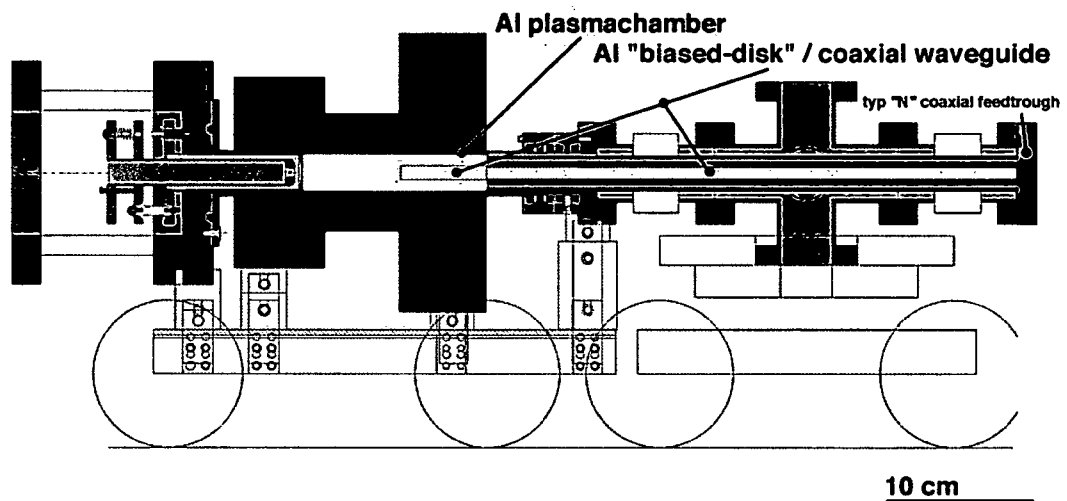


Figure 2.3.3: Schematic view of the setup of “SOPHIE” at the teststand in Gießen. A simple diode extraction system and a coaxial waveguide coupling system have been used.

Therefore it has been decided to use a coupling system as described above, based on hollow waveguides only. To develop such a system, a mock-up of the plasma chamber has been built to allow simple calorimetric measurements of the transmitted microwave power. In this way the dimensions of the coupling system and the microwave window were determined by optimizing the transmitted microwave power. Since the complex interaction of the microwaves with the plasma can not be simulated by measuring the transmission to a water dummy-load, the system had to be fine-tuned at the test stand by way of comparing extracted ion currents.

Fig. 2.3.4 and 2.3.5 show for Ar^{8+} the ion-current dependence on the microwave power and the biased-voltage (see also chapter 2.6).

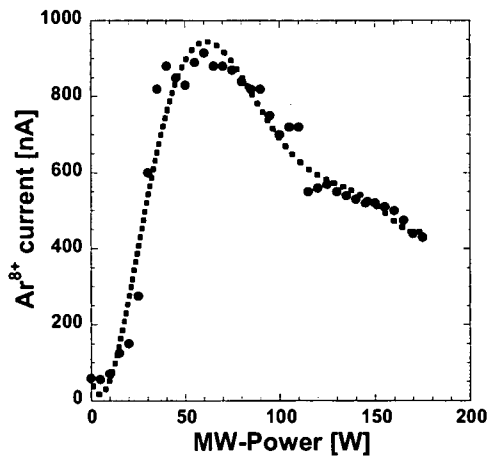


Figure 2.3.4: Ar^{8+} ion current in dependence of the microwave power. Extraction voltage: 5 kV, Mixing-gas: O_2 [43].

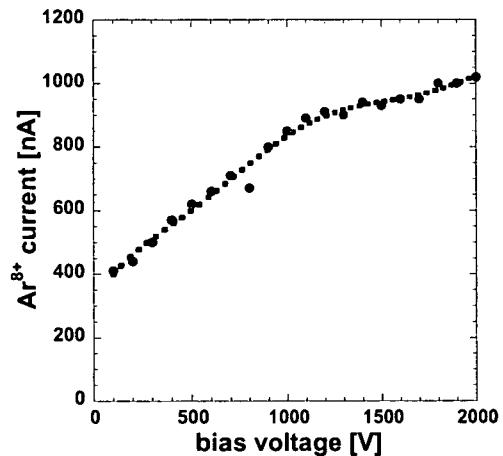


Figure 2.3.4: Ar^{8+} ion current in dependence of the bias voltage. Extraction voltage: 5 kV, Mixing-gas: O_2 [43].

The first months of operation showed that ion currents typically reach saturation well below the maximum available microwave power (fig. 2.3.4). Only for higher charge states (beyond Ar^{+11}) it was necessary to deploy the maximum available microwave power (see also table 2.6.1). Also, biasing of the waveguide proved to be crucial for extraction of higher intensities not only for multiply charge ions, but also for currents of ions in lower charge states.

2.4 The Ion Extraction System

“SOPHIE” is equipped with a triode “Accel-Decel” extraction system. Three concentric electrodes are supported, located and isolated by ceramic spacers, the outermost of which fits smoothly into the plasma chamber, such that the whole system can be easily removed from the ion source.

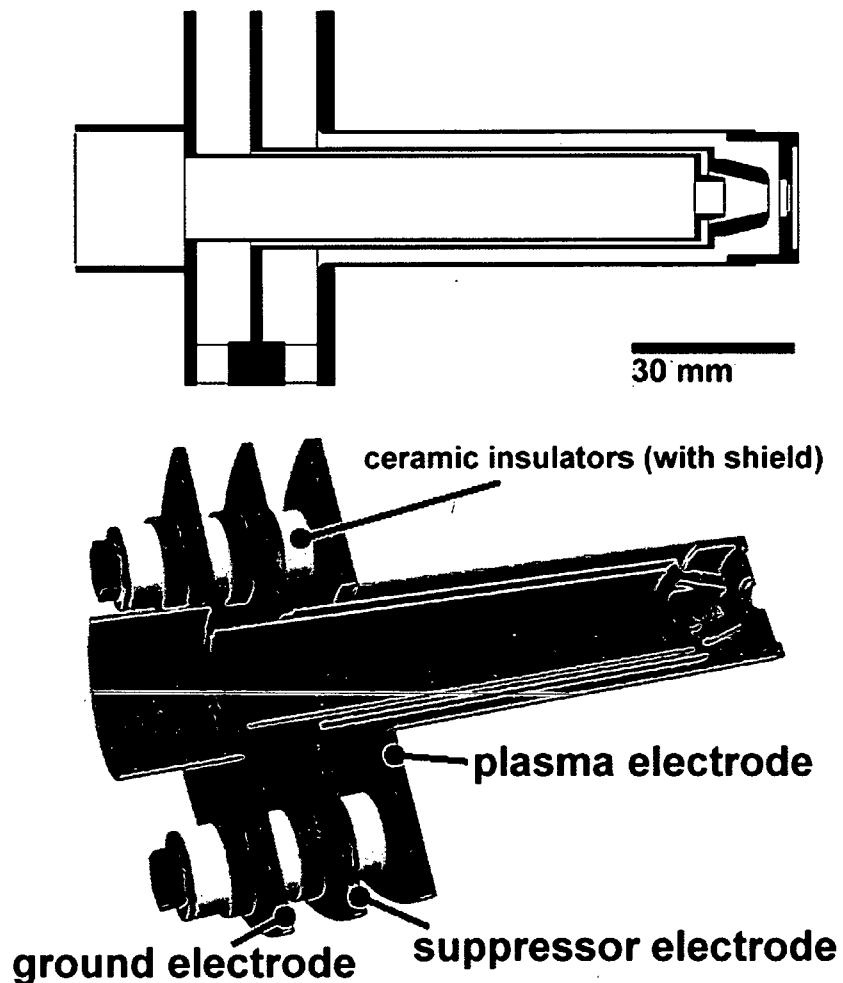


Figure 2.4.1: Schematic view of the triode extraction system.

The ceramic insulators are positioned well away from regions exposed to the ion beam. Additionally, the insulators are shielded from sputtered metal vapour by small metal cylinders. The system can be operated with a potential difference of up to 10 kV between ground potential (inner electrode) and the ion source potential (outer electrode), and for up to 2 kV between the suppressor electrode (middle electrode) and ground potential.

The system has been designed to be operated at “perveance-match” condition by selecting the optimum extraction voltage, as the very limited space available would not allow a reliable operation of movable electrodes.

To allow selection of ion energy independent of the extraction voltage, the original plan was to insulate the beam-line from ground potential. In this manner, the potential difference between source and final ion target could then be defined independently of the extraction voltage which would be defined by the difference between the source and beam-line potentials. As relevant experiments are equipped with deceleration lens systems, the insulation of the beam-line has not been realized at the time of writing.

The shape of the electrodes was optimised by using the ion beam trajectory code “AXCEL-INP” [46] to model the extraction system. This program iteratively calculates trajectories of the ions in two dimensions based on given electrode geometries, electrode potentials and the magnetic field along the axis. The results are provided as a table or graphically. The emittance of the ion beam can be calculated at predefined locations along the beam axis.

With “AXCEL-INP”, the space charge compensation is considered after the calculated potential has passed zero downstream of a minimum below zero. To allow the user to investigate the influence of the space charge compensation, it can be controlled how space charge compensation is considered in the calculation. The user can select influence the of space charge from 0%, corresponding to no space charge compensation, to 100% ,corresponding to fully considering space charge compensation in the calculation.

To optimize the shape of the electrodes within this artificial environment, the extraction voltage was set near 6 kV and the extraction gap to 5.5 mm. The ion mass was defined as 40 amu., assuming singly-charged Ar ions. Figure 2.4.2 shows trajectories calculated

by "AXCEL-INP", assuming complete compensation of the space charge in the drift region.

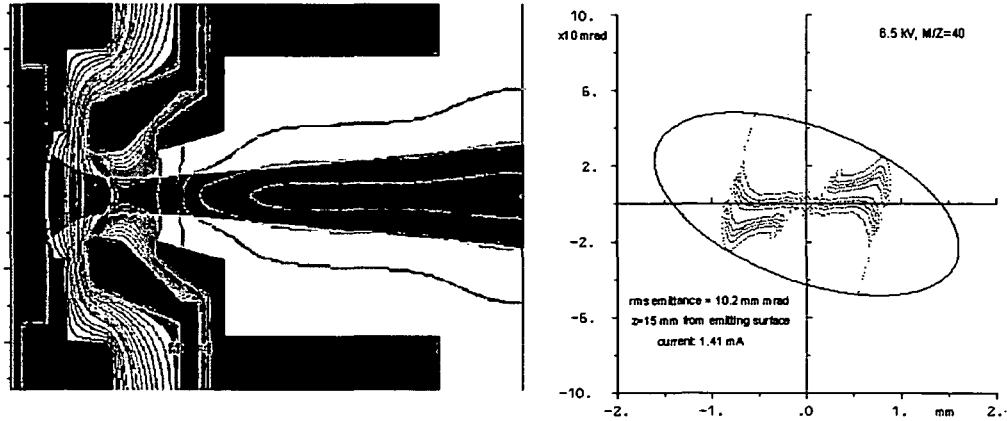


Figure 2.4.2: Result of an "AXCEL-INP" calculation for the triode electrode geometry used for "SOPHIE". (left: ion trajectories, right: emittance at 15 mm distance along the axis) Extraction voltage: 6.5 kV, suppressor electrode: -700 V, "75%" space-charge compensation) [46]

In this simple model many aspects of ion-beam extraction from an ECR-plasma could not be included, since these calculations do not represent the complicated situation found in an ECRIS extraction system. Neither the non-uniform ion beam density distribution across the plasma meniscus nor the composition of the extracted ion current of different charge states could be considered here. As the calculations have been done before first operation of "SOPHIE", the current density had to be chosen rather arbitrarily. Also the assumed charge state is not representing the situation typically for "SOPHIE". Nevertheless, this program gave an environment to test the shape of the electrode geometries.

By optimizing the geometry of the electrodes, aberrations now only found at too low plasma densities could be suppressed. The electrodes were shaped such that the charge compensation for this calculation starts at the waist of the beam, resulting in a minimum emittance of the ion beam.

Although these calculations were based on simplified assumptions, they gave a rough idea of the influence of the space charge and the plasma density on the extracted current.

Fig. 2.4.3 shows the influence of the plasma density (current density of the emitting surface) on the calculated trajectories. As the calculations were done at an early stage, values for the current densities had to be chosen rather arbitrarily. Compared to fig. 2.4.2 a less sophisticated, but similar electrode shape has been used.

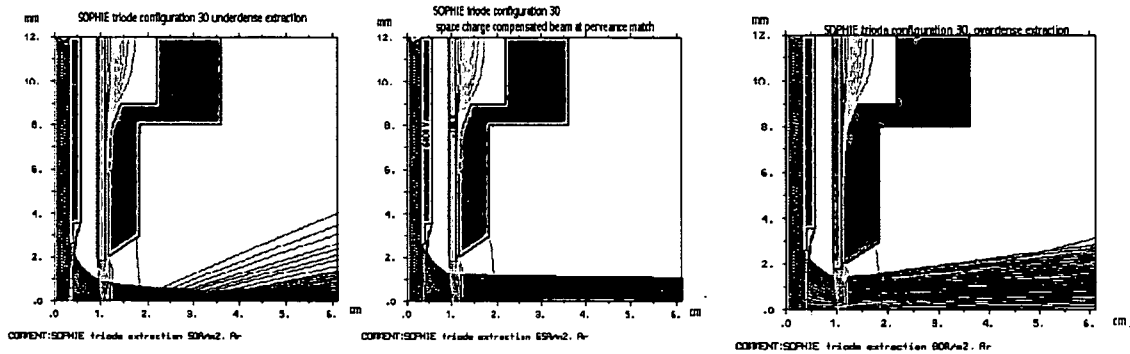


Figure 2.4.3 Calculated trajectories for (from left to right) “under dense” (5 mA/cm^2) “perveance match” (6.5 mA/cm^2) and “over dens” (8 mA/cm^2) operation of the extraction system. Note the aberrations at low plasma-density. Extraction voltage: 6 kV, suppressor electrode: - 700 V [46]

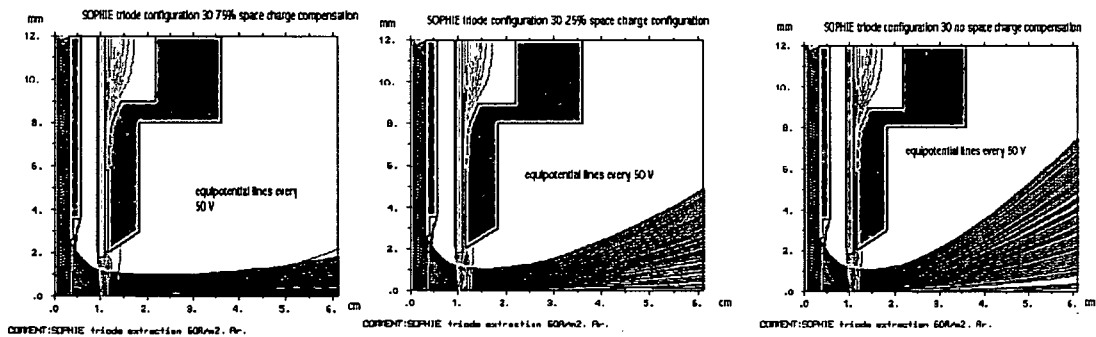


Figure 2.4.4 Calculated trajectories for the “SOPHIE” extraction system, assuming 75 %, 25 % and no space charge compensation (left to right). Extraction voltage: 6 kV, Suppressor electrode: - 700 V [46]

Based on the output data of “AXCEL-INP”, the fraction of the ion beam transmitted into the magnetic quadrupole lens could be calculated for an aperture of 40 mm diameter at approximately 360 mm downstream from the plasma meniscus. According to these calculations even with 50 % space-charge every 50 V 100 % of the ion beam would be transmitted into the magnetic lens.

Although “SOPHIE” is reliably providing currents of sufficient intensities for the ongoing experiments, further investigations on the shape of the electrodes are recommended, especially as these calculations had to be done before operation of “SOPHIE” started and could not be verified experimentally.

2.5 Computer Control and Interlock System

At the Hahn-Meitner Institute in Berlin, the LabVIEW programme “CODIAN” was developed by J. Bundesmann to control different ECR ion sources and beam line components by means of interface electronics like CAMAC (Computer Automated Monitor And Control) or distributed I/O systems (e.g. FieldPoint). The programme is configured by an ASCII database and can therefore be easily adapted to different laboratory setups without major software modifications.

“SOPHIE” was the first ECRIS outside the Hahn-Meitner Institute to be controlled by “CODIAN” [15,16]. Figure 2.5.1 shows a schematic view of the LabVIEW [14] control system used for “SOPHIE”. A custom built BNC interface box connects the two analogue I/O cards in the PC running “CODIAN” with the various components of the ion source. Only the TWT amplifier is controlled via a serial interface.

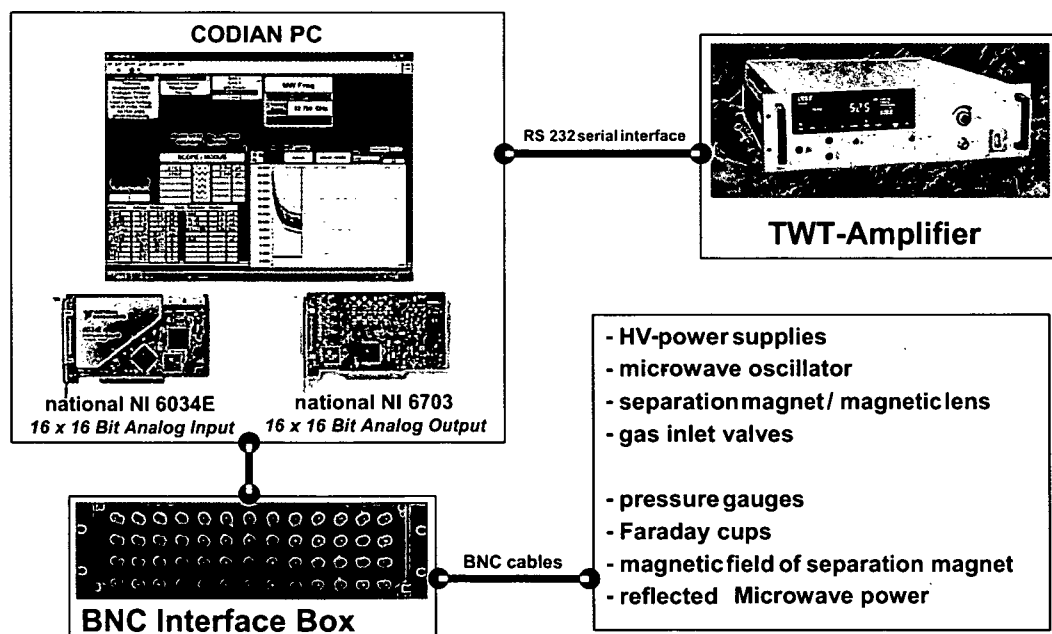


Fig. 2.5.1: Schematic view of the LabVIEW based computer control system.

The main screen (fig. 2.5.2) of the user interface of “CODIAN” shows four major features simultaneously.

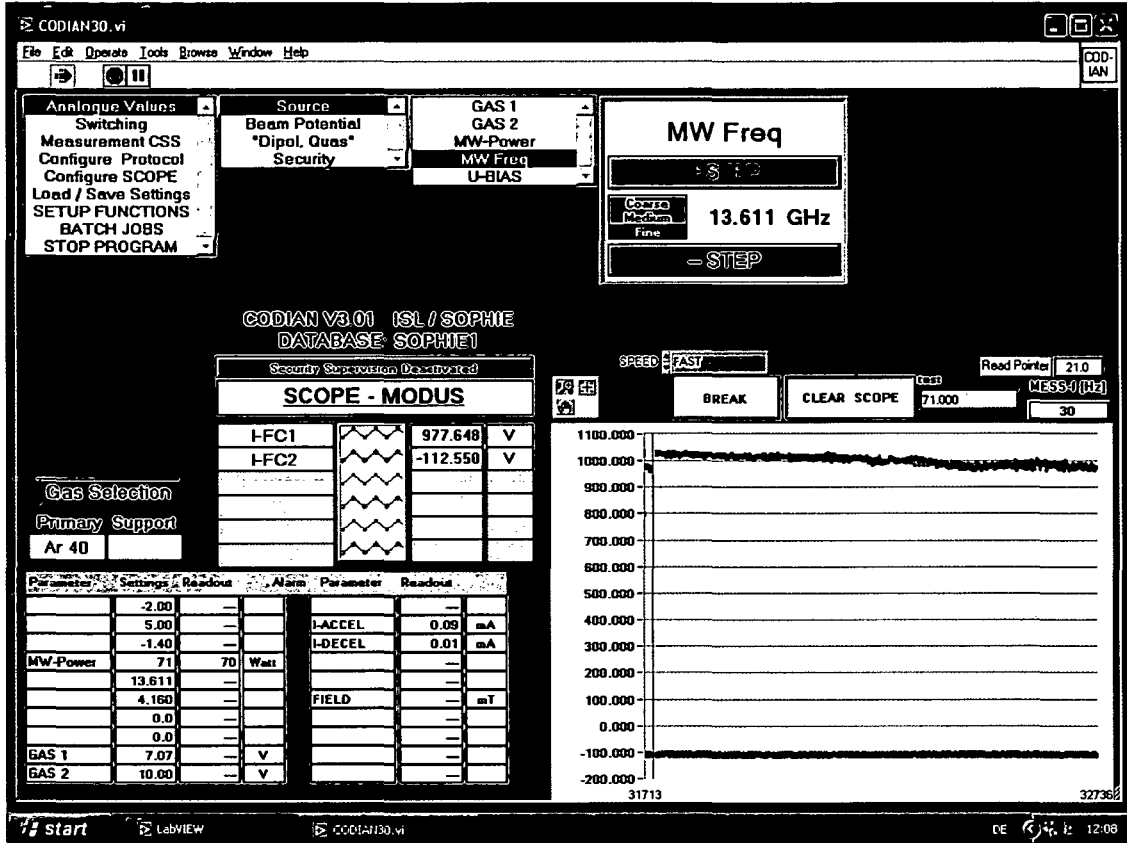


Fig. 2.5.2: Screenshot of the LabVIEW program “CODIAN”.

In the upper part of the screen is a pull-down menu, making each user defined parameter accessible. This menu includes the option to select and start more complex subroutines: measurement of the charge state distribution, saving and reloading of complete beam settings, configuration of the screen for the various beamlines. The menu also allows the user to configure other parts of the screen. The table of parameters in the lower left corner is selected from predefined groups. The scope window which can show up to six time dependent parameters is located in the lower right part of the screen. These parameters can be chosen from a list of predefined groups or online by the user. All these parameters can be plotted interdependently.

The mass-over-charge spectra are acquired by “CODIAN” as a function of the separation-magnet current vs. the detector current/signal. Due to the remanence of the separation magnet currents for achieving a specific mass-over-charge ratio change every time the magnet current is changed. Therefore it is necessary to calibrate the acquired charge-state spectra according to well identified mass-over-charge peaks. For this purpose a short IDL program has been written, which allows the operator to quickly calibrate spectra obtained with “CODIAN”. The program can be executed independently of an (expensive) IDL compiler, using the freely available so-called “IDL Virtual Machine” [48]. To avoid complications due to different versions of IDL, the layout of the program has been kept as simple as possible, using only machine independent standard IDL-routines.

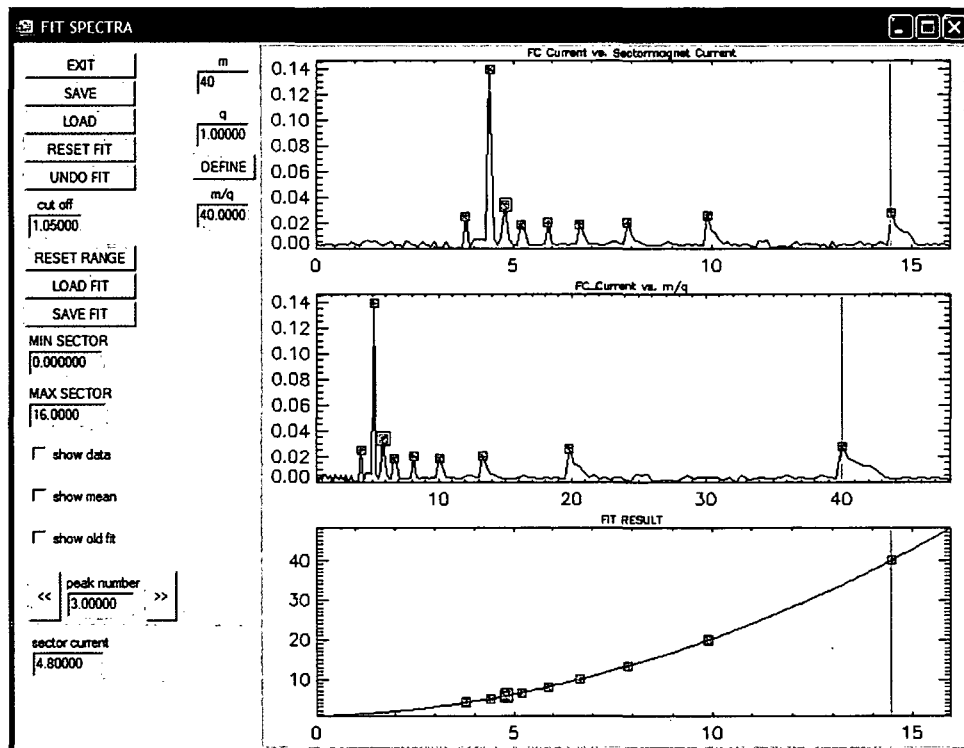


Figure 2.5.3: Screenshot of the IDL-program used to calibrate mass-over-charge spectra acquired with CODIAN.

After loading the raw data, the spectrum is plotted in the graphics window. It is then up to the user to define the mass-over-charge value for two or more peaks, to allow the program to calculate a calibration curve for the spectrum using a least-square fit routine.

The raw spectrum, the calibrated spectrum, and the calibration curve are then all plotted in the graphics window (see fig. 2.5.3). The result of this calibration can be saved as a text file. The program allows to load data from previously achieved calibrations as a first guess for newly acquired data.

Fail-safe hardware is also built into the system, to ensure the safety of the operator or the machine. There are two interlock system, completely independent of the PC running "CODIAN".

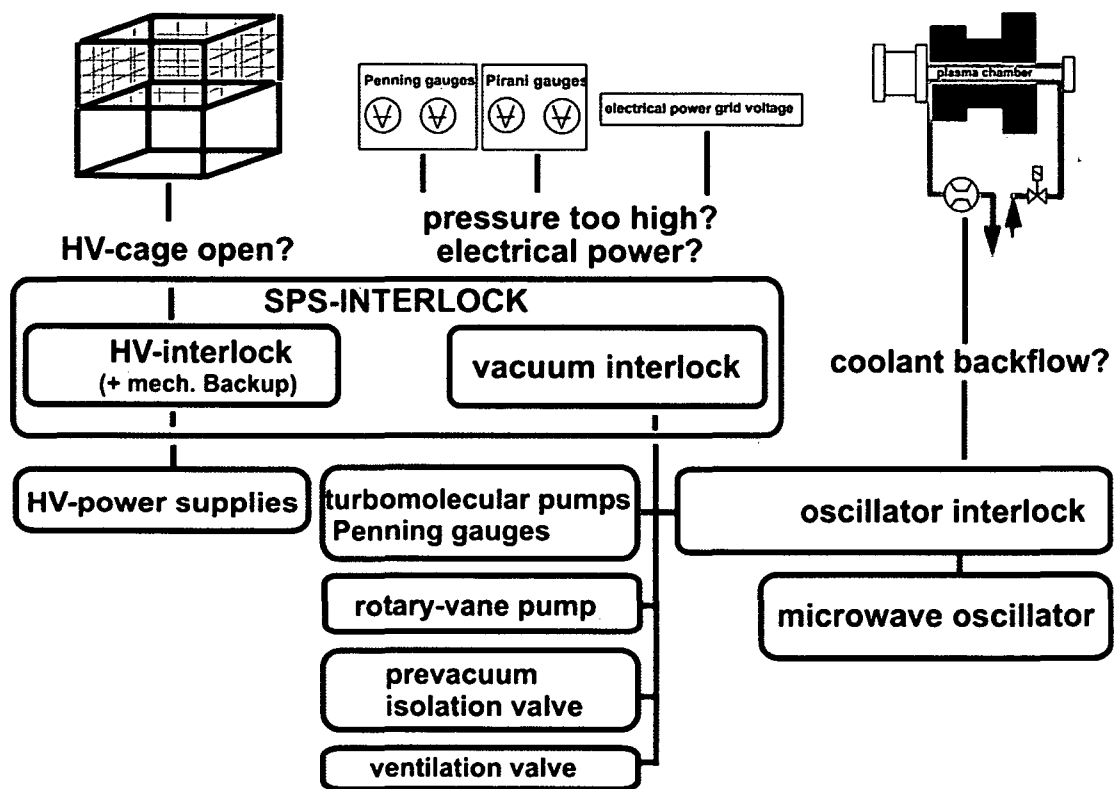


Fig. 2.5.4 Schema of the interlock system.

First, a simple interlock system (in fig. 2.5.4: "oscillator interlock") shuts off both the water supply to the plasma chamber's cooling system and the electricity supply to the microwave oscillator in an event that the cooling water back-flow stops. This protects the permanent magnet system from overheating and prevents flooding of the laboratory.

A more sophisticated interlock system based on a "LOGO! 230RC SPS" unit manufactures by Siemens, monitors the high voltage and vacuum system of "SOPHIE".

This SPS device features four input and four output channels, surveying the access to the ion source, the vacuum system and the electrical power. The SPS interlock system is connected to the emergency power supply of the laboratory to allow a controlled shut down of “SOPHIE” even during a power failure. The function of the SPS based interlock system can be described as follows.

- If a wire cage prohibiting access to the ion source is opened, the power supply to the high voltage system is switched off, thus preventing anyone to touch parts on high potential. This function is backed up by a mechanical switch.
- In case of an electrical power failure or a pressure increase above a predefined value the system is switched off and the vacuum vessel is pressurized in a predefined safe procedure.

The SPS interlock may be overruled by the operator, e.g. for stopping an ongoing ventilation procedure. The high voltage interlock nevertheless stays active.

Altogether, the hierarchy of the control system of “SOPHIE” can be grouped into four operational modes:

- Manual operation over-ruling the SPS interlock system.
- Manual operation with active SPS interlock system.
- Computer controlled operation via “CODIAN”
- remote operation via VNC [17] client/server software (see chapter 3)

The high voltage and the cooling water interlock can not be overruled and are always active. Of course, all interlock systems are completely independent of the “CODIAN” computer.

2.6 Overall Performance of the ECRIS SOPHIE

2.6.1 Investigations at the Test Stand

“SOPHIE” has been first been assembled and operated at the Gießen ECRIS testing facility [6]. A simple coaxial microwave-coupling-system and a diode extraction system have been used (see fig 2.3.3).

The first spectrum obtained with “SOPHIE” is given in figure 2.6.1. For this measurement the ion beam has been collimated by two apertures in front of the Faraday cup. (figure 2.6.2) This geometry has been chosen as a standard within the LEIF [13] network to allow a comparison between the different facilities. No focusing has been used for these very first tests.

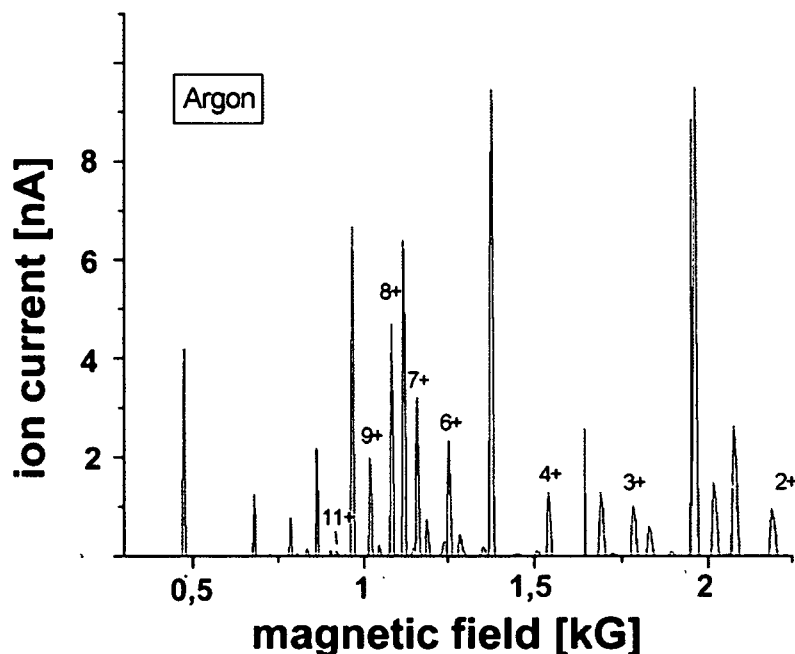


Figure 2.6.1: First spectrum of “SOPHIE” measured at the Gießen ECR testing facility on September 28, 2001 (argon with residual gas).

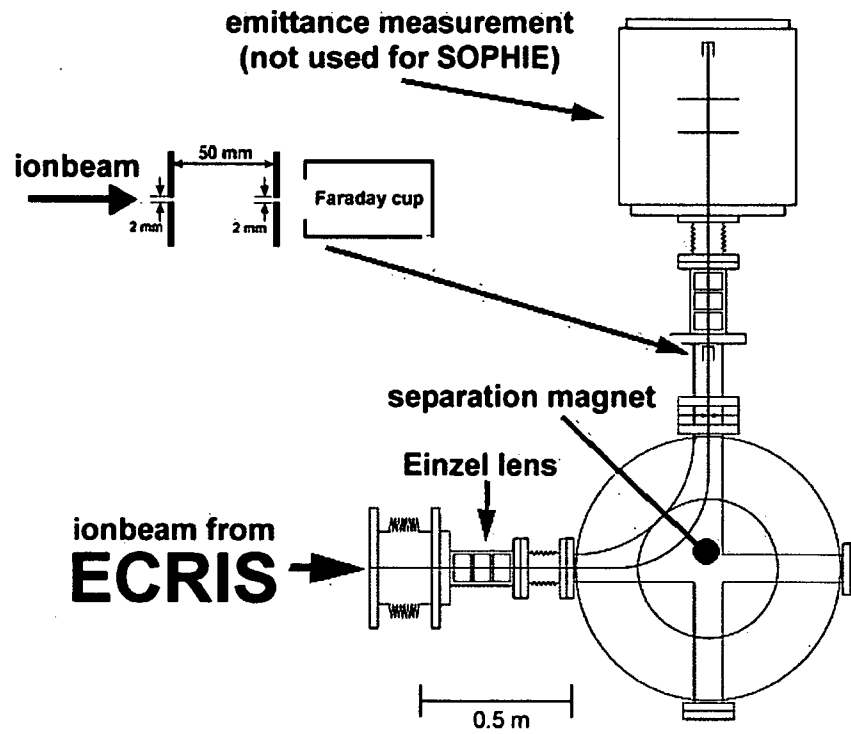


Figure 2.6.2 : Gießen ECR-Teststand with LEIF Faraday cup geometry: Two apertures, with 2 mm diameter each, at a distance of 50 mm collimate the ion beam. The Einzel-lens has not been used [6].

Further investigations on the performance of “SOPHIE” were carried out by using a dedicated test stand at the University of Technology in Vienna. Fig. 2.6.3 gives a schematic view of this setup.

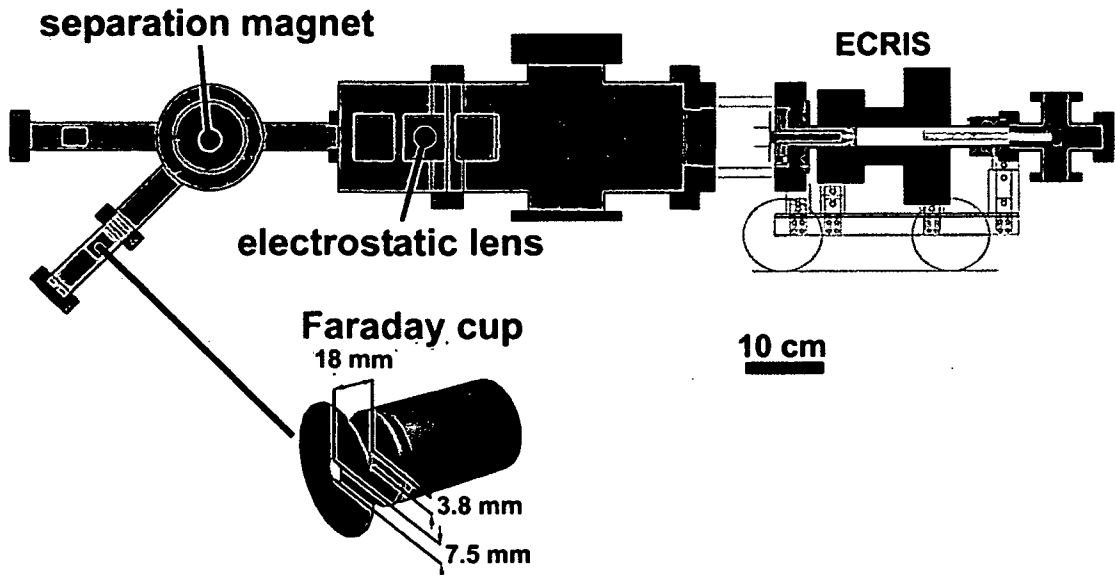


Figure 2.6.3 Schematic view of the test stand at the University of Technology in Vienna.

As no suitable bellow has been available “SOPHIE” has been directly connected to the recipient. Therefore the ion source could not be aligned to the test-stand, thus not allowing to measure the maximum possible ion currents.

The extracted current could be focused with an electrostatic lens. One Faraday cup in the axis of the ion source, and another one to measure the charge to mass separated ion currents have been installed.

Investigations at the test-stand focused on testing the reliability and to a smaller extent on the characterisation of the performance of the ion source. A more efficient microwave window and microwave coupling system (see chapter 2.3) have been developed and the mounting of the extraction system has been improved.

The optimum length of the cylindrical waveguide and the optimum position of the extraction system have been found by operating with different waveguides of different length. For each waveguide length, the ion current has been optimized by moving the ECRIS permanent-magnet. As aluminium tubes with the preferred inner diameter of

13 mm were not available investigations at the test stand had to be carried out using aluminium tubes with 12 mm inner diameter. It has been found that the cylindrical waveguide can be damaged by electrons from the resonance-zones “outside” the confined plasma. Therefore, the waveguide has been positioned at a safe distance from the maximum of the axial mirror field, avoiding these resonance-zones. Nevertheless, negative biasing the waveguide remarkably increased the extractable ion-currents of multiply charged ions (fig. 2.6.5, 2.6.7 and fig. 2.3.5), even with the electrode being retracted from the maximum of the axial field.

For the optimization of the microwave-coupling system, the dependence of the ion currents on the microwave power has been investigated. For all results obtained at the test stand a narrower 12 mm inner diameter waveguide has been used (compare to 2.3.4, measured with the 13 mm inner diameter waveguide).

The results shown in figs. 2.6.4 and 2.6.6 describe the behaviour of the microwave system, the influence of the bias-voltage is presented in fig. 2.6.5 and 2.6.7. For a better overview, fig. 2.6.8 gives the ion-current distribution for 170 W as found in fig. 2.6.4. For figs. 2.6.4 to 2.6.8 all ion source parameters and the electrostatic lens were optimized for a maximum Ar^{8+} ion current.

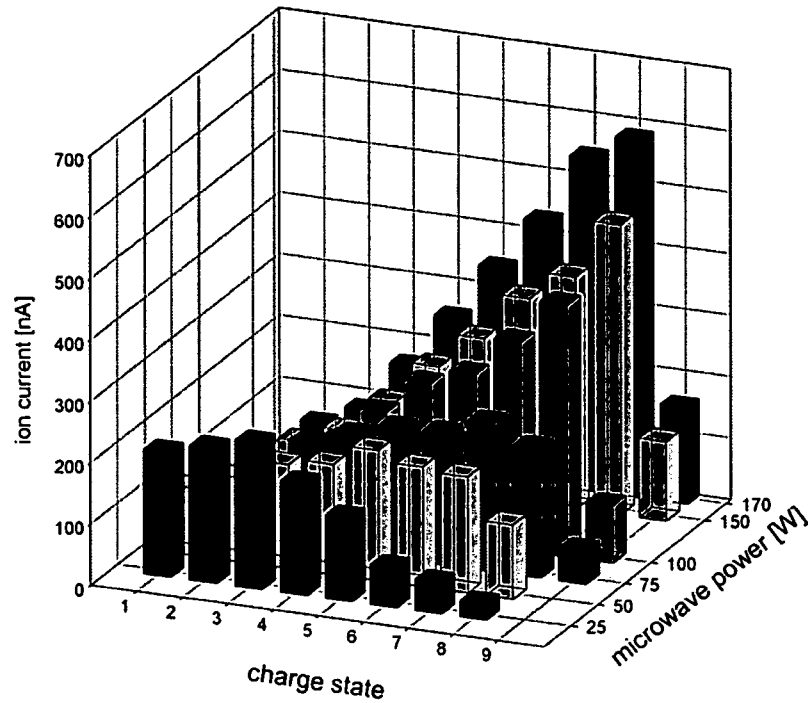


Figure 2.6.4: Argon ion current distribution in dependence of the microwave power. Extraction voltage: 5 kV / Mixing gas: Helium (see also fig. 2.6.7). Other than in fig. 2.6.11 and table 2.6.1 the Ar^{5+} ion current is presented, as helium has been used as mixing gas, and nearly no peaks of other elements were detected [43].

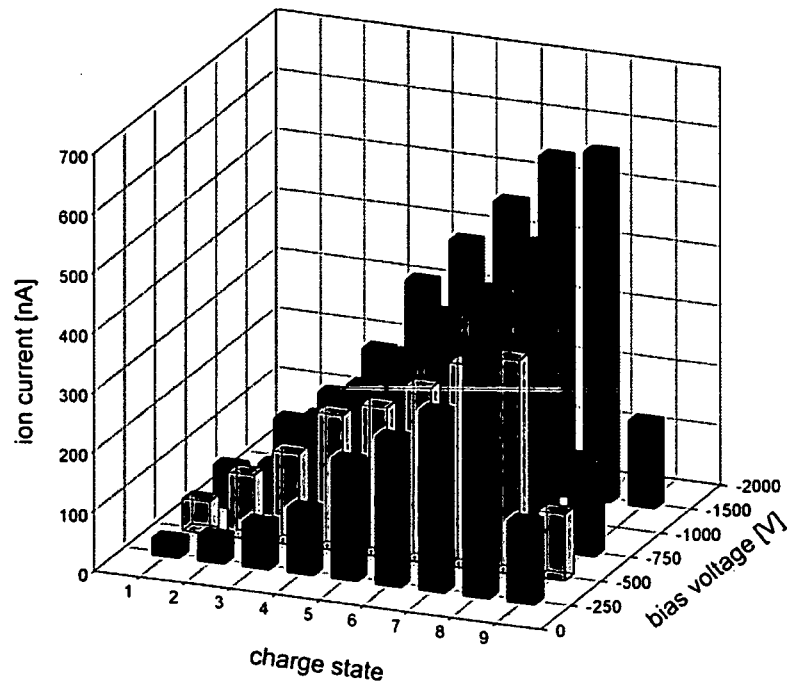


Figure 2.6.5: Argon ion current distribution in dependence of the biased waveguide voltage. Extraction voltage: 5 kV / Mixing gas: Helium (see also fig. 2.6.8). Other than in fig. 2.6.11 and table 2.6.1 the Ar^{5+} ion current is presented, as helium has been used as mixing gas, and nearly no peaks of other elements were detected [43].

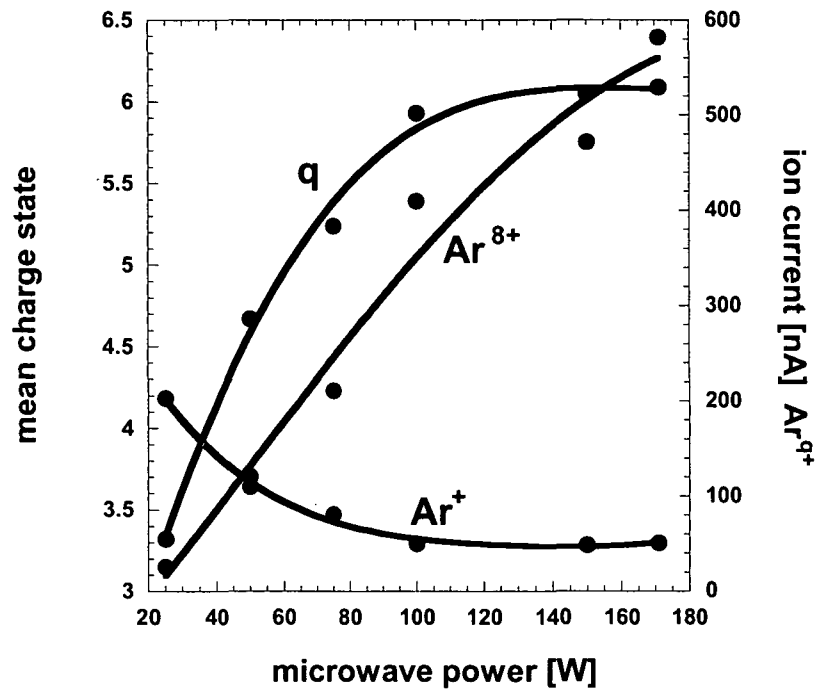


Figure 2.6.6: Mean charge state q of the total extracted current, Ar^+ and Ar^{8+} ion currents in dependence of the microwave power. Extraction voltage: 5 kV; Mixing-gas: Helium [43].

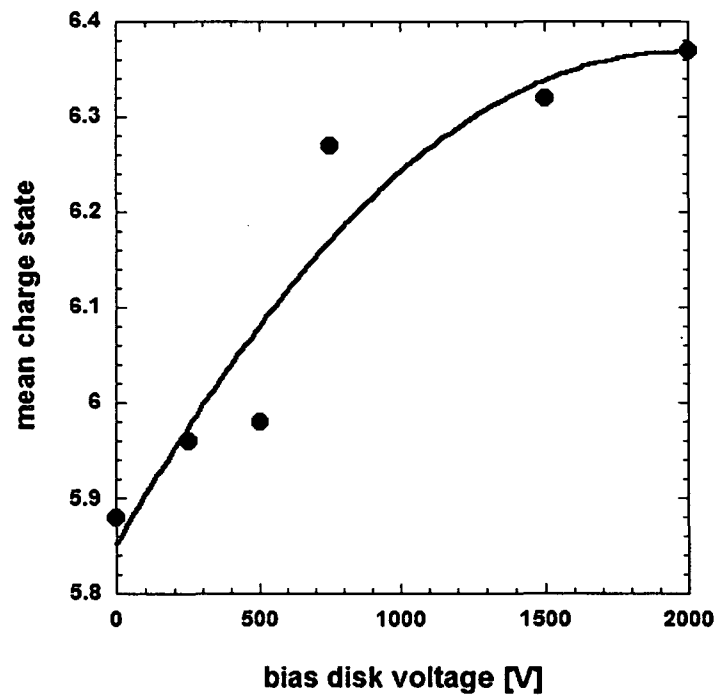


Fig. 2.6.7: Mean charge state q of the total extracted current in dependence of the bias-voltage. Extraction voltage: 5 kV; Mixing-gas: Helium [43].

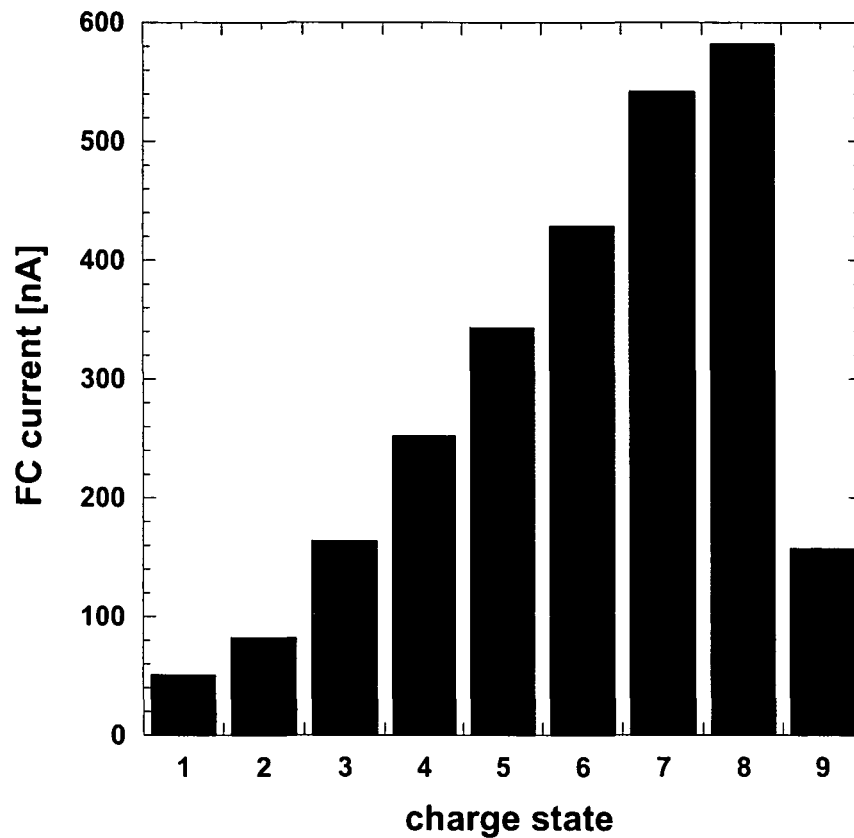


Fig. 2.6.8 Argon ion current distribution of "SOPHIE" measured at the test-stand. Extraction voltage: 4kV / Microwave power: 170 W / helium admixture. (as in fig.2.6.4) [43]. Other than in fig. 2.6.11 and table 2.6.1 the Ar^{5+} ion current is presented, as helium has been used as mixing gas, and nearly no peaks of other elements were detected.

Comparing fig. 2.6.8 with the results obtained with the to be replace 5 GHz ECRIS "BERTA" [4], it has been decided to move the ECRIS "SOPHIE" from the test-stand to "AUGUSTIN" laboratory, especially as higher intensities could be expected with the ion source being better aligned to the beamline.

2.6.2 Performance of SOPHIE at the Ion Accelerator

Fig. 2.6.9 shows a schematic view of the beamline setup in the “AUGUSTIN” laboratory. A magnetic lens consisting of two magnetic quadrupoles allows to focus and steer the extracted ion current. For two beamlines the ions are separated according to their charge-over-mass ratio with a sector magnet. The straight beamline is equipped with a second separation magnet.

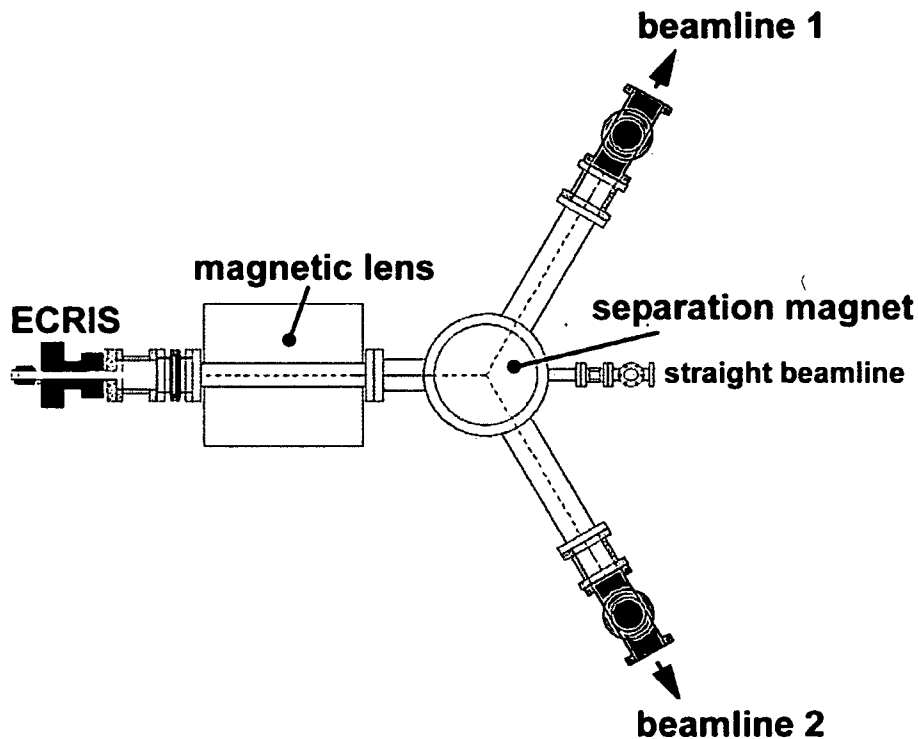


Figure 2.6.9 Schematic view of the “AUGUSTIN” beamline.

Measurements of the performance of “SOPHIE” have been done at the experiment “NINA” [49], intended for investigations on ion induced electron emission from solid surfaces. Figure 2.6.10 shows a schematic view of the experiment “NINA”. The ion currents have been measured on the empty target holder which has been biased against the surrounding grid and cage to suppress secondary electron emission. A pair of deflection plates and an electrostatic lens were used to focus and steer the ion beam.

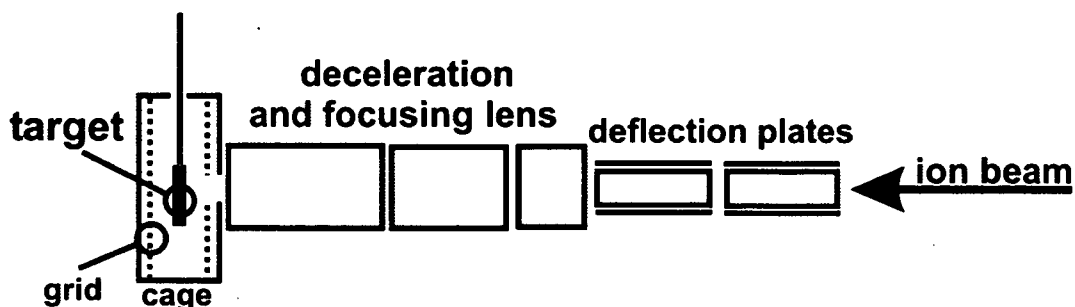


Figure 2.6.10: Schematic view of the experiment "NINA".
The diameter of the aperture of the cage is app. 3 mm [49]..

Figure 2.6.11 shows an argon ion current distribution for "SOPHIE" [50] in comparison with ion current distributions of "BERTA" [4] (with and without biased voltage). For "SOPHIE" as well as for "BERTA" all parameters besides the extraction voltage (5 kV) have been optimized to achieve a maximum ion current for each charge state (see also table 2.6.1). In both cases oxygen has been added as mixing gas, and a Faraday Cup with an 3 mm diameter aperture has been used.

Figures 2.6.12 to 2.6.14 show typical argon-, neon- and xenon- [51] spectra of "SOPHIE" measured at "NINA". These spectra have been acquired by varying the field of the separation magnet only. All other beamline- and ion-source parameters have previously been optimized for a certain charge-over-mass ratio, and were left unchanged during the whole acquisition process. The stability of the ion source during the acquisition process has been verified by comparing the extracted current before and after collecting the spectrum. It has to be pointed out that the height of the peaks in the charge-over-mass spectra does not represent the ion current distribution in the ion source. Optimizing the intensity of a certain charge-over-mass ratio peak by changing not only the ion source but also the beam line parameters may well result in lower currents measured for higher mass-over-charge ratio peaks. Also, due to such a "misalignment" double peaks might be detected. The finite step-width with which the LabVIEW program changes the field of the separation magnet might also contribute to the distortion of the peak height by way of "stepping over" the actual peak maximum during data acquisition (e.g. see Ne^{9+} and Ne^{+8} or ^{20}Ne and ^{22}Ne peak height in fig 2.6.13).

The necessity of a biased electrode is again demonstrated by the results presented in figure 2.6.12. Leaving all ion-source and beamline parameters constant, spectra have been taken with and without bias voltage. The influence of oxygen admixture on the xenon spectrum is shown in fig. 2.6.14. (again, all parameters have been left unchanged, with, and without oxygen admixture) Additionally, xenon ion currents with the respective ion-source parameters are given in table 2.6.2. Higher charge states than here presented have also been detected but could not be considered in this work, as the currents were not stable enough. The stability of "SOPHIE" could probably be considerably improved by operating the ion source with the same gas all around the clock for a longer period (from experience with other ECR ion sources some days, maybe one or two weeks) However, since experiments using a variety of gases had to be carried out this has not yet been possible.

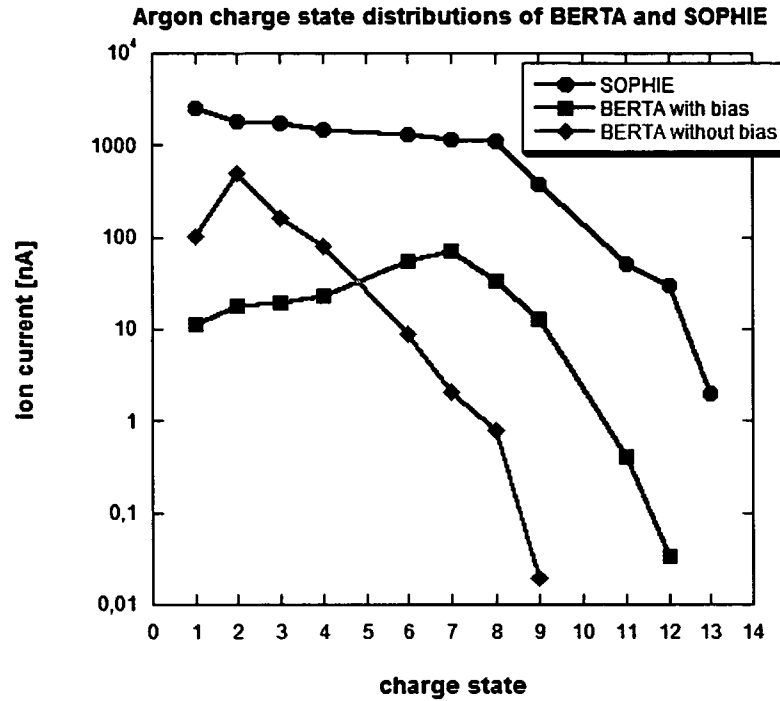


Fig. 2.6.11 Argon ion current distribution of “BERTA” and “SOPHIE”. Extraction voltage: 5 kV / Oxygen admixture [4,50]. Ion currents of Ar^{5+} and Ar^{10+} , could not be measured, because they involve the same charge-over-mass ratio as ions from other elements.

argon charge state	FC current [nA]	microwave-power [W]	microwave-frequency [GHz]	total pressure [mPa]
1	2500	75	13.97	8
2	1850	75	13.954	6
3	1750	74	13.650	7.2
4	1480	94	13.937	7
6	1300	69	14.027	6.2
7	1140	69	14.025	6.7
8	1100	69	14.021	6.7
9	380	120	13.75	5.8
11	50	169	13.757	5.7
12	30	170	13.562	5.4
13	2	170	13.55	5.1
14	2	170	13.547	5.3

Table 2.6.1: Optimized argon ion currents with related ion source parameters for different charge states [50]. Ion currents of Ar^{5+} and Ar^{10+} , could not be measured, because they involve the same charge-over-mass ratio as ions from other elements.

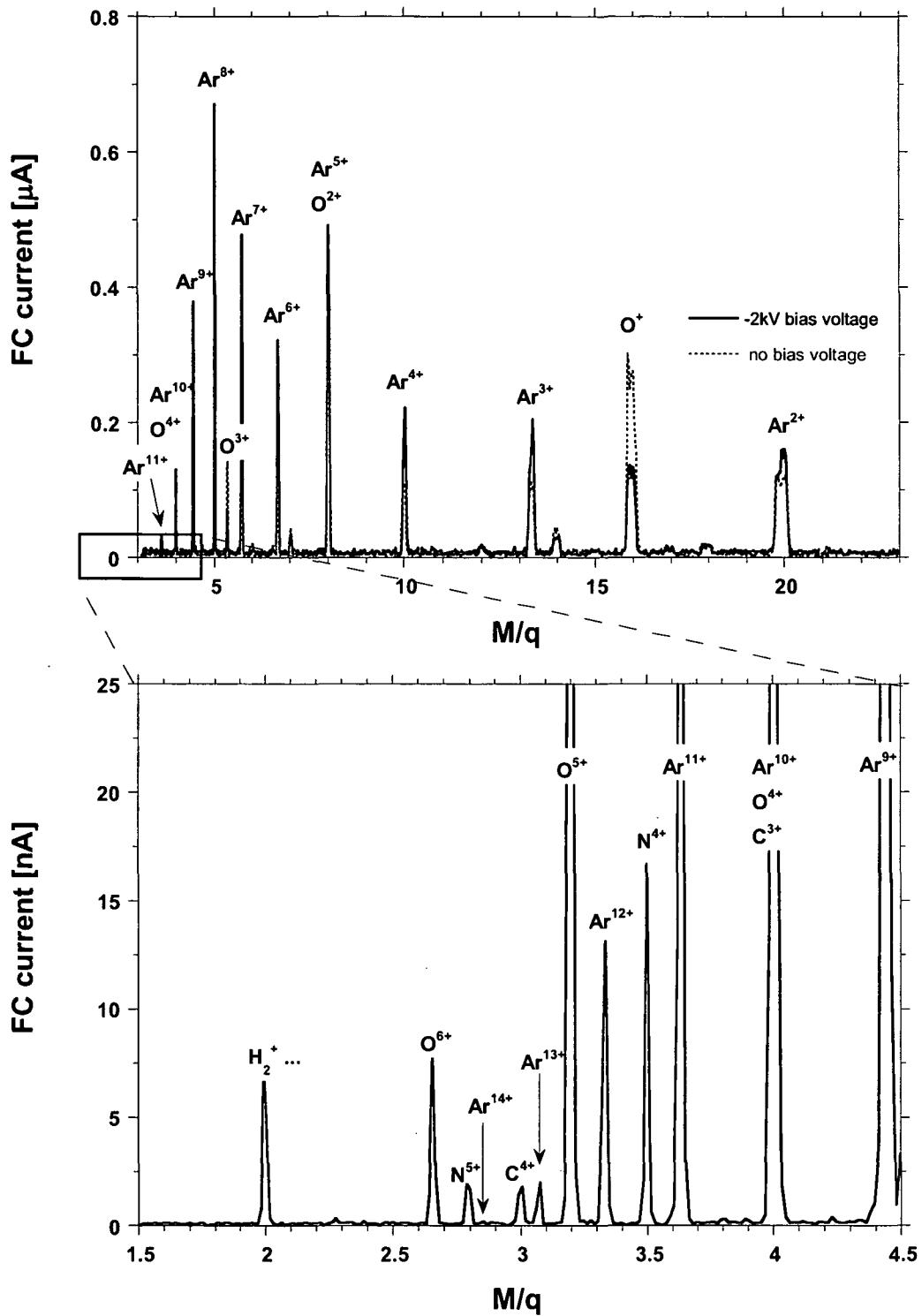


Figure 2.6.12 Argon charge state spectra with and without bias voltage. Optimized for highest achievable charge state. Microwave power: 170 W / total pressure 3.6 mPa / gas admixture: oxygen [51].

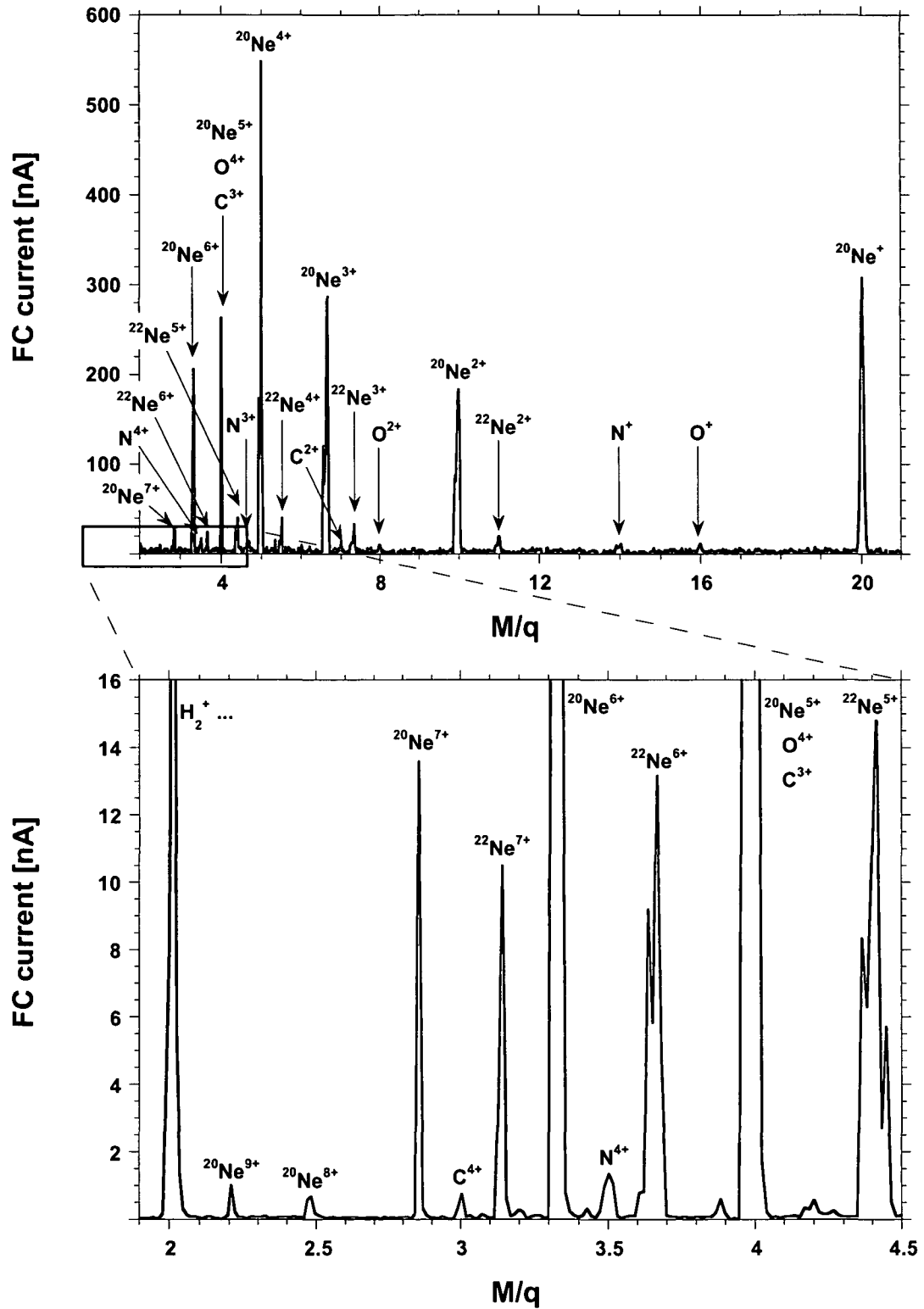


Figure 2.6.13: Neon charge state spectra optimized for Ne^{9+} .
 Microwave power 100 W / Total pressure: 1.4 mPa [51]

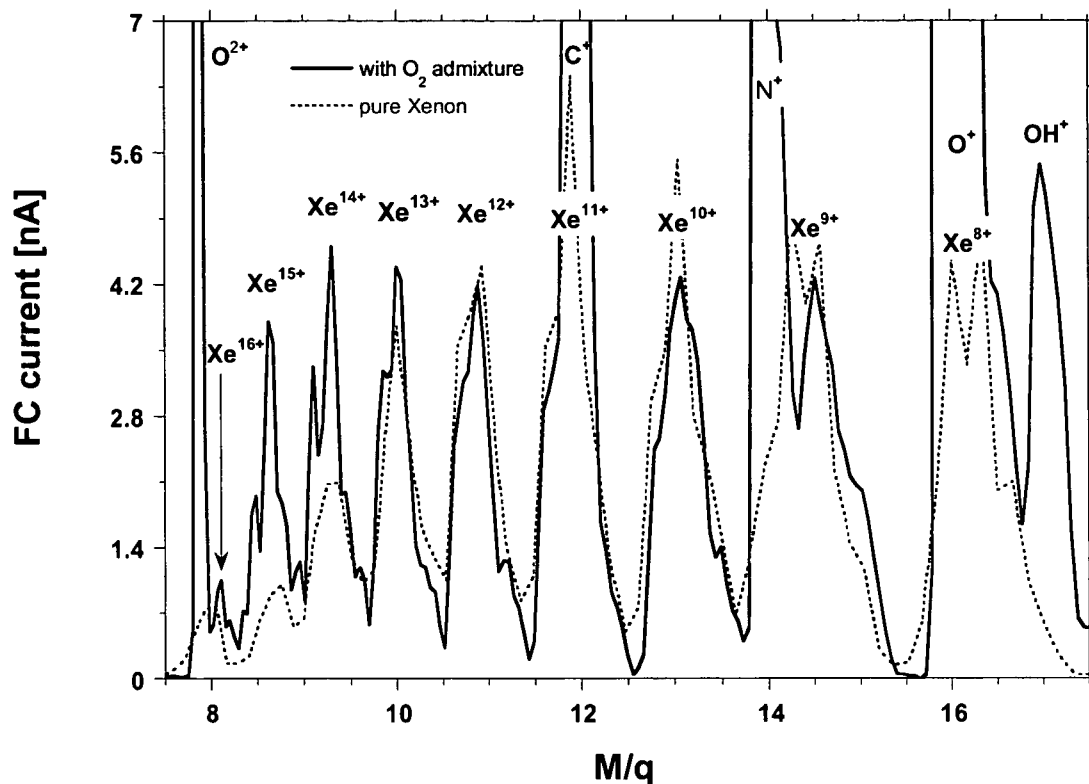


Figure 2.6.14: Xenon charge state spectrum with and without oxygen admixture, optimized for Xe^{15+} . Microwave power: 100 W / total pressure: 2.8 mPa [51].

xenon charge state	FC current [nA]	microwave-power [W]	Microwave-frequency [GHz]	total pressure [mPa]
1	240	37	14.205	5,6
2	160	52	14.019	5,6
3	160	62	14,453	4,4
5	37	92	13,997	3,6
7	2,3	122	13,950	3,6
12	3,7	103	14,007	2,4

Table 2.6.2: Optimized xenon ion currents with respective ion source parameters for different charge states. Gas admixture: oxygen [52].

3. Remote Participation

For an infrastructure network like LEIF [13], with facilities distributed over the laboratories of 12 participants, easy and simple-to-use tools for communication between these different laboratories is crucial. During the last years "Remote Participation" became common among international fusion research laboratories like JET (Joint European Torus) and ASDEX Upgrade (AxialSymmetrisches DivertorEXperiment Upgrade). Therefore it has been decided to introduce the techniques and the know-how gained during fusion related research projects into the LEIF network.

Since the year 2000 the JET fusion experiment is operated under the auspices of the European Fusion Development Agreement (EFDA), with direct involvement of researchers of all major European fusion research laboratories. Scientist from laboratories outside JET can participate personally in JET Task Force work by travelling to the JET site. However, this is not always possible for the entire time interval needed to prepare and execute experiments and analyse respective results. For this reason a large effort has been made to facilitate "Remote Participation" in EFDA-JET using a number of mainly Internet based techniques. This system is operational since the start of experimental campaigns in May 2000. "Remote Participation" has been widely used by scientists to prepare, perform and analyse experiments at JET.

At JET a number of dedicated Windows NT servers are installed to run the CITRIX Metaframe software [53], whereas remote client machines use the free available CITRIX ICA client software to communicate with the servers at the JET site. Access to the Metaframe server is subject to user authentication with SecureID [53] token cards.

Using a preliminary hardware-setup at the University of Technology, Vienna it was possible to participate remotely in JET meetings via teleconferencing. "Virtual Rooms Videoconferencing System" (VRVS) [54], a multi-platform public domain software package, which allows the user to receive and transmit audio and web-camera video pictures to the other participating sites, was used to communicate between the participants of the

meeting. "Power Point" presentations were displayed using VNC [17] (a web-browser/Java based image broadcast system used by EFDA-JET to transmit the presentation viewgraphs to the meeting participants).

A short description of the tools used is given in chapters 3.1, 3.2 and 3.3. The activities within the LEIF network [13] involving LabVIEW [14] are summarized in chapter 3.4. Chapter 3.5 gives an overview of the JET and AUG based experiments involving edge plasma diagnostics with fast helium beams, where these tools have been used on a regular basis and thus served as a good training ground for applying remote participation methods.

3.1 VNC

VNC stands for Virtual Network Computing [17]. It is a remote control software which allows one to view and interact with one computer (the "server") using a simple program (the "viewer") on another computer anywhere on the Internet. The two computers do not even have to be of the same type, so for example one can use VNC to view an office Linux machine on the Windows PC at home. VNC is freely and publicly available.

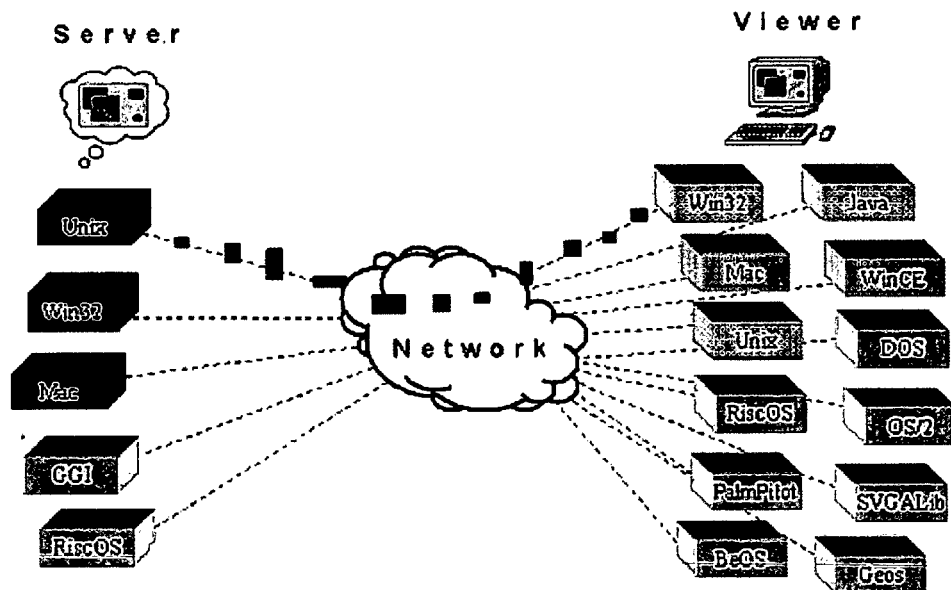


Figure 3.1.1: VNC client/server software allows interaction between computers independent of the platform used.

Within the fusion community, VNC is used for "JTV", a web-browser/Java based image broadcast system used by EFDA-JET to transmit presentation viewgraphs to meeting participants. Via VNC the current presentation desktop image of an ongoing

presentation is transferred into the "JTV" system for broadcast to the presentation for the meeting participants.

Based on the experience from participating in "JTV" broadcast meetings, VNC has been introduced to the LEIF [13] network. Other than in the fusion research community, the use of VNC is not only limited to broadcast meetings. Using VNC client server software, fully computer controlled experiments like "SOPHIE" can in principle be controlled from any computer anywhere in the world. VNC is now frequently used to control "SOPHIE" from different locations in the "AUGUSTIN" laboratory, allowing the experimenter to run the ion-source right from the control/data acquisition system of his experiment.

In the future, VNC might also be used for guests from outside laboratories who wish to follow ongoing experiments. For test-purposes, the control of "SOPHIE", being operated in Vienna, has been successfully transferred to a personal computer in Gießen, Germany. Of course extra precautions had to be taken when connecting the control-computer of "SOPHIE" to the Internet for protection of the system from unauthorized access.

3.2 VRVS

VRVS (Virtual Room Videoconferencing System) [54] is a web oriented system for videoconferencing and collaborative work over IP networks. VRVS provides a low cost, bandwidth-efficient, extensible means of videoconferencing and remote collaboration over networks within the High Energy and Nuclear Physics (HENP) communities. Recently VRVS also has extended the service to various other academic/research areas. VRVS works under all operating systems includes Windows, Linux, Mac, Solaris and Irix.

Since it went into production service in early 1997, deployment of the web-based system has expanded to more than 11,000 identically by registered users running the VRVS software on more than 37,000 computers in 106 countries.

For a meeting, participants can join and talk inside a virtual place called "Virtual Room." Participants at any location join videoconferences (in one or several virtual rooms) by contacting their closest "Reflector". A "Reflector" is a host that interconnects each user to a "Virtual Room", by a permanent IP tunnel. A set of 81 VRVS "Reflectors", interconnected by unicast tunnels and multicast, manage the traffic flow at HENP labs and universities in the US, Europe, Asia, and South America.

Using their browsers user can join the same virtual space ("Virtual Room") and see and talk among each other, like if they would be together in the same physical room. To join a "Virtual Room" somebody must have booked it previously, in the same way people make reservations of physical rooms to carry on a meeting.

The "Reflectors" and their links form a set of virtual sub-networks through which an audio-, video- or data-stream flows. The use of the reflector technology allows the

system to be highly extensible and assures the quality needed for videoconference transmission.

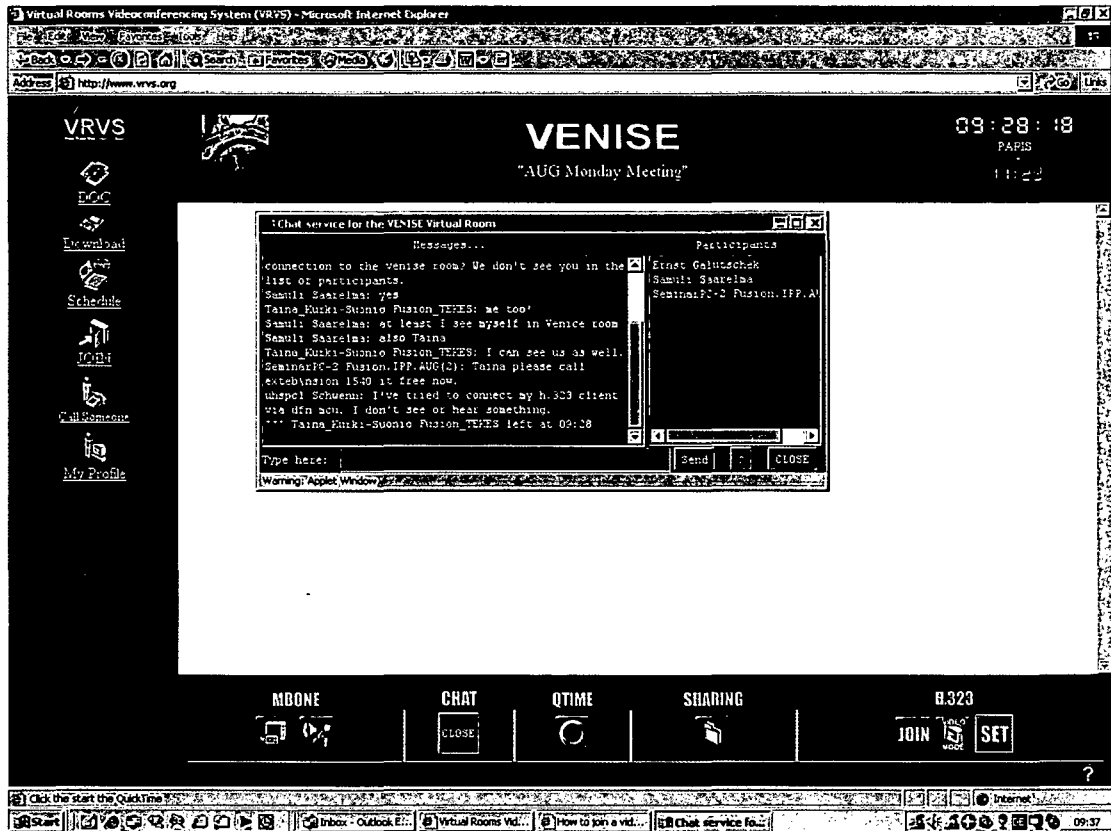


Fig 3.2.1: Screenshot of a typical VRVS screen.

In order to make efficient use of bandwidth, packets (video, audio and data stream) are just sent through the tunnel that links two “Reflectors”, if there are participants in the same virtual room on both sides. In addition, the network reflector topology is chosen by taking into account both geography and the bandwidth available on each network link, in order to optimize the network-connectivity paths.

Recent and ongoing developments include support for MPEG2/MPEG4 and “High Definition” videoconferencing, shared collaborative environments, etc. The goal is to support a set of new and essential requirements for rapid data exchange, and a high level of interactivity in large-scale scientific collaborations.

3.3 Yahoo! Messenger

Instant messaging is the ability to exchange messages in real time with other people over the Internet. To send and receive instant messages, one needs a connection to the Internet and instant messaging software. “Yahoo! Messenger” [55] is a free instant messaging service that one can use to communicate with other people who also use “Yahoo! Messenger”.

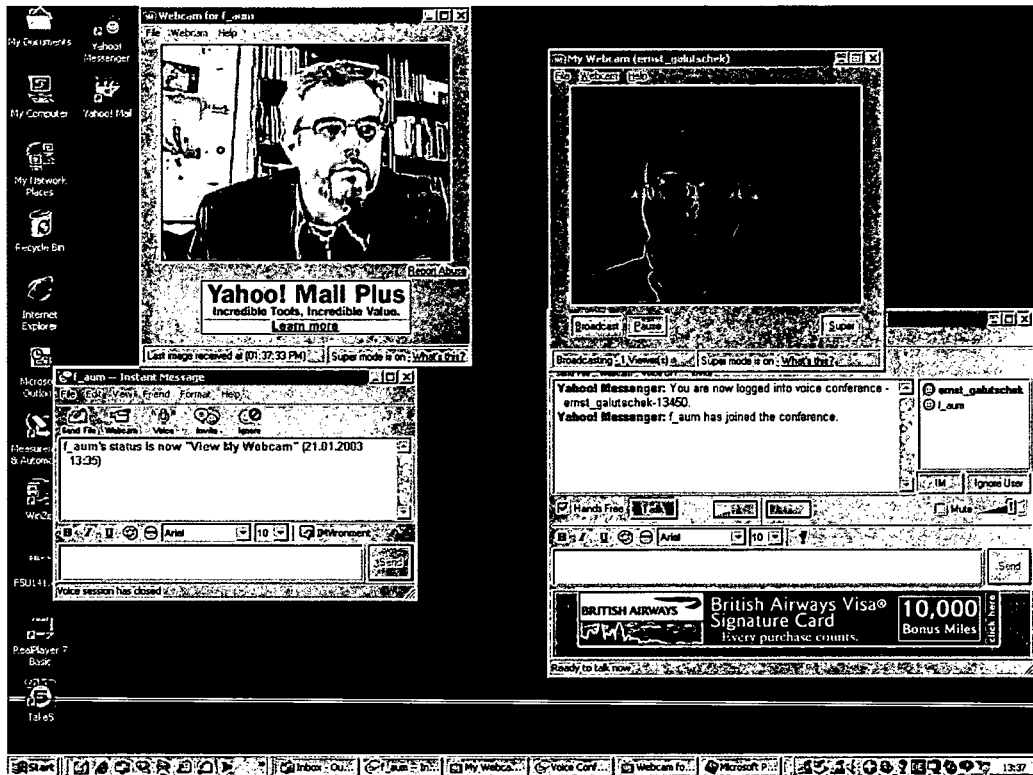


Fig. 3.3.1: Screenshot of a typical yahoo! Messenger conference.

The instant messaging software enables one for setting up a list of “friends” who also use the program. Once one has set up this list, one can see if each “friend” is online at a particular moment. If so, one can begin a conversation with them quickly and easily. Most conversations are typed text messages that are sent back and forth, though more advanced users can exchange voice, video, files and more.

3.4 LabVIEW Activities within the LEIF Network

National Instruments's LabVIEW [14] is a widely used graphical programming environment designed for measurement and automation tasks, giving the flexibility of a programming language without the complexity of traditional development tools. This software package provides tools to assist with application development, as well as functions for data acquisition, instrument control, data analysis, and report generation.

During the last years, LabVIEW established itself as a reliable standard software for controlling experiments.

Encouraged by the pertinent work of Mr. Jürgen Bundesmann (HMI in Berlin) on the use of National Instruments LabVIEW for the control of ECR ion sources, it has been decided to agree on LabVIEW as a standard for the computer based control of experiments throughout all LEIF laboratories (see chapter 2.5).

To introduce LabVIEW to the LEIF community, a well received introductory LabVIEW course, embedded in the 2nd annual LEIF meeting, was held at the University of Heraklion on September 12 and 13, 2001. The 42 participants, split up into two classes, not only attended lessons on LabVIEW programming but also had the opportunity to develop and discuss their own LabVIEW programs.

A second workshop on LabVIEW techniques was organized by Prof. N. Stolterfoht and coworkers (in particular Mr. J. Bundesmann) at the Hahn-Meitner Institute (HMI) Berlin on May 10 and 11, 2002. Detailed results of this workshop are given on the LEIF website. In contrast to the LabVIEW course organised in 2001 in Heraklion, where the basic principles of LabVIEW and some advanced applications have been explained and studied, it was now the aim to work on concrete applications of LabVIEW for the control of ECR ion sources.

The LEIF LabVIEW workshop in Berlin triggered many more activities at several laboratories within the LEIF network. First results of these activities were presented at the third LabVIEW workshop on August 27, 2003 in Vienna, embedded in a first summer school of the LEIF Young Scientist Forum.

Within this workshop, the 14.5 GHz ECRIS "SOPHIE" in Vienna has been presented. It is the first ion source outside the HMI where the LabVIEW based "CODIAN" control system has been implemented. The HMI has kindly agreed to provide "CODIAN" related software without licensing costs until the end of the present LEIF network period. Thereafter, non-profit use will probably be made possible for moderate costs only. Other laboratories have meanwhile expressed their preference for "DAQ" I/O cards in connection with "CODIAN" for their ion sources. The experience gained with the setup at the University of Technology, Vienna will help to further distribute "CODIAN" within the LEIF network.

3.5 Fast Helium Beam Diagnostics as a Learning Case for Remote Participation

3.5.1 Principles of Fast He BES

A precise knowledge of the plasma edge parameters is essential for the development of reactor relevant plasmas. Active spectroscopy of injected atomic beams is a well established diagnostics for a wide range of plasma parameters.

Optical emission from energetic lithium beams [56] has been successfully used as a diagnostics of tokamak plasma density. Electron temperature as well as plasma density can be measured with thermal helium diagnostic beams [57]. However, both beam emission spectroscopies (BES) are limited in range to the outer plasma region because of small penetration depth of the injected neutral particles. More energetic (≥ 20 keV) helium atoms penetrate much deeper into the plasma and therefore offer the prospect of locally measuring electron temperature and plasma density over a much wider range. For developing electron density and -temperature diagnostics based on fast helium beam emission spectroscopy (fast He-BES), different proof-of-principle experiments have been performed in recent years at ASDEX Upgrade (AUG) in Garching and JET in Culham [58]. For generation of fast helium beams the injectors of the neutral particle heating system have been used to produce either pure helium beams or helium doped deuterium beams. [59] For observation of the helium beam emission existing charge-exchange spectroscopic systems have been used at both experiments (see fig. 3.5.1).

The HeI beam emission appears in the spectrum as a clean Doppler-shifted peak, largely undisturbed by impurity emission. Emission from the triplet levels is limited to the outer region of the plasma. The singlet emission could be detected over the full observation range, but its maximum is about one order of magnitude lower than the maximum of the most intense triplet emission (see fig. 3.5.2).

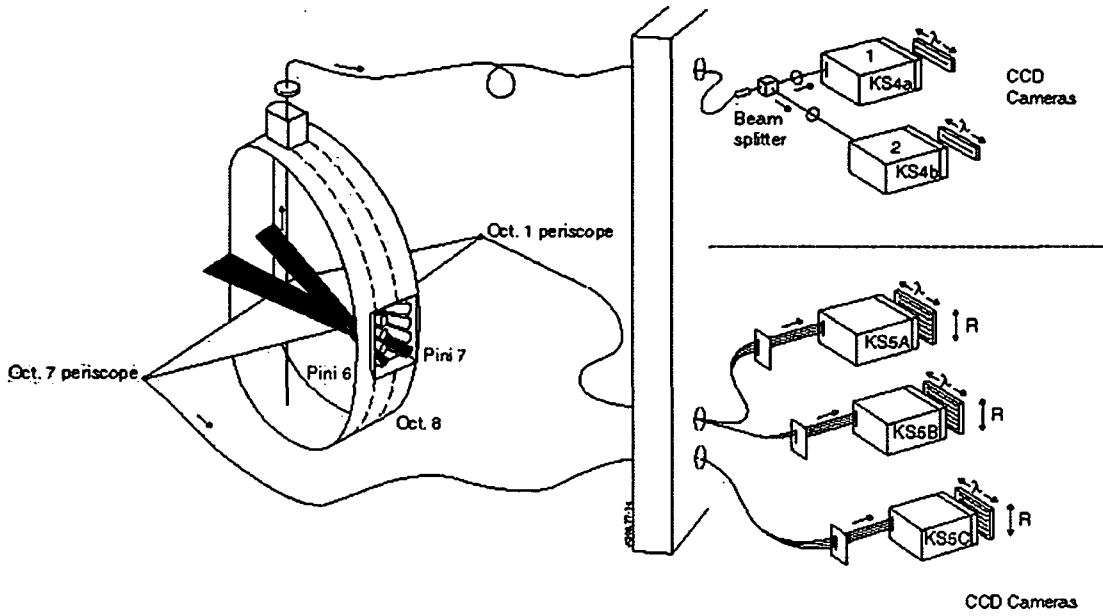


Fig 3.5.1: Schematic view of the „KS5a“ and “KS5c” charge exchange spectrometers (red and blue Octant 7 and Octant 1 viewing lines) used for measuring the He beam emission profiles of the He doped D₂ beam (green) produced by the neutral beam source “PINI7” [60].

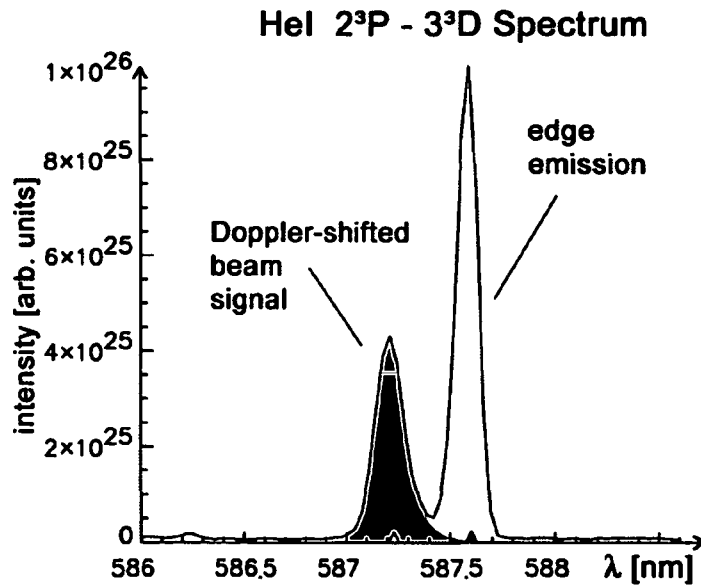


Fig 3.5.2: Typical HeI beam emission spectrum [58].

The initial metastable 2^1S fraction of the beam could be derived from the shape of the singlet HeI beam emission profile. Out of eleven HeI emission lines observed, seven showed sufficient intensity and the 667.8 nm (2^1P-3^1D) singlet- and the 587.6 nm (2^3P-3^3D) triplet line proved to be most suitable.

The measured HeI emission profiles agree comparably well with model calculations which are based on a collisional-radiative model developed by the ADAS group. With the aim to reconstruct plasma density and temperature profiles from the measured HeI beam emission profiles, a so called "reversion code" based on these model calculations [58] has been developed.

For the first tests of this reversion code, synthetic data were generated in order to overcome possible errors in the look-up tables generated from the atomic data. With these synthetic data the code showed good convergence, and both electron density and - temperature could be derived from sets of two synthetic HeI emission profiles. These first results led to the decision to collect a set of beam emission profiles for the above mentioned wavelengths for different plasma discharges.

3.5.2 Measurements at JET in October 2002

To build a database of beam emission profiles the same type of plasma discharge as previously used for the measurement of He beam emission profiles has been used. To achieve a good spatial resolution, the plasma has been swept radially by 120 mm with a ramp rate of 40 mm/s across the viewing lines of the spectrometers. Besides the higher resolution this experimental technique also made it possible to cross-calibrate neighbouring channels, which yielded significantly reduced measurement errors. The plasma shape was made very slim, in order to avoid interaction between the plasma and the vacuum vessel. Also, the sweep range had to be limited, to avoid the strike-point passing over the gap between horizontal and vertical target in the divertor, maintaining a constant density profile during the sweep.

To allow operation of the doped deuterium/helium beam for the duration required for sweeping experiments with the plasma, the total number of operating beam sources has been limited to avoid excessive helium accumulation in the beam duct. Also, to avoid the noise introduced in H-mode plasmas by ELMs a so-called L-mode plasma has been used. Therefore the total heating power had to be kept below the H-mode transition threshold.

Due to problems with the valve sealing the neutral beam duct in "Octant 4", the preferred 70 kV PINI together with the "KS7" plasma edge charge exchange diagnostics could not be used for these measurements.

Therefore the 140 keV diagnostic "PINI 7" at "Octant 8", also equipped with a helium doping system, had to be used instead to produce the He beam [60]. The beam emission was observed with the core plasma charge exchange spectrometers "KS5a" and "KS5c" (with 9 and 12 channels, respectively), allowing to measure the beam emission profiles of the two preferred wavelengths simultaneously.

3.5.3 Experimental Results

To investigate the capability of the method for temperature profile reconstruction, the plasma temperature has been varied by adding a neutral beam source and RF power from pulse to pulse. A list of the successful pulses can be found in table 3.5.1.

Pulse	KS5A wavelength	KS5C wavelength	aim	Comments
57188	667.8 nm	587.6 nm	4 PINIs +1MW RF	
57189	667.8 nm	587.6 nm	2 PINIs	
57227	667.8 nm	587.6 nm	4 PINIs	Lost 1 pini
57231	667.8 nm	587.6 nm	1 PINI	

Table 3.5.1: List of the successful He beam emission pulses.

Fig. 3.5.3 and fig. 3.5.4 show the density and temperature profiles of different diagnostics for these pulses, fig. 3.5.5 and fig. 3.5.6 show the measured helium beam emission profiles compared with calculations from a numerical collisional radiative model [61] based on atomic collision data supplied by the ADAS group. Up to now error bars for the atomic data are not available in the ADAS data base. Therefore, to estimate the error propagation, a normally distributed error of 10% standard deviation has been assumed for the atomic data and the initial meta stable population. This has been realized by M. Proschek [62] in a Monte-Carlo approach. The such obtained results show that the variation of the different measured beam emission profiles for different plasma temperature profiles is well below the error of the ADAS model calculations. Therefore, the rather small temperature difference of the different discharges of this data set can not be resolved, which might be explained by the dominance of ion collisions at the comparably high beam energy which had to be used for these measurements. Significantly improved atomic data are unlikely available for the foreseeable future, due to the complex nature of the involved helium-proton collisions. Nevertheless, measurements at lower beam energies, which were not possible at JET, could lead to more satisfying results.

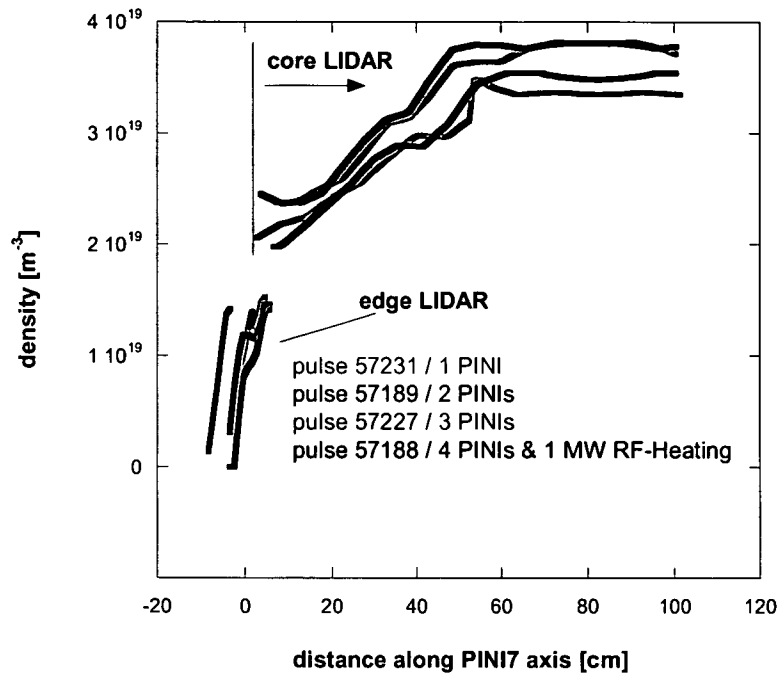


Fig. 3.5.3.: Plasma density profiles obtained with edge- and core LIDAR diagnostics. Zero distance indicates the position of the last closed flux surface. The plasma centre is at app. 80 cm.

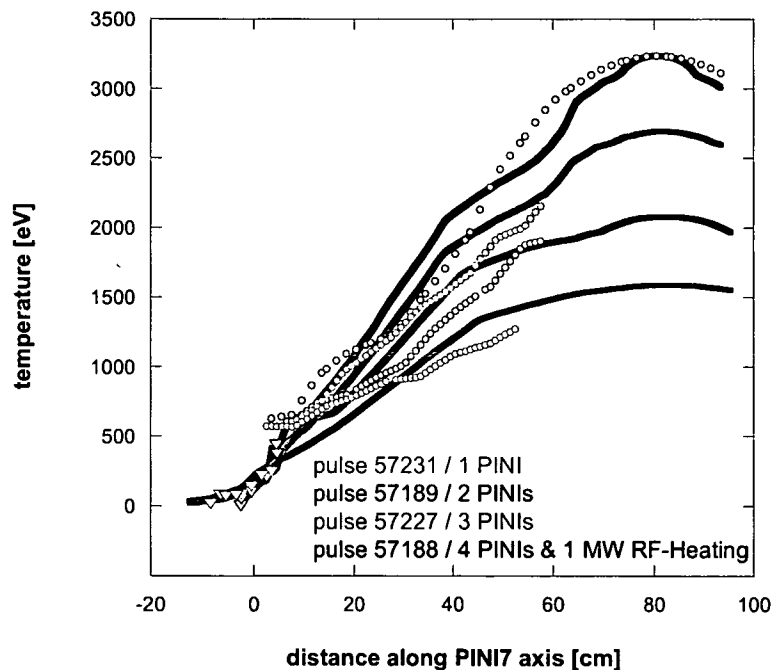


Fig. 3.5.4.: Plasma temperature profiles obtained with Electron-Cyclotron Emission (line), edge (triangles)- and core (circles) LIDAR diagnostics. Zero distance indicates the position of the last closed flux surface. The plasma centre is at app. 80 cm.

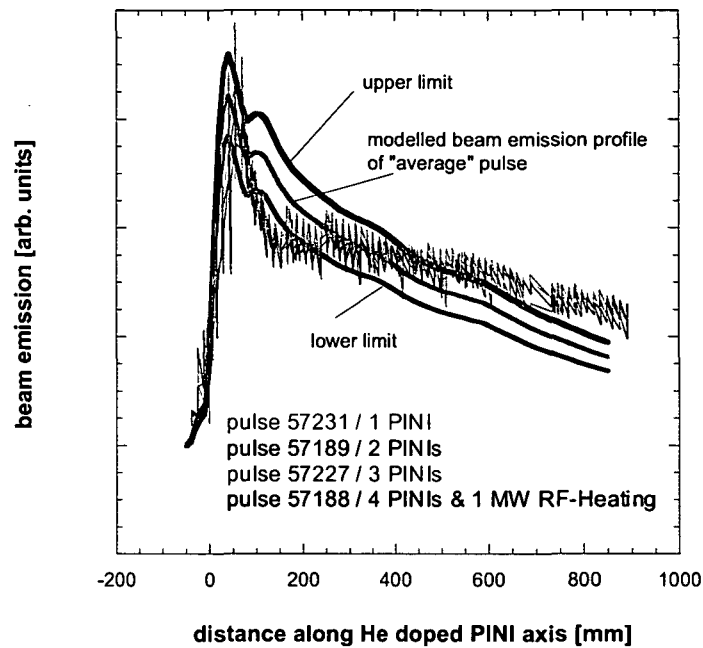


Fig 3.5.5 Measured singlet beam emission profiles compared to the modelled beam emission profile (grey line), using the average temperature and density profiles of the here given pulses. The black curve indicate the estimated error of the model calculation. Zero distance indicates the position of the last closed flux surface.

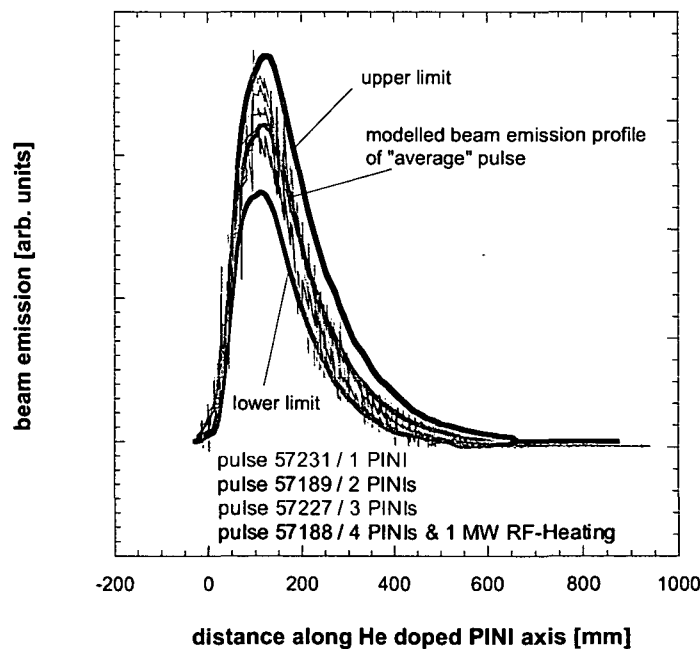


Fig 3.5.6 Measured triplet beam emission profiles compared to the modelled beam emission profile (grey line), using the average temperature and density profiles of the here given pulses. The black curve indicate the estimated error of the model calculation. Zero distance indicates the position of the last closed flux surface.

Conclusion and Outlook

At the time this work was being written the new ECR ion source “SOPHIE” had already been successfully operated for more than one year. Starting from the design of the Gießen type all-permanent-magnet ECR ion sources an in many respects new design of ECR ion source has been developed. Not only the different needs at the University of Technology in Vienna, but also the higher operation frequency made it necessary to redesign many components of the ion source.

An efficient microwave coupling system, based on hollow waveguides only, has been developed. Avoiding any coaxial waveguides, the whole coupling system serves also as “biased-electrode” to enhance the production of multiply charged ions. Despite the rather limited space available, the ion source has been equipped with an aluminium liner and an “Accel-Decel” extraction system. Two leakage valves allow “mixing-gas” operation to further improve the performance of the ion source.

As expected, the new ion source gave access to higher ion charge states and the power consumption of the laboratory could be reduced considerably with respect to the previously used conventional ECR ion source. The LabVIEW based computer control system dramatically simplified the operation of the laboratory, a large part of standard components resulted in low equipments costs, easy maintainance and high reliability.

Although these first results are very satisfying, there is of course room for further improvements. Beside many, less important, details concerning the mechanical and electronic setup, it is the shape of the extraction electrodes in particular which needs further consideration. The efficiency of the microwave system is satisfactory but could be further enhanced by allowing the end-plate position to be adjusted from outside the vacuum vessel during operation. Replacing the PTFE window with another material, such as mica, could well improve the quality of the vacuum in the ion-source. Addition of an oven for operation with plasmas involving non-gaseous elements, is relatively straightforward.

The described “remote participation” tools have been evaluated and successfully implemented into daily routine. However, these programs have to be maintained and updated frequently.

For the example project “Fast Helium Beam Diagnostics” a first set of pulses has been collected during two dedicated experimental sessions at JET. Due to technical limitations the data gained from these pulses can only be seen as preliminary and not meant to be sufficient to clarify the capabilities of this method. Experiments at lower beam energies and more accurate atomic data are necessary to finally assess the applicability of fast helium beam emission spectroscopy for plasma diagnostics.

Bibliography

- [1] S. Fiedler,
„Entwicklung einer 2.45 GHz – ECR – Ionenquelle“
diploma thesis, Vienna University of Technology 1991
- [2] D. Wutte,
„Entwicklung und Aufbau eines Lithiumatomstrahl-Injektors und Beiträge zur
Lithiumatomstrahl-Plasmarandschichtdiagnostik bei Kernfusionsexperimenten“,
doctoral thesis, Vienna University of Technology 1995
- [3] D. Wutte, M. Leitner and HP. Winter
Rev. Sci. Instrum. **65** (4) (1994) 1091
- [4] D. Wutte, M. Leitner, J. Brandstätter, F. Aumayr and HP. Winter
Rev. Sci. Instrum. **65** (4) (1994) 1094
- [5] M. Schlapp,
„Entwicklung einer 14 GHz und einer "vollpermanenten" 10 GHz Elektron-Zyklotron-
Resonanz (EZR) Ionenquelle zur Erzeugung hochgeladener Ionen“
doctoral thesis, Justus-Liebig University Gießen 1995
- [6] R. Trassl,
"Entwicklung "vollpermanenten" EZR Ionenquellen und Untersuchung des
Ladungsaustausches in Stößen zwischen 4-fach geladenen Bismut-Ionen"
doctoral thesis, Justus-Liebig University Gießen 1999
- [7] F. Brötz
„Weiterentwicklungen und Untersuchungen an einer "herkömmlichen" 14 GHz und
verschiedenen "vollpermanenten" 9-10.5 GHz Elektron-Zyklotron-Resonanz (EZR)-
Ionenquellen“
doctoral thesis, Justus-Liebig University Gießen 2000
- [8] M. Schlapp, R.W. McCullough, R. Trassl, E. Salzborn and H.B. Gilbody
Nucl. Instr. and Meth. in Phys. Res., B **98** (1995) 525
- [9] M. Schlapp, R. Trassl, P. Hathiramani, E. Salzborn, R.W. McCullough and
J.B. Greenwood
"Application of Accelerators in Research and Industry"
eds. J.L.Duggan and I.L.Morgan
AIP Press **CP392** (1997) 1199
- [10] R. Trassl, P. Hathiramani, F. Brötz, J.B. Greenwood, R.W. McCullough, M. Schlapp
and E. Salzborn
Physica Scripta, **T73** (1997) 380
- [11] R. Trassl, W.R. Thompson, F. Brötz, M. Pawlowsky, R.W. McCullough and
E. Salzborn
Physica Scripta, **T80** (1999) 504

- [12] F. Broetz, R. Trassl, R.W. McCullough, W. Arnold and E. Salzborn
Physica Scripta **T92** (2001) 278
- [13] LEIF (Low Energy Ion Beam Facilities)
European Network HPRI-CT-1999-40012) *see also* www.leif-network.org
- [14] LabVIEW , National Instruments Corporation , www.ni.com
- [15] J. Bundesmann
"Das Kontrollsystem Codian - Steuerung und Visualisierung eines Ionenquellen-Teststands",
Begleitband zum Kongress VIP2001 - "Virtuelle Instrumente in der Praxis",
Hüthig Verlag Heidelberg (2001) 125-130
- [16] J. Bundesmann,
"Developments in a Control-System for the ECR Facility"
LEIF Report 5, European Network HPRI-CT-1999-40012
- [17] VNC (Virtual Network Computing)
AT&T Laboratories, Cambridge, <http://www.realvnc.com/>
- [18] K. Bethge (Ed.)
"Lecture Notes in Physics":
Chapter 1: "Production of Multiply Charge Ions" by HP. Winter
Springer-Verlag, Berlin Heidelberg 1978
- [19] R. Geller
"Electron Cyclotron Resonance Ion Sources and Plasma" Institute of Physics
Publishing, Bristol 1996
- [20] Ian. G. Brown (Ed.)
"The Physics and Technology of Ion Sources, Second Edition"
WILEY-VCH Verlag GmbH & Co. KGaA, Weinheim 2004
- [21] A.G. Drentje
Rev.Sci.Instrum., **74** (5) (2003)2631
- [22] A. Girard, D. Hitz and G. Melin
Rev.Sci.Instrum. **75** (5) (2003)1381
- [23] R.J. Goldstone and P.H. Rutherford
"Introduction to Plasma Physics"
Institute of Physics Publishing, Bristol and Philadelphia 1995
- [24] F.F. Chen
"Introduction to Plasma Physics and Controlled Fusion Volume I: Plasma Physics, Second Edition"
Plenum Press, New York 1984

- [25] HP. Winter and F. Aumayr,
Europhysics News **33** (6) (2002)
- [26] D. Leitner, Lawrence Berkeley Laboratory, Berkeley, USA
(2004, private communication).
- [27] B. Lehnert
Dynamics of Charged Particles
North Holland Publishing Company, 1964
- [28] Z.Q. Xie and C.M. Lyneis,
Rev.Sci.Instrum. **65** (1994) 2947
- [29] C. M. Lyneis
*Proceedings of the international Conference on
ECR Ion Sources and their Applications,*
Michigan State University, East Lasing, Michingan 1987
- [30] R. Geller, C. Barue, F. Bourg, P. Briand, J. Debernardi, M. Delaunay, B. Jaquot, P.
Ludwig, R. Pauthenet and P. Sortais
*Proceedings of the international Conference on
ECR Ion Sources and Their Applications,*
Michigan State University, East Lasing, Michingan 1987
- [31] S. Gammino, J. Sibring and A.G. Drentje,
Rev. Sci.Instrum. **63** (1992) 2872
- [32] G. Melin, C. Barue, F. Bourg, P. Briand, J. Debernardi, M. Delaunay, R. Geller, A.
Girard, K.S. Golovanivsky, D. Hitz, B. Jaquot, P. Ludwig, J.M. Mathonnet, T.K.
Nguyen, L. Pin, M. Pontonnier, J.C. Rocco, F. Zadworny
*Proceedings of the 10th Workshop on ECR Ion Sources, Oak Ridge ORNL CONF-
9011136* (1990) 1
- [33] H. Beuscher, W. Krauss-Vogt and H.G. Mathews,
Proceedings of the 5th International Workshop on ECR Ion Sources
ORNL, Knoxville, Tenesse 1990
- [34] R. Geller, *Annu. Rev. Nucl. Part. Sci.* **40**, 15 (1990)
- [35] R. Geller, *Proceedings of the international Conference on ECR Ion Sources and their
Applications*, ed. J. Austin and S. Shafroth (Chapel Hill, 1996)
- [36] A.G. Drentje, U.Wolters, A. Nadzeka, D. Meyer and K. Wiesemann
Rev. Sci. Instrum. **73** (2) 516(2002)
- [37] V. Mirnov, K.E. Stiebing, O. Hohn, L. Schmidt and H. Schmidt-Böckling
Rev. Sci. Instrum. **72** (2) 623 (2003)

- [38] A. Heinen, M. Rütter, H. W. Ortjohann, Ch. Vitt, S. Rohde, H. J. Andrä
Proceedings of the 14th International Workshop on ECR Ion Sources
CERN (Geneve), Switzerland (1999) 224
- [39] A. Girard, D. Hitz, G. Melin and K. Serebrenikov,
Rev. Sci. Instrum. 75 (2004) 1381
- [40] Ian. G. Brown (Ed.)
"The Physics and Technology of Ion Sources"
John Wiley & Sons Inc., New York 1989
- [41] K. Halbach, Nuc. Instr. Meth. **169** (1980) 1
- [42] Selten-Erd-Dauermagnete VACODYM, VACOMAX
brouchure published by Vacuumschmelze
- [43] SUPERFISH Code
Los Alamos National Laboratory, USA (1996) LA-UR-96-1834
- [44] M. Fürsatz
„Messungen zur Optimierung des Mikrowelleneinkoppelsystems der 14.5 GHz EZR-Ionenquelle SOPHIE“
project report, 2003
- [45] E. Galutschek, R. Traßl, E. Salzborn, J. Bundesmann, HP. Winter and F. Aumayr
Poster presented at the
„Final LEIF Meeting“, 5-10 December 2003 Stockholm, Sweden
- [46] Ingenieurbüro für Naturwissenschaft und Programmentwicklung,
Peter Spädtke, 65205 Wiesbaden, Junkernstr. 99, Germany
see also www.inp-dme.com
- [47] H. Falter
„Ionenabsaugung aus dem Plasma der SOPHIE ECR Quelle“
internal report, 2001
- [48] IDL "Interactive Data Language", RSI Research Systems Inc.
- [49] H. Eder, W. Messerschmidt, HP. Winter and F. Aumayr
J. Appl. Phys., **87** (2000) 8198
- [50] C. Mayrhofer
„Aufnahme der Leistungsdaten der ECR-Ionenquelle SOPHIE“
project report, 2003
- [51] E. Galutschek, HP. Winter and F. Aumayr
Poster presented at the
"12th International Conference on the Physics of Highly
Charged Ions" September 2004, Vilnius, Lithuania

- [52] F. Wimmer
„Erstellung der Leistungsdaten der ECR- Ionenquelle SOPHIE
in Bezug auf Xenon“
project report, 2004
- [53] Citrix Metaframe Software, Citrix Systems, Inc, www.citrix.com
- [54] Virtual Rooms VideoConferencing System, www.vrvs.com
- [55] www.yahoo.com
- [56] E. Wolfrum, F. Aumayr, E. Hintz, D. Rusbült, R.P. Schorn, D. Wutte,
and HP. Winter,
Rev. Sci. Instrum. **64** 2285-92 (1993)
- [57] B. Schweer, M. Brix, and M. Lehnen, J. Nucl. Mater. **266-269** 673 (1999)
- [58] M. Proschek,
“Towards fast He beam edge plasma diagnostics”,
doctoral thesis, Vienna University of Technology 2001
- [59] M.G. v. Hellermann, W. Mandl, H.P. Summers, H. Weisen, A. Boileau,
P.D. Morgan, H. Morsi, R. König, M.F. Stamp and R. Wolf,
Rev. Sci. Instrum., **61**, 3479 (1990)
- [60] H. D. Falter, M. Proschek, S. Menhart, F. Aumayr, D. Ciric, S. Cox, A. Dines, D.
Godden, N. Hawkes, T. T. C. Jones and HP. Winter,
Rev. Sci. Instrum. **71** 3723 (2000)
- [61] S. Menhart,
“On the applicability of fast neutral He beams for fusion plasma diagnostics”,
doctoral thesis, Vienna University of Technology 2000
- [62] M. Proschek, private communication

List of Abbreviations

- ADAS** Atomic Data and Analysis Structure;
An atomic database provided by Strathclyde University Glasgow
- ASCII** American Standard Code for Information Interchange. The basis of character sets used in almost all present-day computers.
- ASDEX Upgrade**
Axial Symetrischens Divertor Experiment Upgrade
Tokamak Experiment in Garching, Germany
- AUG** ASDEX Upgrade
- AUGUSTIN** Atom- und Grenzflächenphysikalische Untersuchungen bei STößen mit Ionen und Neutralteilchen; laboratory at the University of Technology Vienna.
- AXCEL-INP** A program to simulate the ion extraction from plasmas. [46]
- BERTA** Big Electron cyclotron Resonance Trap for Augustin ,
5 GHz ECRIS developed at the University of Technology Vienna. [4]
- BES** Beam Emission Spectroscopy
- BNC** Bayonet Neil-Concelman or British Naval Connector. A bayonet-style locking connector for coaxial cable connections commonly used for the higher frequency radio and video signals.
- CAMAC** Computer Automated Monitor And Control
An electronics standard used primarily in scientific research applications.
- CITRIX Metaframe**
The world's first server-based computing software for Microsoft Windows NT 4.0 Server, Terminal Server Edition multi-user software (co-developed by Citrix).
- CODIAN** LabVIEW based program for the control of ECR ion sources. [15,16]
- CF-35, CF-100**
Types of metal seal flanges.

DAQ I/O	Type of data acquisition card.
ECR	Electron Cyclotron Resonance
EFDA	European Fusion Development Agency
ECRH	Electron Cyclotron Resonance Heating
ERNST	ECR NeutralSTrahlquelle 2.45 GHz ECRIS developed at the University of Technology Vienna. [1-3]
ECRIS	Electron Cyclotron Resonance Ion Source
ELM	Edge Localized Mode (plasma instability)
FieldPoint	National instruments data acquisition system
He-BES	Helium Beam Emission Spectroscopy
H-mode	High confinement mode
HENP	High Energy and Nuclear Physics
HMI	Hahn Meitner Institute, Berlin
IDL	Programming language. [48]
I/O	Input/Output
Irix	A version of Unix for Silicon Graphics machines.
IP	Internet Protocol
JET	Joint European Torus; Tokamak fusion experiment in Culham, England.
JTV	VNC based broadcast system operated at JET.
Ku-Band	Radio spectrum in the 10.9 GHz to 17 GHz range used by satellite communications systems.
KS5a	Core plasma charge exchange spectrometer at JET. [60]
KS5c	Core plasma charge exchange spectrometer at JET. [60]
KS7	Edge plasma charge exchange spectrometer at JET.

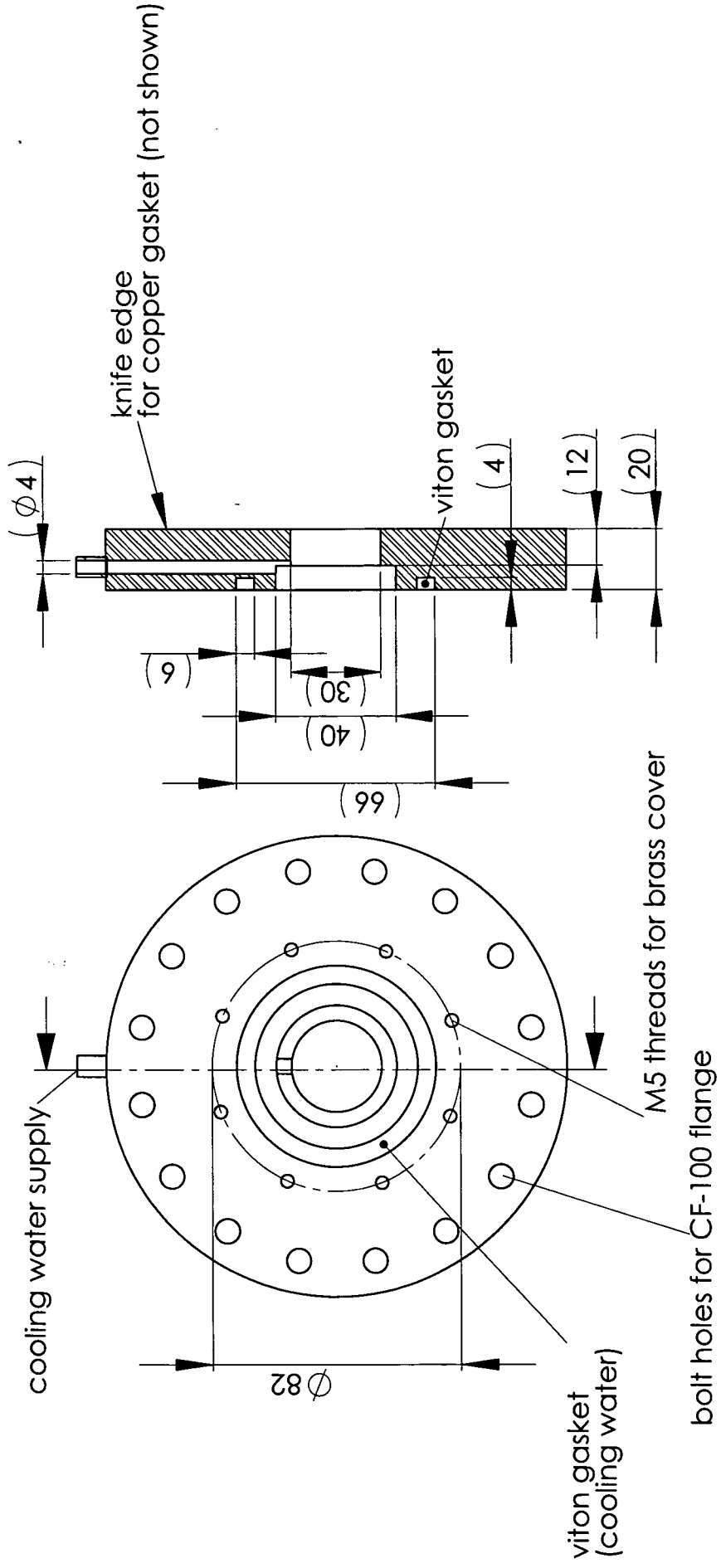
List of Abbreviations

LabVIEW	Programming language for experiments automation and data acquisition. [14]
LEIF	Low Energy Ion Facilities [13]
LIDAR	Light Detection And Ranging (in this context a plasma diagnostics method)
L-mode	Low confinement mode.
Linux	Linux is an open-source operating system derived from the Unix operating system.
LOGO!SPS	Automation system manufactured by system by Siemens.
Mac	Short for Macintosh, a type of personal computer that employs a graphical user interface and is made by Apple Computer, Inc.
MCI	Multiply Charged Ion
MHD	MagnetoHydroDynamic
MPEG	Moving Picture Experts Group. A standard for a digital video & audio compression. MPEG2 This group has defined MPEG-1, MPEG-2 and MPEG-4 video compression standards.
NINA	Experiment for measuring the ion induced electron emission. [49]
OS	Operating System, the basic software running on a computer
PANDIRA	Program to solve ferroelectric and magnetostatic problems. [43]
PC	Personal Computer
PINI	Positive Ion source Neutral Injector (at JET)
PINI7	Positive Ion source Neutral Injector 7 (at JET)
PTFE	PolyTetraFluoroEthylene
RF	RadioFrequency
SOLARIS	A UNIX operating system developed by Sun Microsystems that runs on multiple platforms.
SOPHIE	SOURCE for PROduction of HIGHly charged Ions using ECR; 14.5 GHz ECRIS developed at the University of Technology Vienna

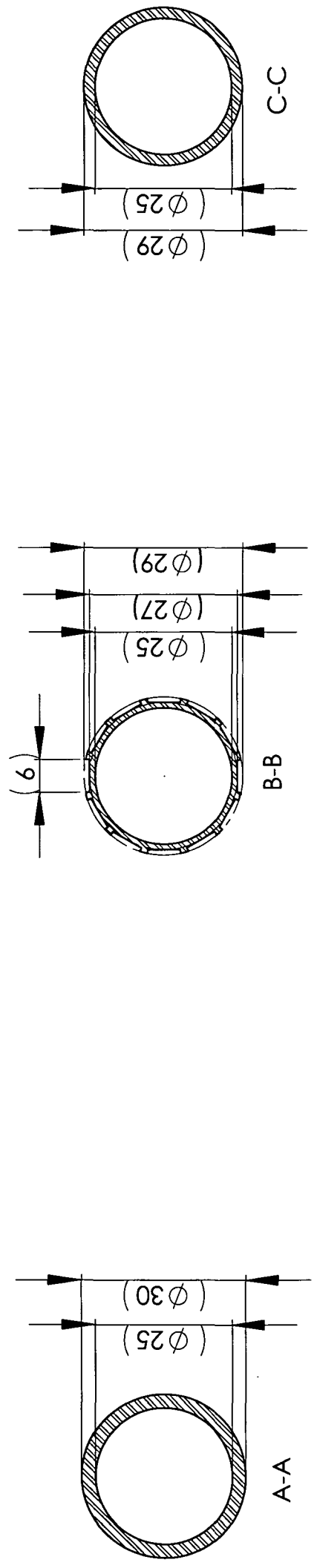
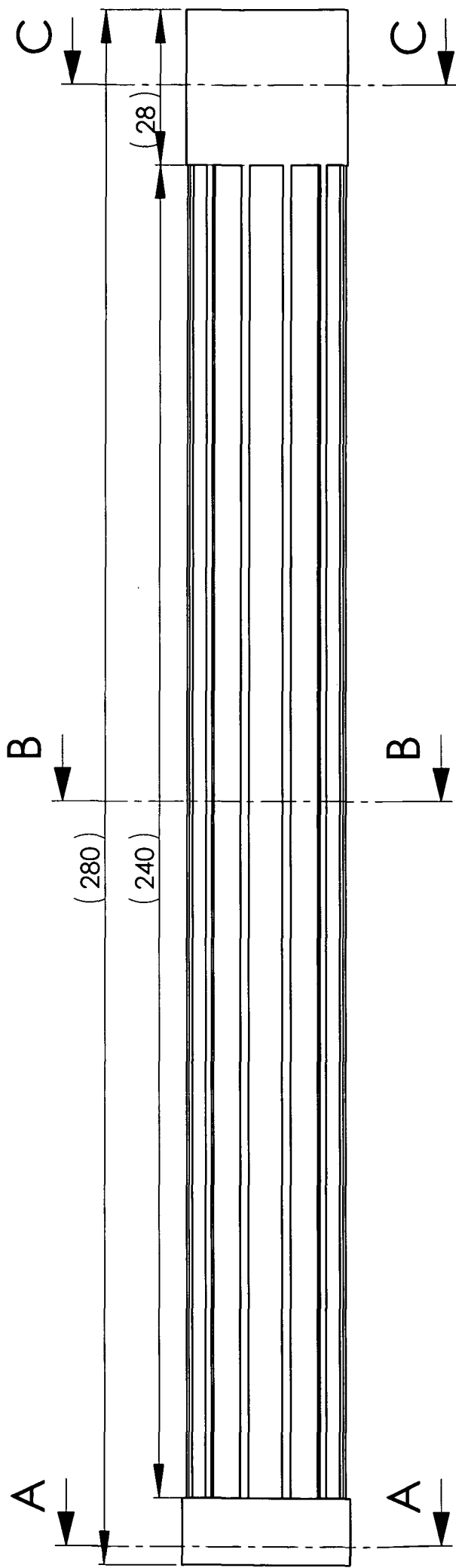
List of Abbreviations

SPS	Speicher Programierbare Steuerung
TU-Wien	University of Technology Vienna
TWT	TravellingWaveTube
UNIX	An operating system developed by Bell Laboratories that supports multiuser and multitasking operations.
VNC	Virtual Network Computing
VRVS	Virtual Room Video Conferencing System
Windows	A family of personal computer operating systems developed by Microsoft Corporation.
Windows NT	Abbreviation of Windows New Technology, a 32-bit multitasking operating system developed by Microsoft Corporation that supports preemptive multitasking.
WR-75	Standardized rectangular hollow waveguide for the Ku-Band.
Yahoo!	Internet search engine.

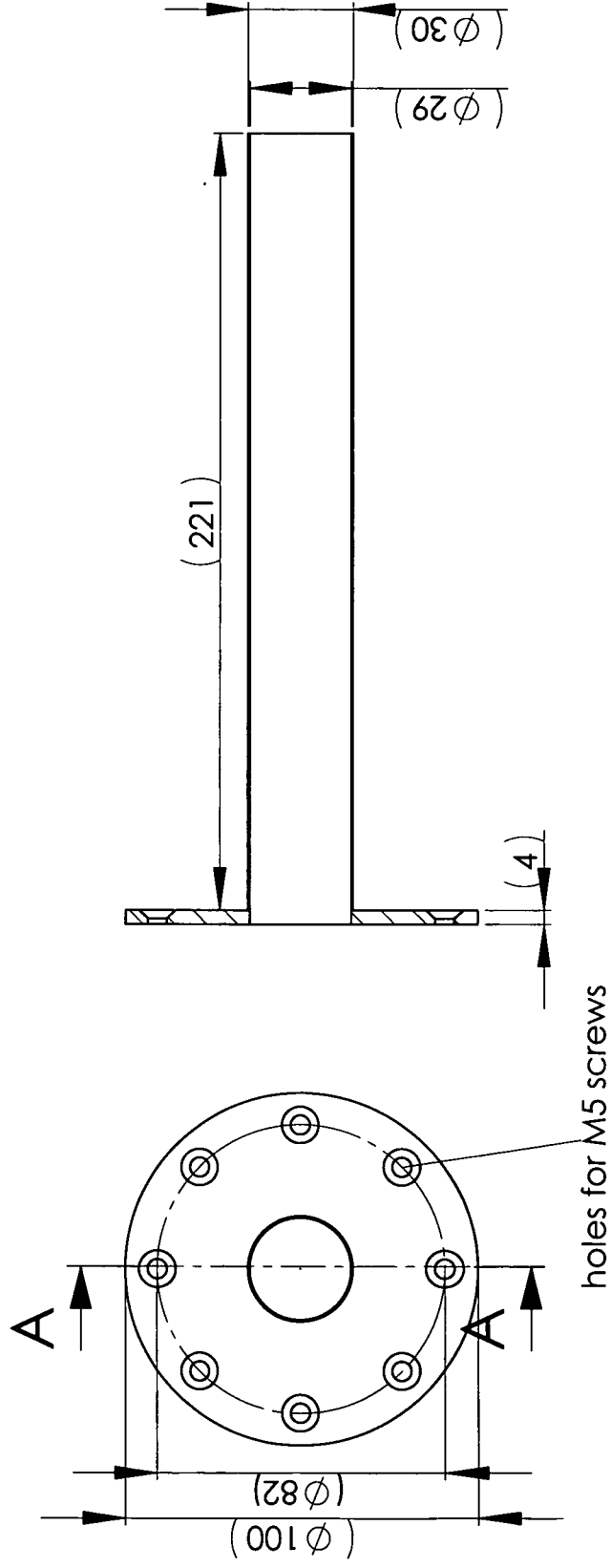
Appendix



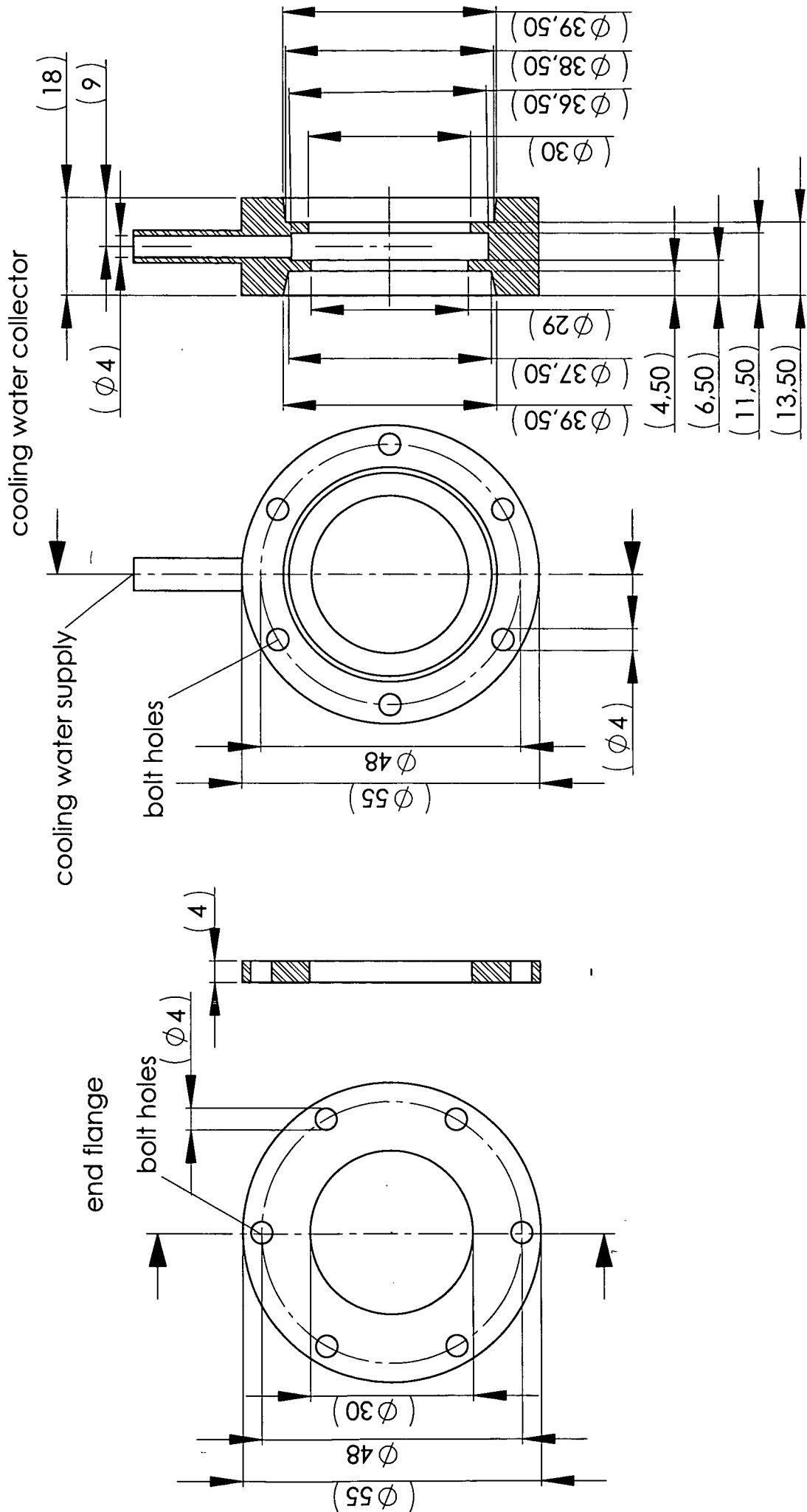
modified CF-100 flange / scale 1:2 / material: stainless steel / all dimension in mm



plasma chamber / scale 1:1 / material: stainless steel / all dimensions in mm

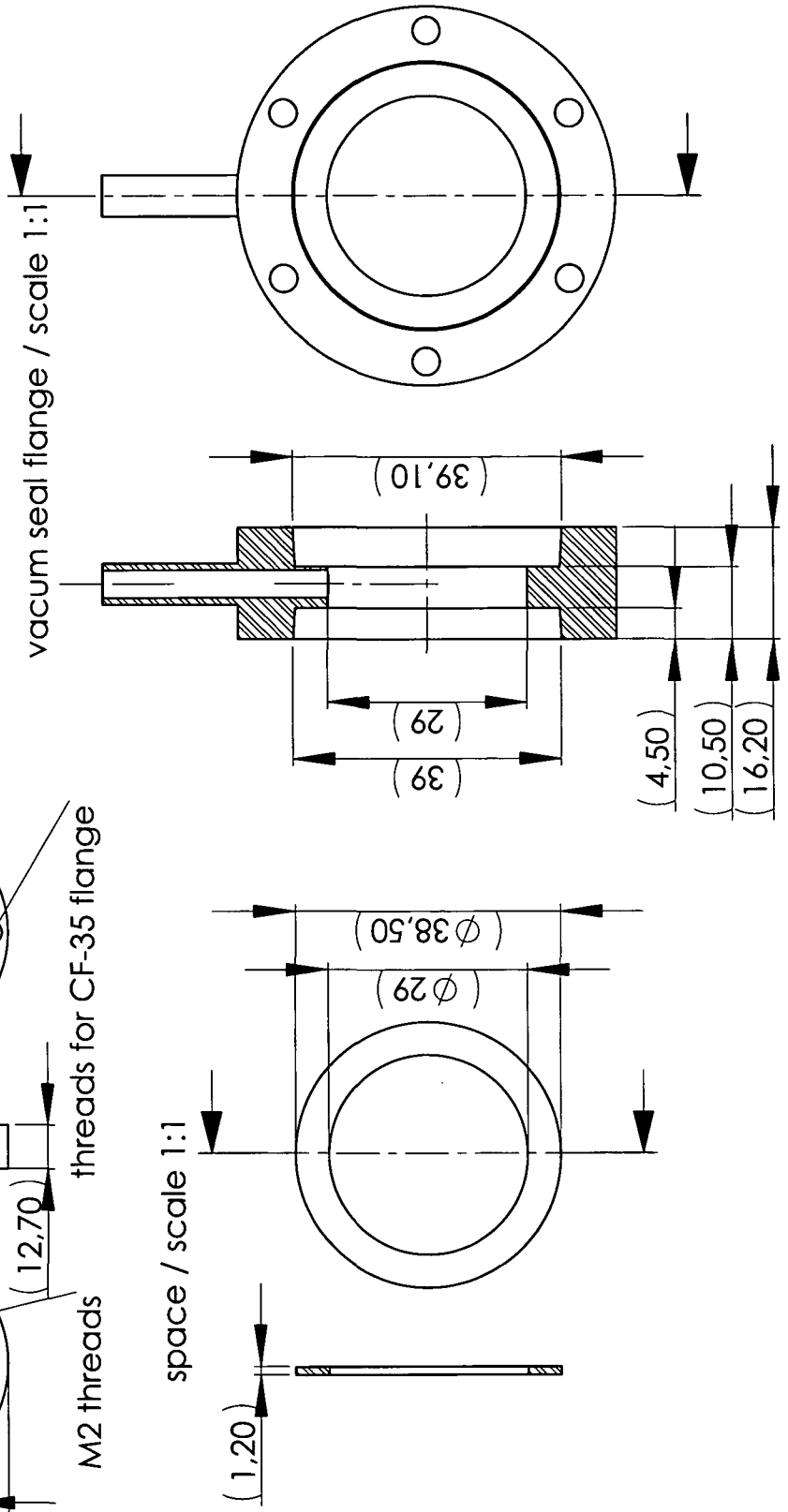
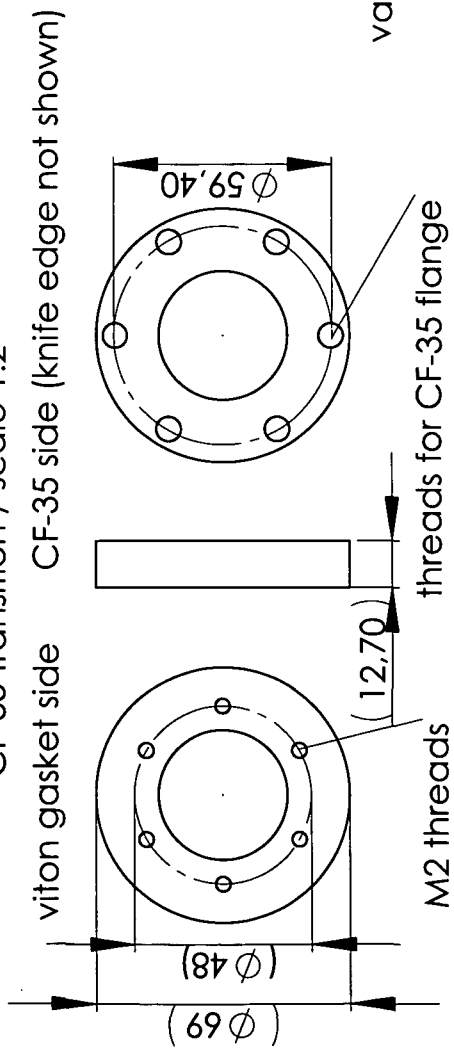


brass cover tube / scale 1:2 / material: brass / all dimensions in mm

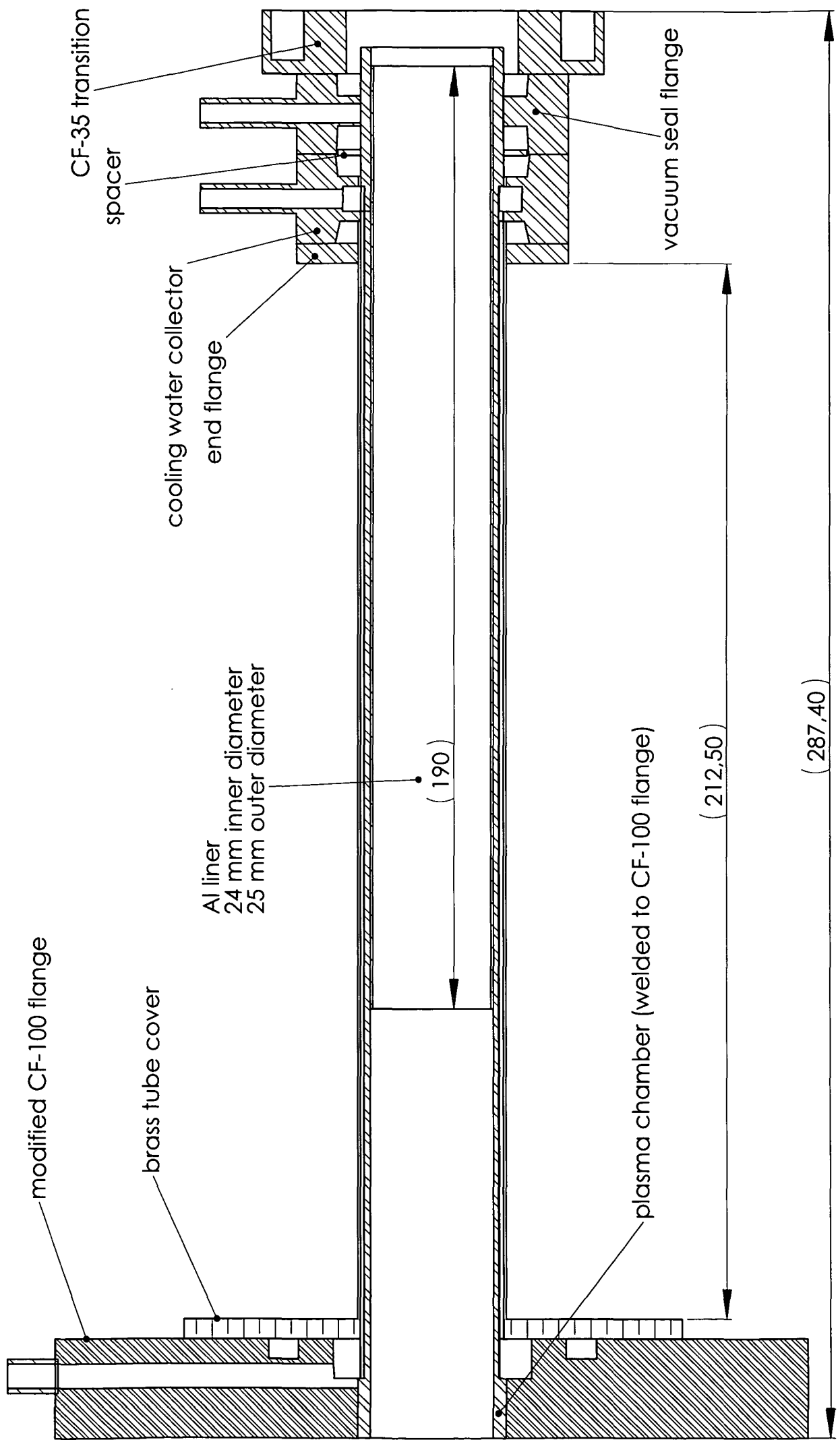


parts for the viton gasket seal system / scale 1:1 / material: stainless steel / all dimensions in mm

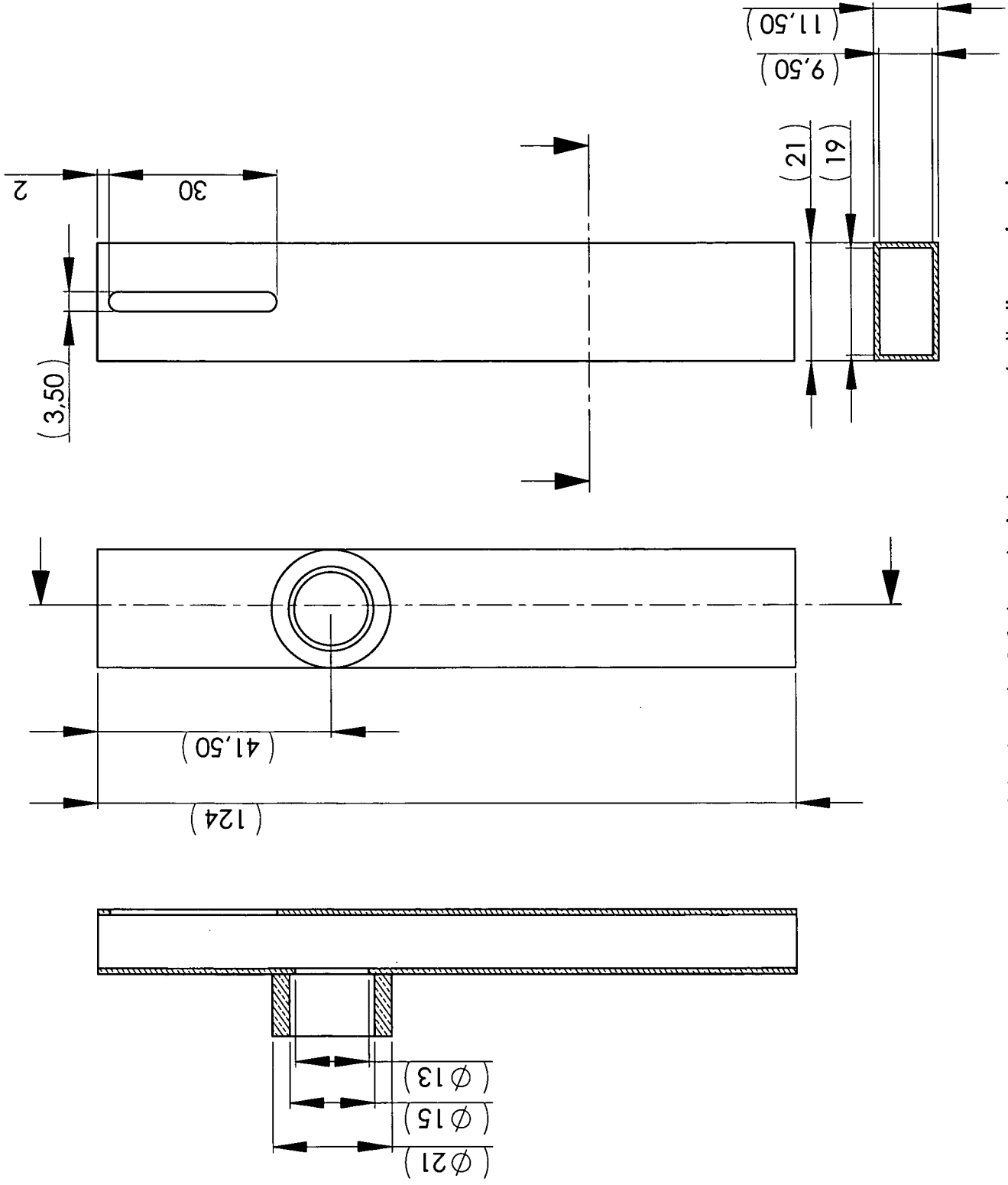
CF-35 transition / scale 1:2



parts for viton gasket seal system / scale 1:1 / material: stainless steel / all dimensions in mm

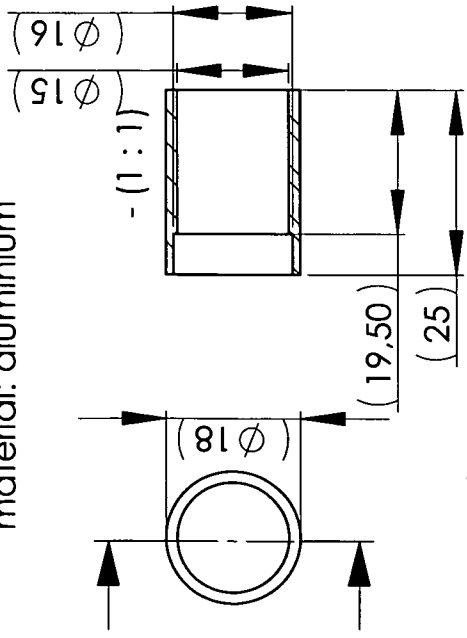


plasma chamber assembly / scale 1:1

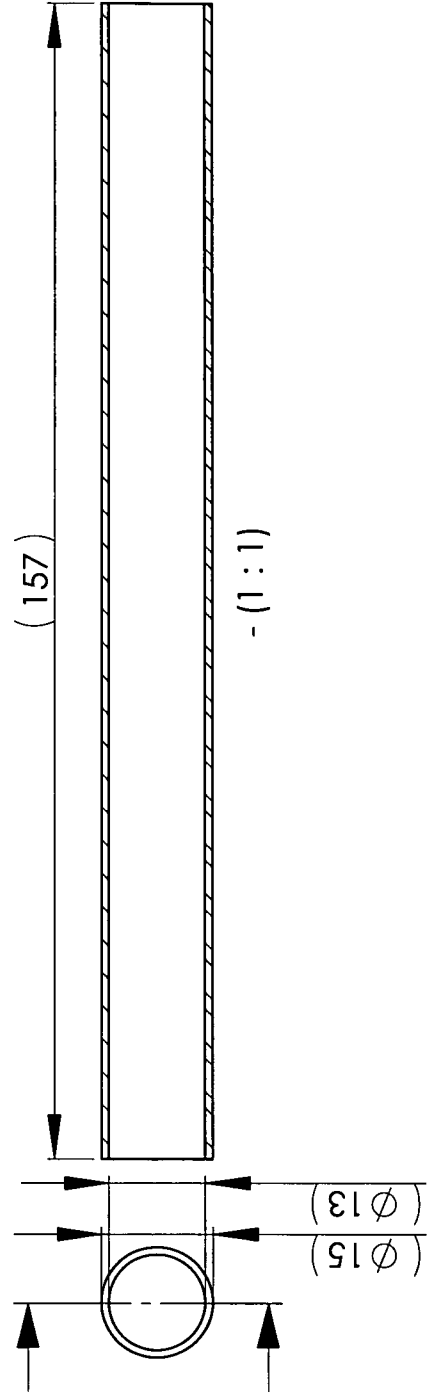


modified WR-75 waveguide / scale 1:1 / material: copper / all dimension in mm

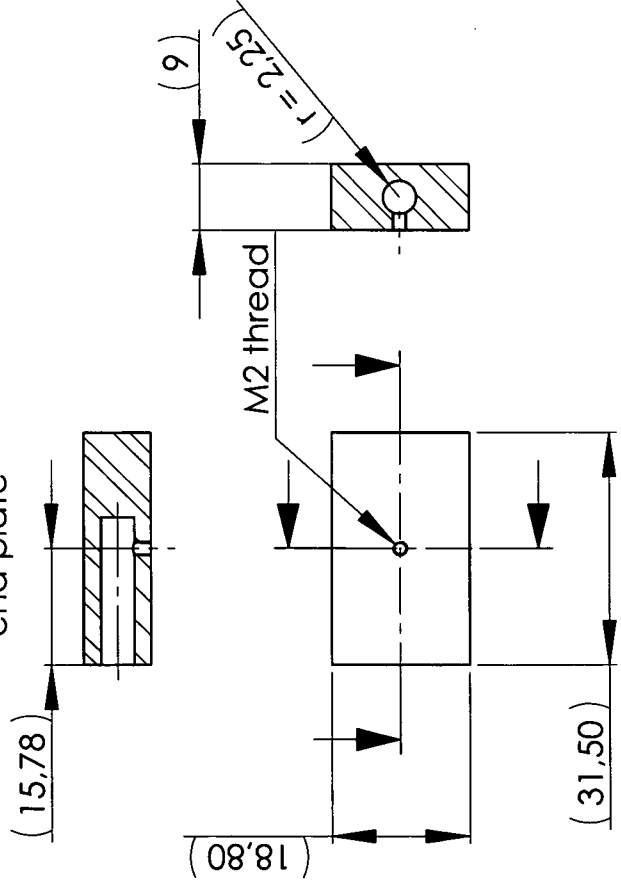
quarter-wavelength transition
material: aluminium



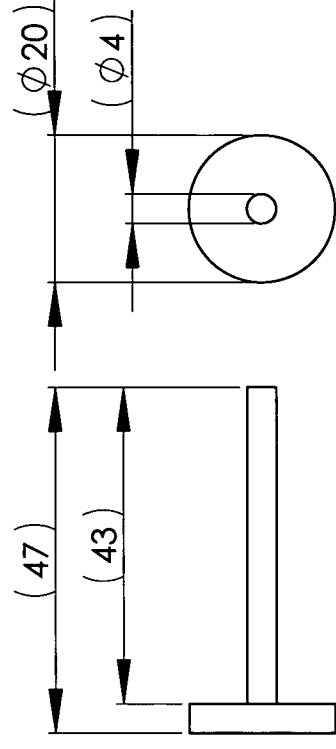
cylindrical waveguide / material: aluminium

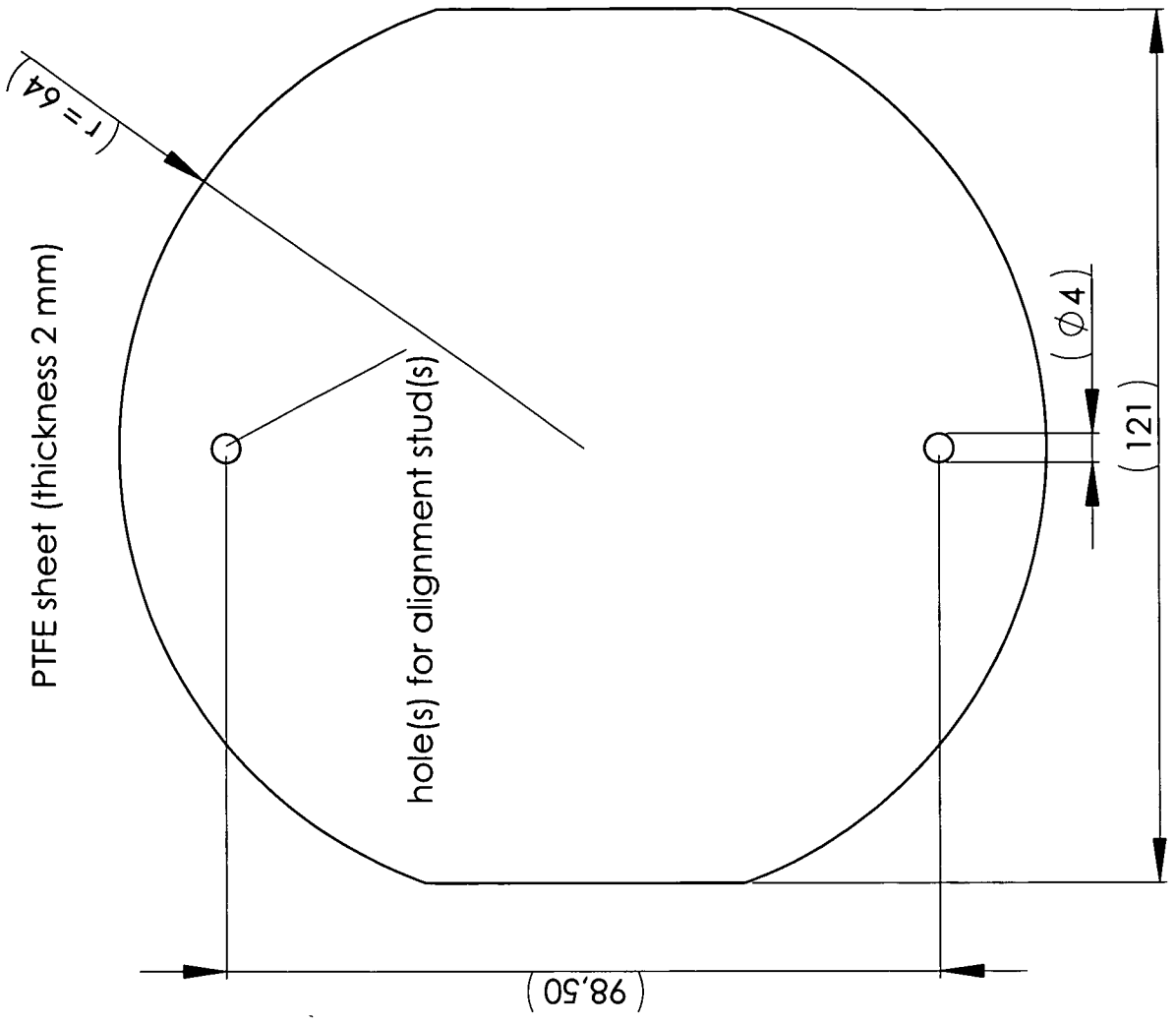
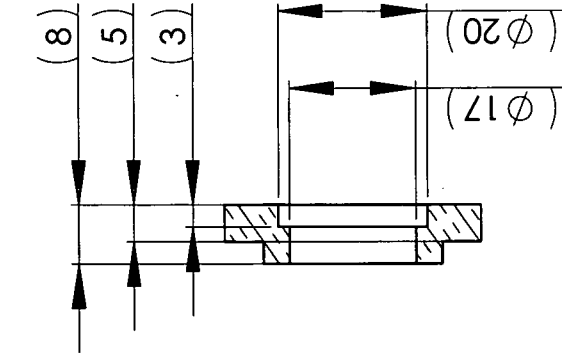
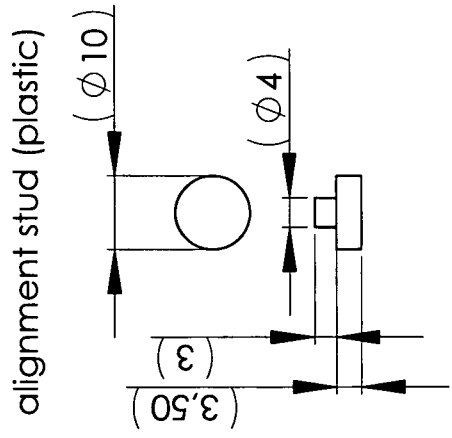
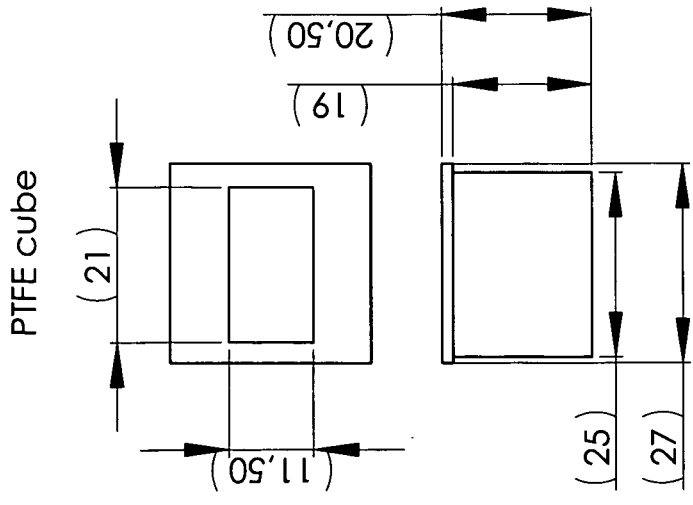


end plate

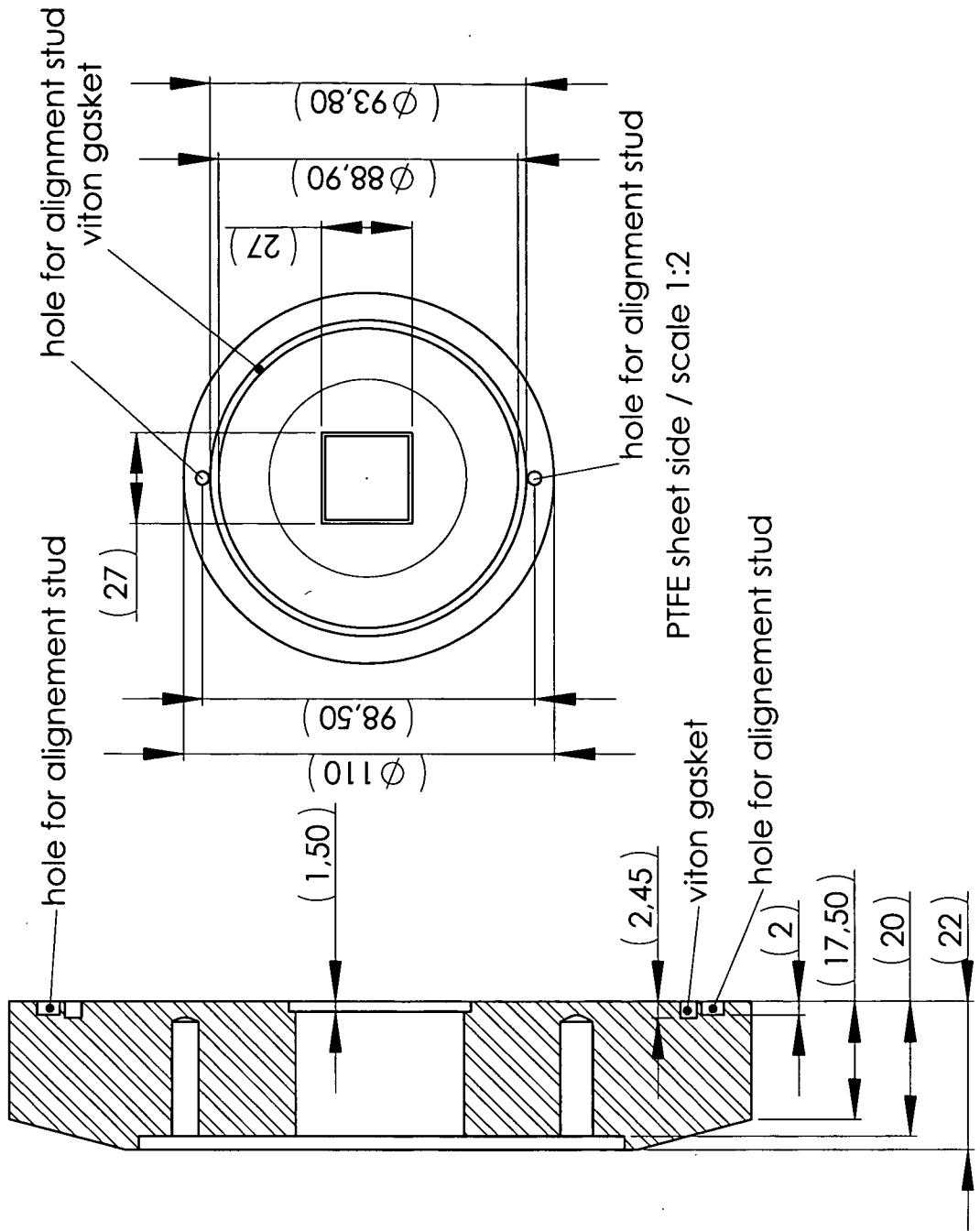


stamp

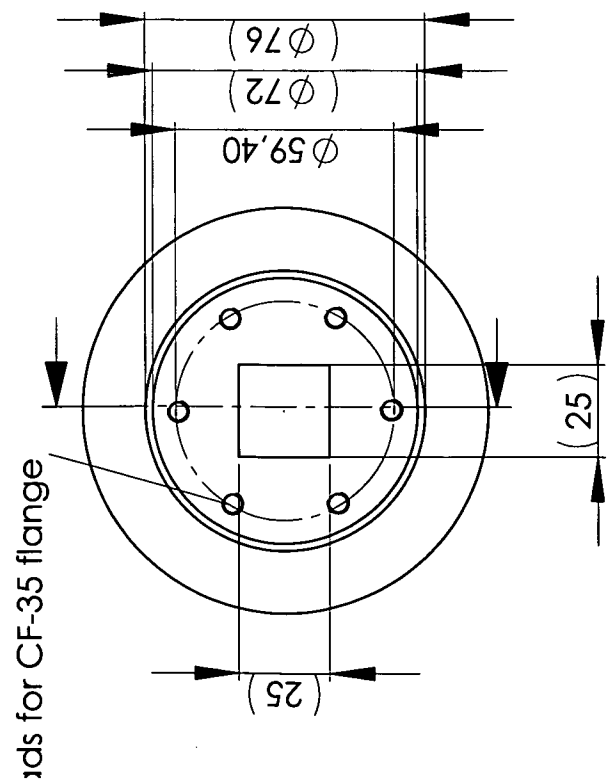




parts for the microwave system / scale 1:1 / material: PTFE (& plastic) / all dimensions in mm

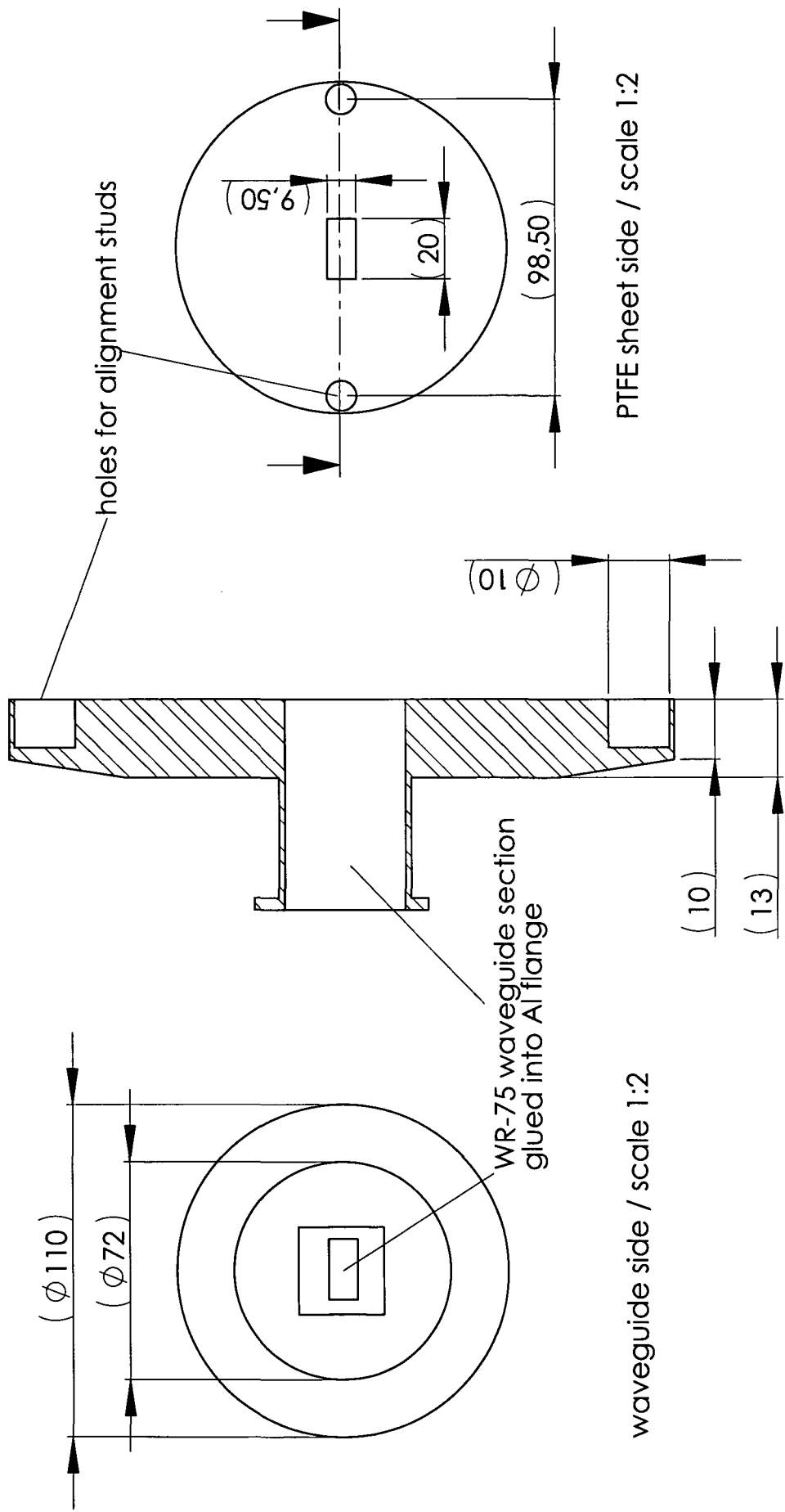


cutaway view / scale 1 : 1



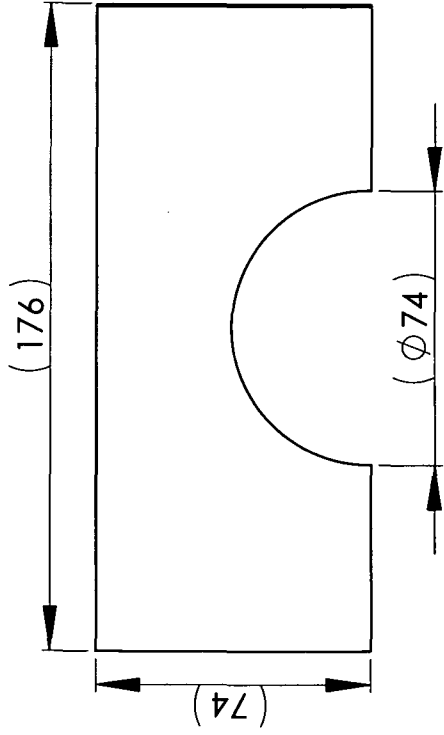
connection to CF-35 flange
(knife edge not shown) / scale 1:2

microwave window - inner flange / material: stainless steel / all dimensions in mm

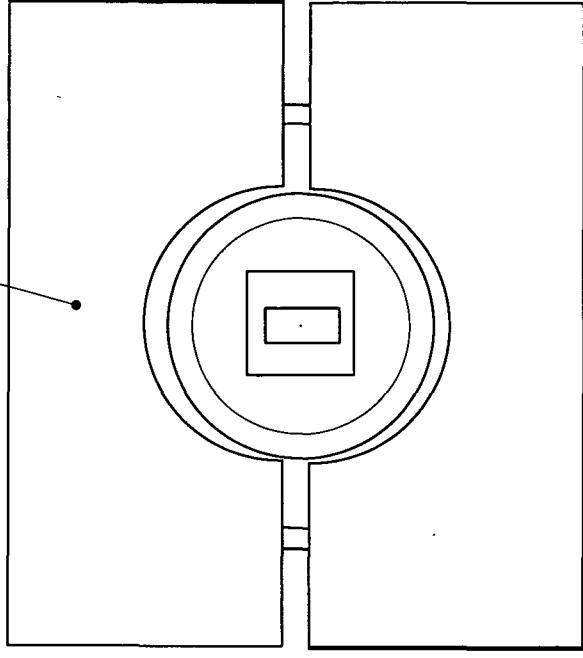


microwave window - outer flange / material: aluminium / all dimensions in mm

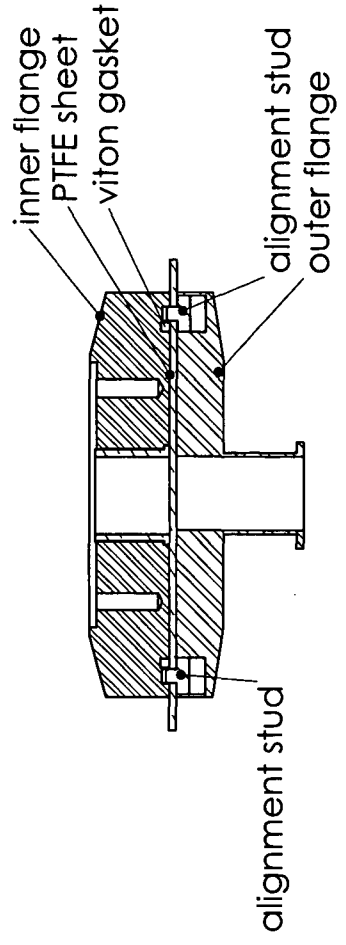
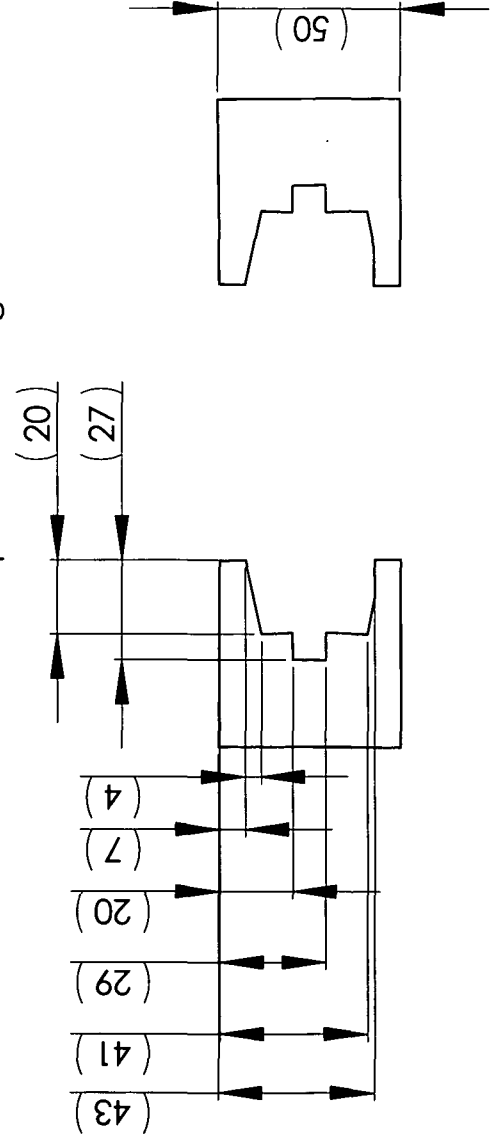
plastic "wedge" (2x)

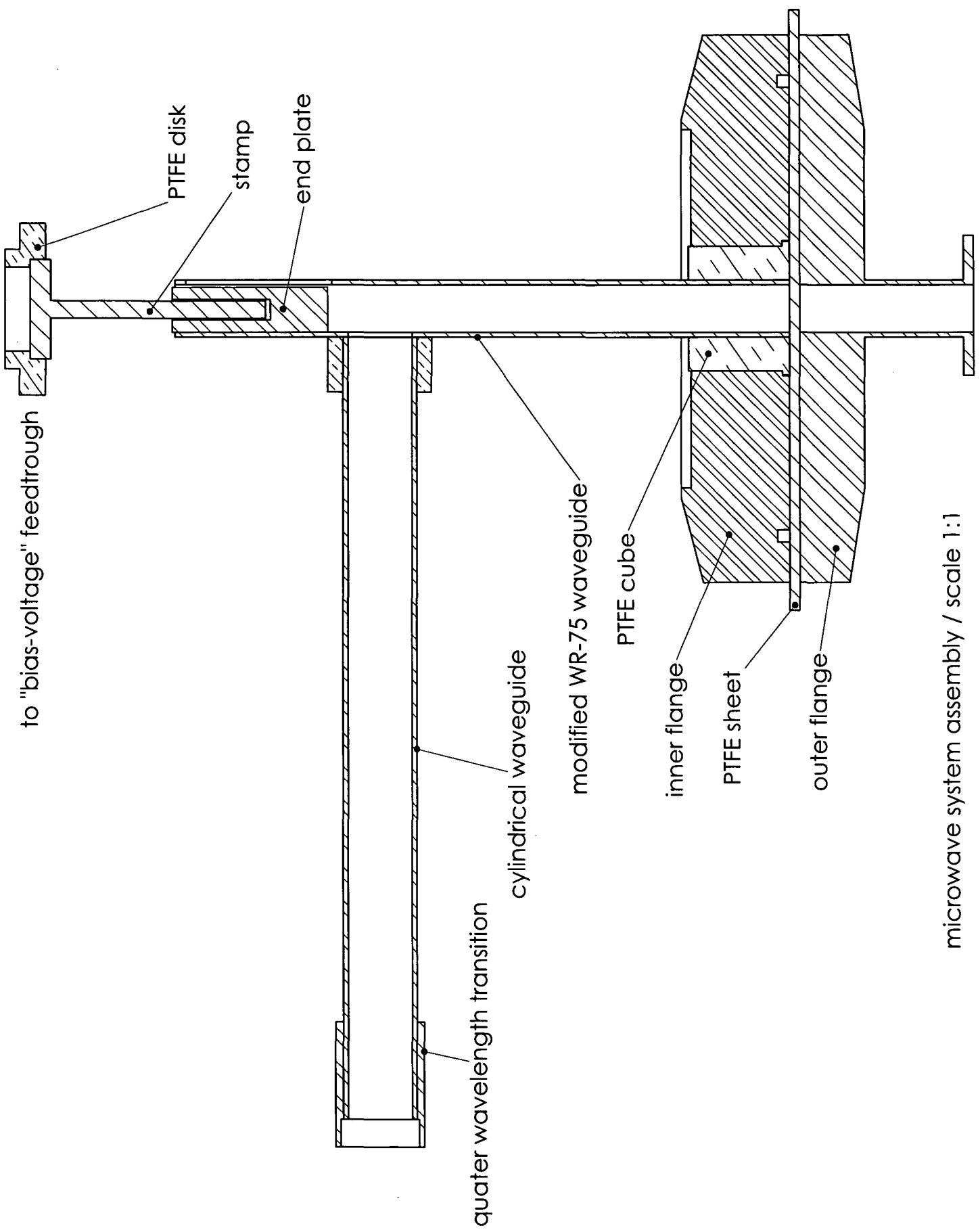


plastic "wedges" press flanges to tighten window

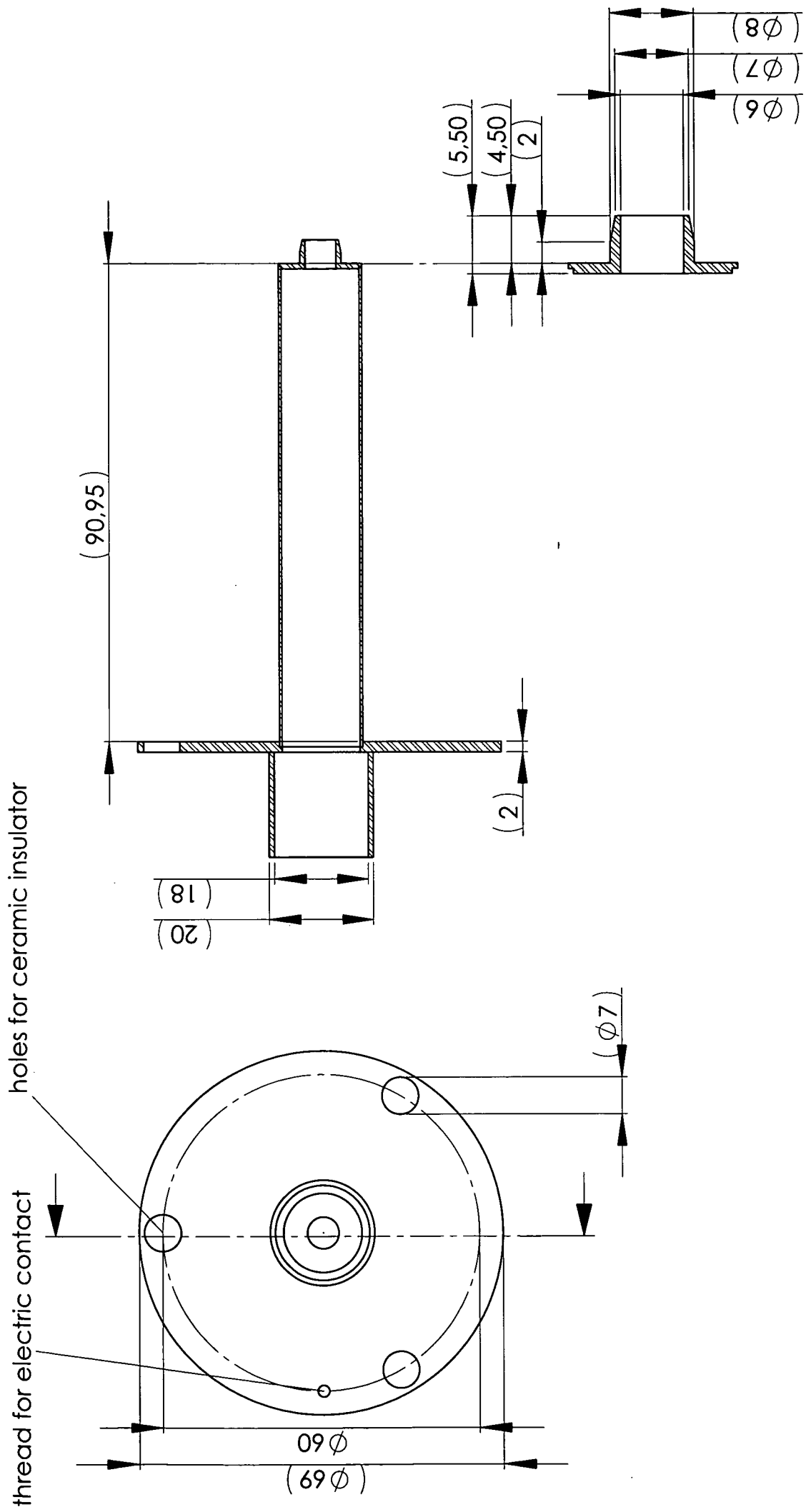


profile of "wedge"



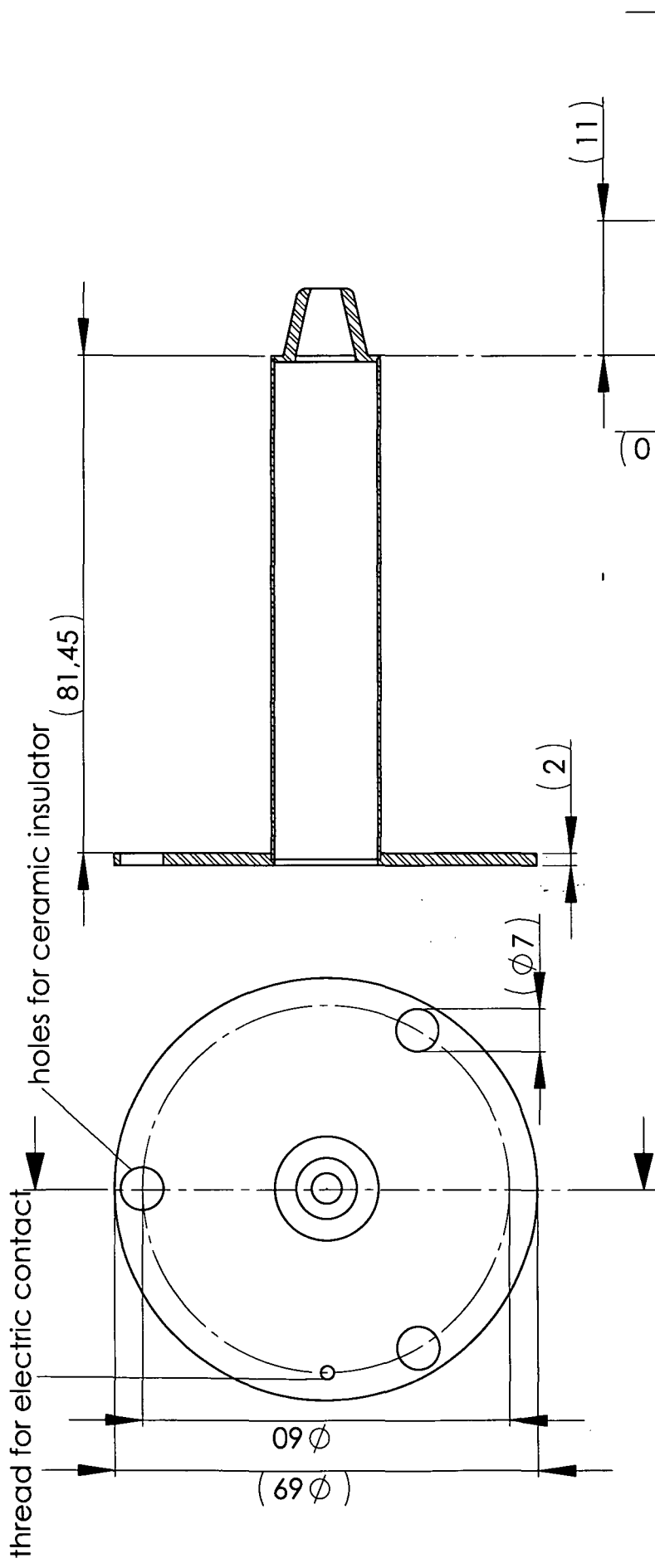


microwave system assembly / scale 1:1



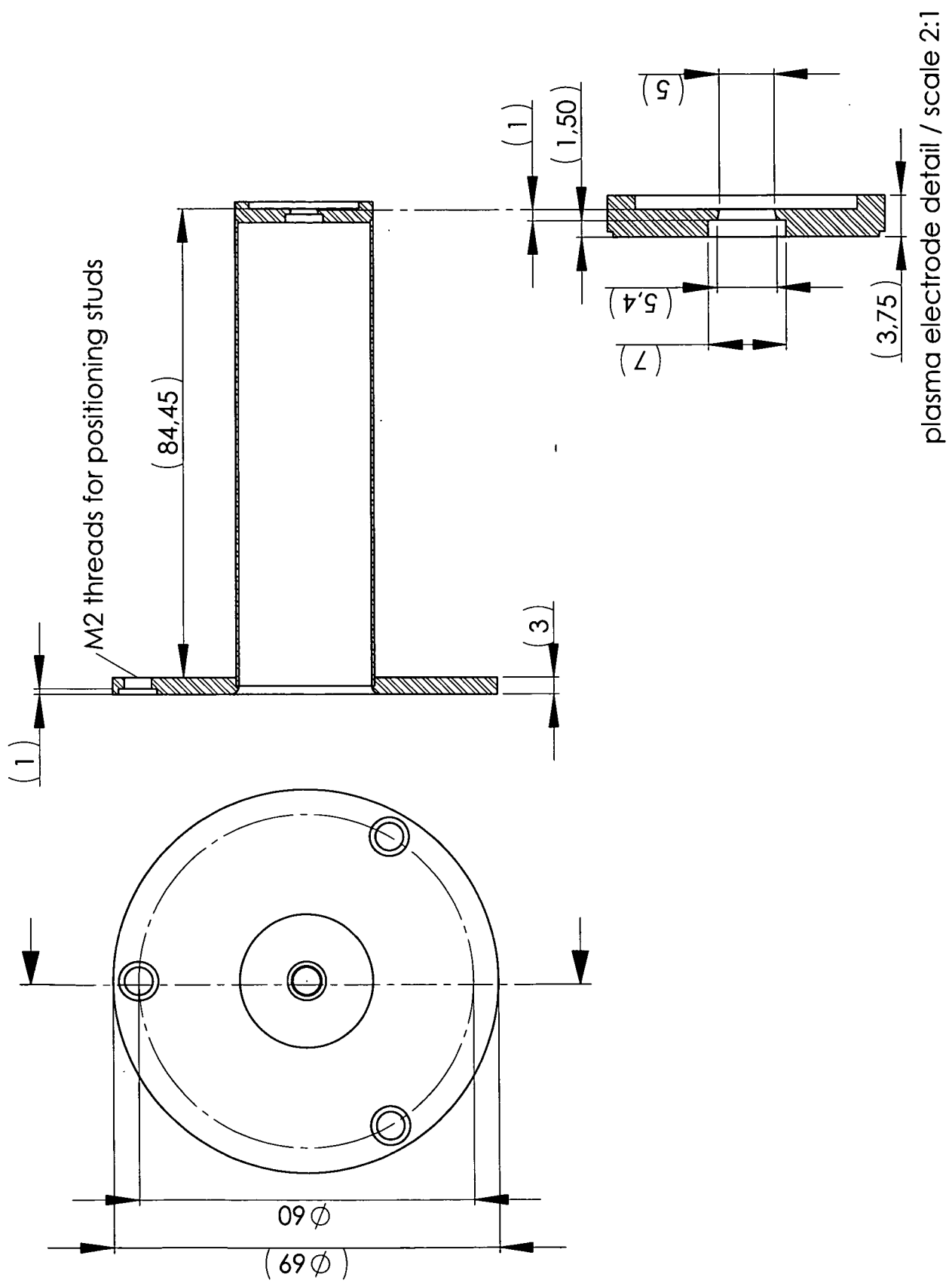
extraction electrode - detail / scale 2:1

extraction electrode / scale 1:1 (1:2) / material: stainless steel / all dimensions in mm

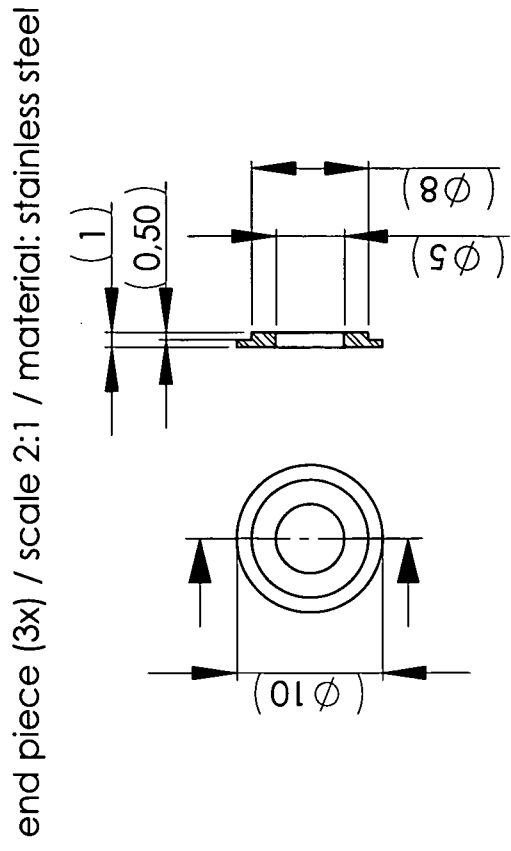
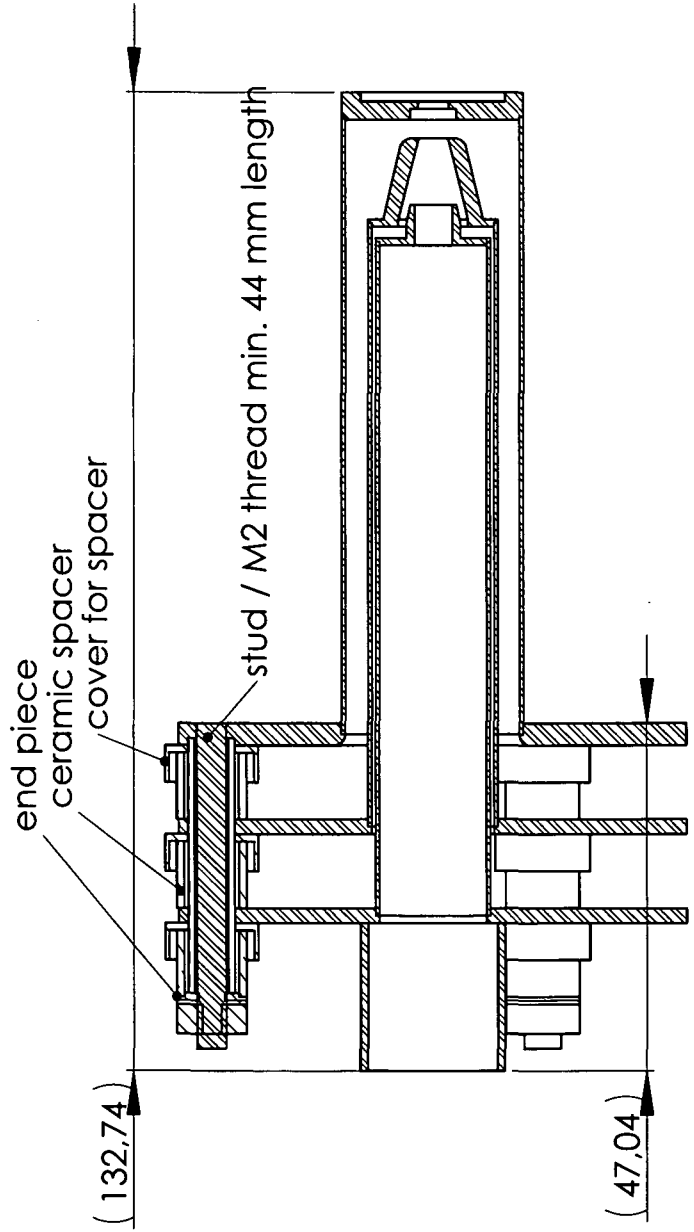
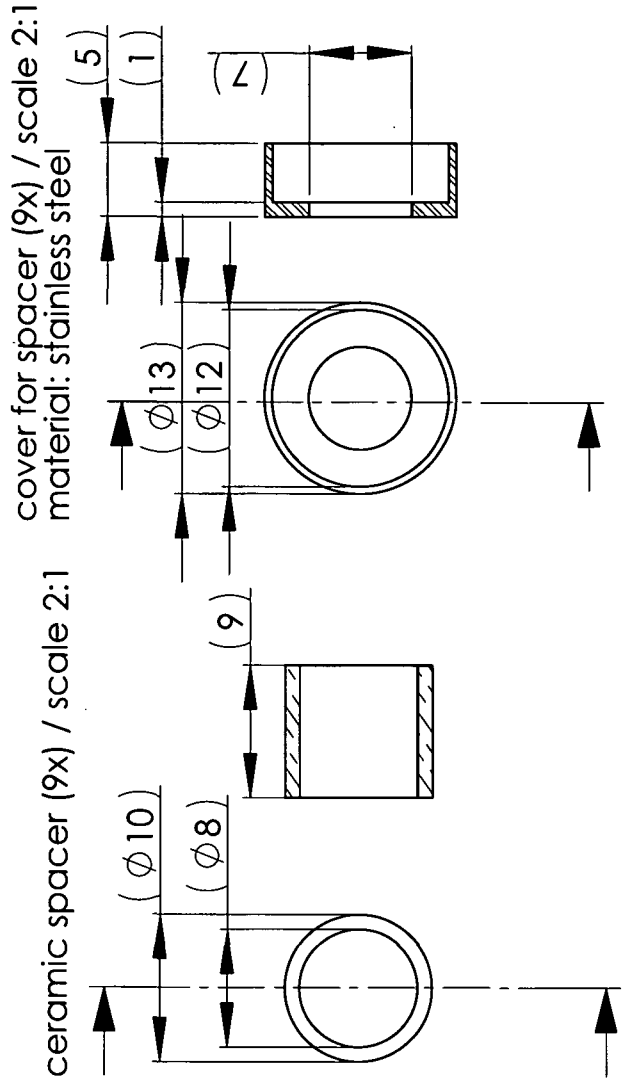
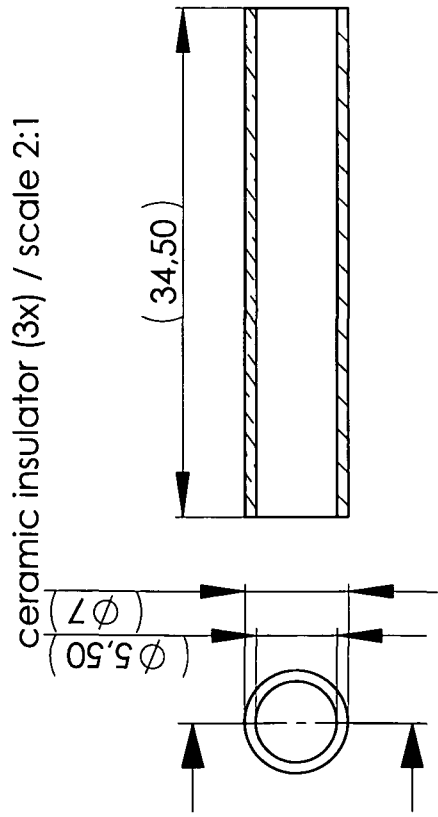


suppressor electrode - detail / scale 2:1

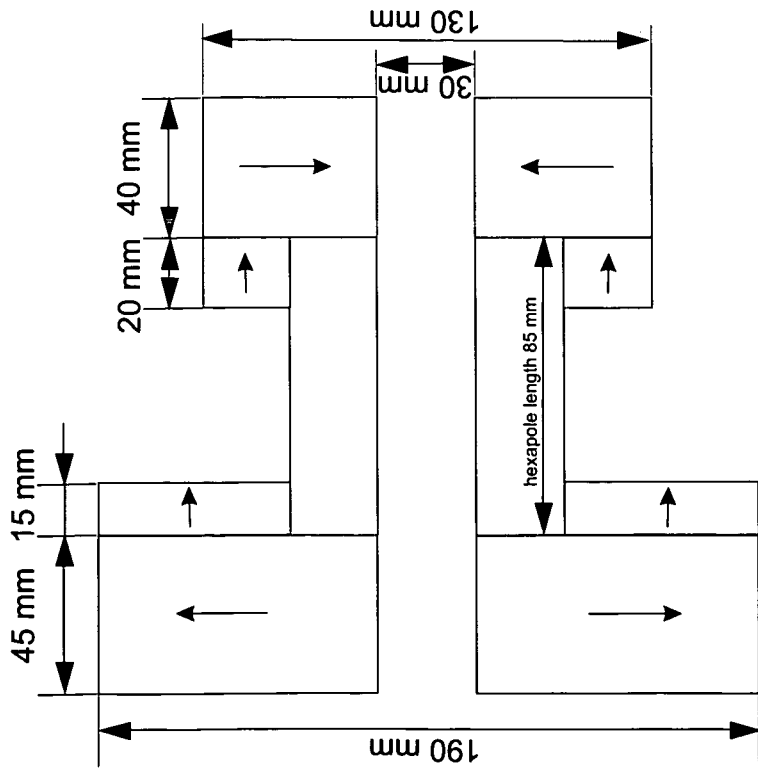
suppressor electrode / scale 1:1 (1:2) / material: stainless steel / all dimensions in mm



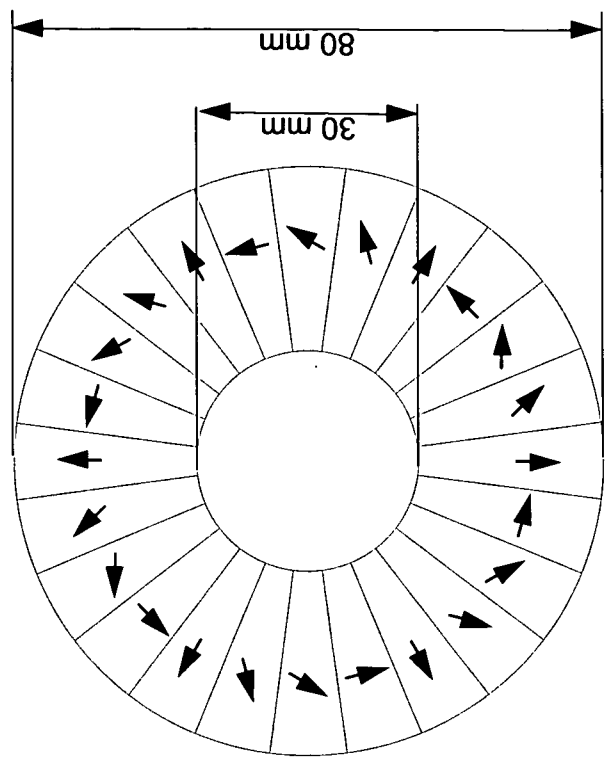
plasma electrode / scale 1:1 (1:2) / material: stainless steel / all dimensions in mm



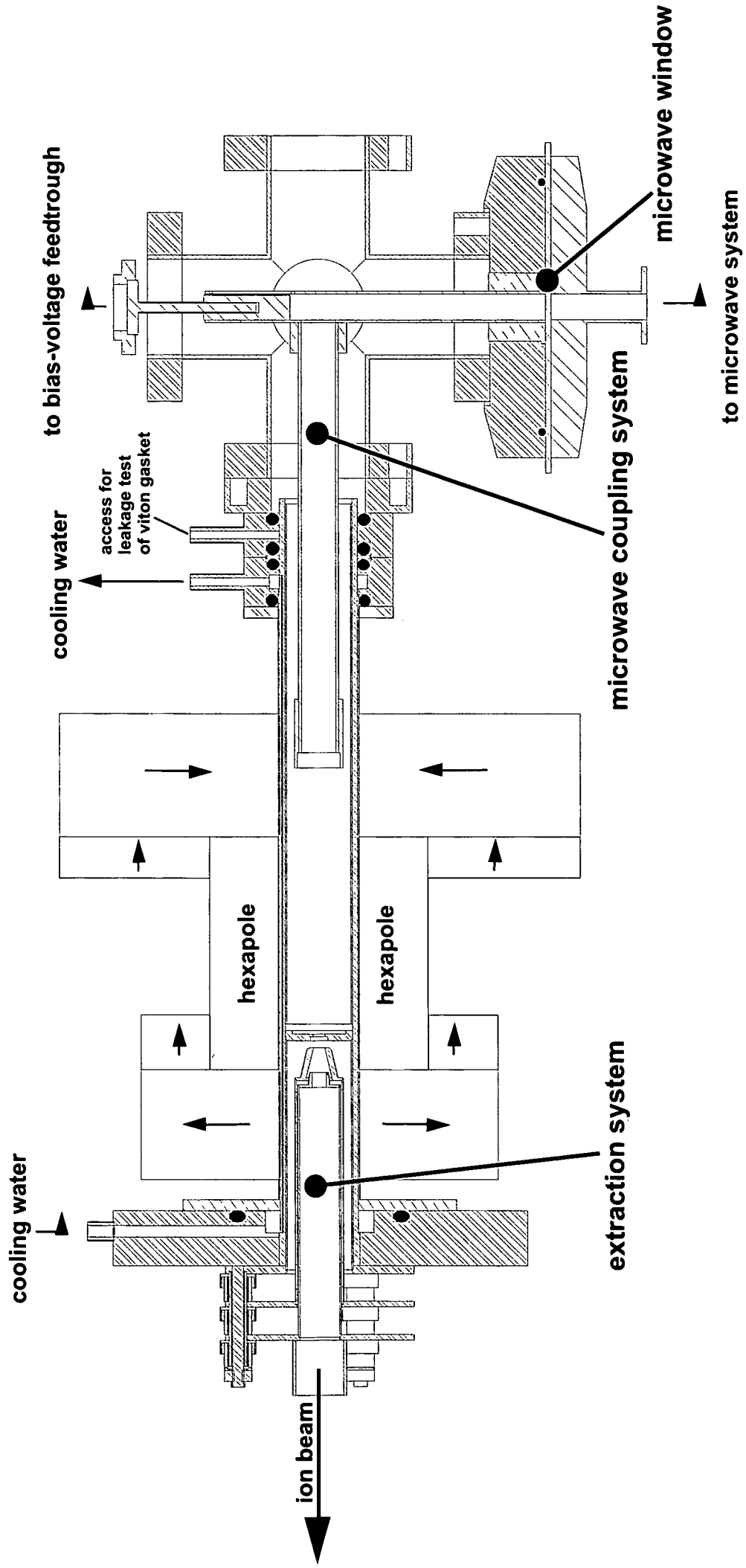
parts for extraction system / scale 2:1 and extraction system assembly / scale 1:1



hexapole cross section



magnet system / VACODYM HR 655



SOPHIE assembly / scale 1:2

Acknowledgement

I would like to thank my supervisor, o.Univ. Prof. Dr. Hannspeter Winter. His support for my work went far beyond the usual, in not only organizing the funding for this work but also allowing me to visit several laboratories, conferences and workshops.

I am very grateful for the advice and support that ao. Univ. Prof. Dr. Friedrich Aumayr, leader of the group of Atomic and Plasma physics, has always been ready to give me. Without his group and the nice atmosphere it would not have been possible to finish this work.

A very special thank-you goes to the workshop team, Ing. Wolfgang Beck, Herbert Schmidt and Rainer Gärtner. In the same manner my thanks go to Ing. Paul Berlinger, responsible for all the ion source`s electronics and Christoph Vetter who supported him. It was the skills and hard work of these people that allowed the ion source presented in this thesis to become reality.

A major contribution to the development of this ion source came from Prof. Dr. Erhard Salzborn and Dr. Roland Trassl, both at the Justus Liebig University Gießen. I am very grateful for their support in designing the magnet system and also their allowing me to carry out the first tests of the new ion source in Gießen.

I am indebted to Jürgen Bundesmann from the Hahn Meitner Institute, Berlin, for providing the excellent "CODIAN" control and interface programme; all users of the ion source have benefitted from its presence in the set-up.

The cooperation with the Justus Liebig University Gießen and the Hahn Meitner Institute were carried out under the auspices of the LEIF network, whose coordinator Prof. Dr. Bernd A. Huber should be thanked here, along with the many other supporters of this network.

The helpful advice of Dr. Walter Ehrlich-Schupita concerning the microwave system also has to be appreciated here.

For my work at JET, I have to thank Dr. Klaus-Dieter Zastrow and his group for their very friendly support. Special thanks go to Dr. Carine Giroud, who maintained the spectrometers used in that part of the work, Dr. Yasmin Andrew and last but not least Dr. Mathias Brix. All these experiments at JET were based on the work of Dr. Michael Proschek, whom I also want to thank for assisting in the data evaluation.

My thanks also go to Dr. Hans-Dieter Falter. His dedication and support were the fundament for the work on the ion source and on the helium beam diagnostics.

Dr. Volker Schmidt deserves thanks for having been very supportive in implementing some of the remote participation tools and organizing a workshop on this topic.

Of all colleagues, I especially want to thank Alfred Pairs, Klaus Schiessel, Martin Fürsatz, Katharina Kaska, Christoph Mayrhofer and Katharina Kaska, Florian Wimmer Katharina Kaska, who all contributed to the construction and characterization of the ion source during their undergraduate project work. Special thanks go to Dr. Richard Smith for reading through this thesis and correcting my English.

There were others who worked concurrently who deserve to be thanked, but are simply too numerous to be mentioned here.

My most heartfelt gratitude goes to my parents, Erika Galutschek and Dr. Ernst Galutschek, for their ever present support and encouragement throughout this sometimes difficult endeavour. Thank you!

Lebenslauf

26. April 1974 geboren in Wien, Österreich
Vater. Dr: Ernst Galutschek, öffentlicher Notar
Mutter: Erika Galutschek, Hausfrau
- 1980 -1984 Volksschule Kolonitzgasse 15, 1030 Wien
- 1984 – 1992 Akademisches Gymnasium, 1010 Wien, neusprachlicher Zweig
- 1992 – 2000 Studium der „Technische Physik“ an der Technisches Universität
Wien
- 1998 – 2000 Diplomarbeit am Institut für Allgemeine Physik
„ Ioneninduzierte Elektronenemission aus Kohlenstoff- und
Litiumfluoridoberflächen“,
betreut von ao.Univ.Prof. Dr. Friedrich Aumayr.
- 2000 Abschluß des Studiums „Technische Physik“
mit den Grad „Diplom-Ingenieur“
- 2000-2003 Arbeit als wissenschaftlicher Mitarbeiter und Dissertation
„Development of a 14.5 GHz All-Permanent Magnet
Multicharged ECR Ion Source for Remote Participation“,
betreut von o.Univ.Prof. Dr. HP. Winter,
am Institut für Allgemeine Physik
der Technischen Universität Wien.
- 2004 Ableistung des Präsenzdienstes